THE UNIVERSITY OF CHICAGO

CORRELATED EVOLUTION OF PECTORAL FIN MECHANICS, MORPHOLOGY, AND MECHANOSENSATION

A DISSERTATION SUBMITTED TO

THE FACULTY OF THE DIVISION OF THE BIOLOGICAL SCIENCES

AND THE PRITZKER SCHOOL OF MEDICINE

IN CANDIDACY FOR THE DEGREE OF

DOCTOR OF PHILOSOPHY

GRADUATE PROGRAM IN INTEGTRATIVE BIOLOGY

BY

BRETT RONALD AIELLO

CHICAGO, ILLINOIS

DECEMBER 2017

TABLE OF CONTENTS

LIST OF TABLES

LIST OF FIGURES

ACKNOWLEDGEMENTS

I believe that graduate school will be one of the most unique experiences I will have in my life. Someone once explained graduate school to me as being thrown in to the deep end of a pool and then being asked to learn how to swim. As I wrote this thesis, I certainly do not feel as though I have learned to swim, at least not efficiently and not always effectively. However, I do think that each chapter represents my ability to tread water just long enough for one or a group of the people in my life (friends, family, colleagues, mentors, etc) to provide the love, support, encouragement, and intellectual guidance needed to help me reach a goal. It is because of the people I am fortunate to have in my life that I was able to conduct the work presented here and achieve any of the successes it might represent. The list of people that need properly thanked is surely too long and I will surely forget many of the people that helped along the way. To the many people that are deserving of thanks, but not mentioned here, please know that your support was appreciated and essential to the completion of this thesis. Thank you.

The most important lesson I learned throughout my graduate education was the value of collaboration and teamwork. While my advisor continually explained the value of teamwork to me, it took interactions with two individuals for me to fully grasp this concept. Adam Hardy was instrumental in teaching me this lesson. Adam is one of the most patient and logical people I have ever had the pleasure of meeting. It is because of Adam's patience and willingness to work with me that I learned this great lesson. While Adam and I will publish at least two projects together, it was the help he gave me with coding and experimental design on projects that he was not apart of and his guidance and support during my two year long search for a postdoctoral research position where I became fully aware of the importance of teamwork. It is my only hope that in our time together, I was able to provide Adam with similar help and support. To Tom

Stewart, it was my greatest pleasure, and still to this day, my greatest accomplishment working on the adipose fin project with you. I didn't know that failing an experiment twelve consecutive times could be so much fun, and after 40 attempts at recording from a tiny nerve, we finally had our N=4 dataset. Despite my constant stubbornness and impatience with analyses and writing, you continually supported me. Furthermore, throughout graduate school you taught me a countless number of lessons about life and general scientific inquiry. You mentored me from my first week in the department through today, and it is largely because of you that I was able to navigate the complexities of the graduate school process. I will do my best to continue to pay forward the insurmountable debt I owe you. Because of Adam, Tom, Melina Hale, and others, I learned that the whole is always greater than the sum of its parts. Thank you.

Aaron Olsen is another individual I owe incredible thanks. Aaron is one of the most brilliant, kind, and hardworking individuals on the planet. Of the four data chapters presented in this thesis, Aaron was a coauthor on three, and provided incredible advice on the fourth. Aaron's positivity and encouragement to dream big and then attempt to make those dreams a reality was instrumental to my time in graduate school. Aaron certainly exemplified the value of collaboration and teamwork. The time I spent working with Aaron was fun, and exactly how I always imagined science to take place – a few people sitting in front of a white board sketching up crazy ideas. The difference was that Aaron and I actually proceeded to do the things we had sketched. Typically, I would provide the crazy and Aaron would provide the brilliance to make these ideas a reality. Further, Aaron is an incredibly hard worker that could often be found in his office on a Saturday or Sunday afternoon. One of my fondest memories of graduate school is coming in to school on Saturday and Sunday afternoons, often after a long brunch at the Valois Cafeteria, and combining our offices for a work party. It was the ideas exchanged on these long

days that greatly improved the way I think about the world and how things work. I am certain that Aaron will go on to do extraordinary things in this world, and I can't wait to see it happen. Thank you for all that you have done for me.

Thank you to the extraordinary students (past and present) of the Darwinian cluster. The students in cohorts preceding my matriculation to the university provided invaluable mentorship and advice. Most notably this list includes: Tom Stewart, Aaron Olsen, Kate Criswell, Haley Stinnett, Justin Lemberg, Andrew Gehrke, David Reed, Caroline Albertin, Joyce Pieretti, Jonathan Mitchel, Amy Henry, Timothy Sosa, Joanna Mandecki, Laura Merwin, Colin Kyle, Ben Krinsky, Charlene McCord, and David Reed. The current students that matriculated to the university after me were similarly instrumental in my education. I appreciate the time you spent teaching me a countless number of things. Notably, I am grateful to Andrew George, Katrina Whitlow, K. Supriya, Laura Southcott, Katherine Silliman, Courtney Orsbon, David Grossnickle, and Jackie Lungmus. I am also incredibly grateful to my entire Darwinian cohort – you were amazing friends and scientists, and you each taught me something so different about the world. Particularly, you each showed me how amazing the world is by sharing your own experiences and exposing me to a variety of different things (foods, games, traditions, ideals, etc) from across the world. Because my cohort and the time we spent together, I learned more about how the world works and the opportunities that exist in it.

I am also overwhelmingly grateful to various students and postdoctoral researchers I was fortunate enough to share lab space: Pepe Jose-Iriarte Diaz, Heather King, Yen-Chyi Liu, Richard Williams, Tom Stewart, Aaron Olsen, Katharine Henderson, Adam Hardy, Andrew George, Hilary Katz, and Evi Menelaou. The patience you all showed me throughout the difficult process of graduate school is second to none. Your guidance, support, and wisdom were

invaluable. I cannot put in to words the amount of happiness and joy you each brought me. I feel like you are all truly part of my family and I love and appreciate you all from the bottom of my heart. I look forward to continuing to watch you bring success to all of your endeavors. Finally, I am extremely thankful to the number of undergraduate students that helped me along the way. I am forever in debt to Chery Cherian, Sihyun Ahn, and Chris Matthis.

I was fortunate to meet an amazing group of people in graduate school and I know we will continue our friendships after we part ways. My friends were there for me throughout the highs and lows of graduate school. These friends include every person previously mentioned in this section as well as Evan Koch, Jenn Stanley, Max Winston, Daniel Hooper, Shane Dubay, Daniela Palmer, Darcy Ross, Victoria Flores, Peter Lido, Mo Siddiq, Joel Smith, Lexi Moore, Kara Feilich, Nicolai Konow, Emily Kane, Michael Korus, Kevin Korus, Warren McClurg, William Lee, Mathew Michael, Michael Bowen, and Carl Jackett. I'd like to thank two of the greatest human beings to have ever walked the earth, Simon Lax and Dallas Krentzel (aka Big Feta, aka Rondo, aka the Maine event, aka gourdson). I would also like to thank Sandy Kawano who has been my friend and mentor since the day I met her at a regional SICB conference at Wake Forest University during the first year of my Masters program. Sandy is another person who has been instrumental to anything I have or might accomplish in the future. I do not believe words exist to describe the gratitude you deserve. Finally, I must thank my two advisors throughout my Masters degree, Michael Butcher and Richard Blob. I would not have made it to a Ph.D. program without your encouragement and help.

Two additional people were instrumental to my development as a scientist. I met both Dallas Krentzel and Michael LaBarbera during the summer prior to my first year in graduate school, and I am very fortunate that I did. For some reason, these two people saw past my

substantial ignorance and were there to teach me anything and everything whenever I was (and in the case of Dallas, also wasn't) in need of advice. I cannot point out one thing they each did and it would be impossible to mention everything they did. I believe that speaks to the investment these two made in my education. These two seemingly have a grasp on how the universe works in a way that I have never seen prior to meeting them. Further, LaB is an amazing teacher in the classroom. Not only did I learn fluid mechanics from LaB, but I tried to learn how to be an amazing educator too. Thank you both for the time you invested in my education, and please know that I will continue to contact you for advice and help the rest of my life.

I am also thankful to the faculty and staff of the Drawinian cluster. The staff, especially Cindy King, Carolyn Johnson, Libby Eakin, Alison Anastasio, and Audrey Aronowsky, was crucial to the navigation of deadlines, completion of paperwork, and the other tasks that are needed to ensure a successful department. Carolyn Johnson and Alison Anastasio showed me exceptional kindness and thoughtfulness, and I thank you for the countless number of conversations we shared. The faculty of the Darwinian cluster was exceptional in their willingness to meet and chat about anything and everything. The expertise you shared with me was invaluable and there is no other place on the planet that I would have been subjected to so much brilliance at the same time. Most gracious with their time were Robert Ho, Stephanie Palmer, Vicky Prince, Neil Shubin, and Michael Coates.

I am most grateful and in debt to my thesis advisor and committee. Each one of you was a source of mentorship, support, wisdom, and education throughout my time in graduate school. In addition to providing all of the things mentioned about others above, you each took it one step further and welcomed in to your labs, homes, and, most importantly, lives. I look at each of you

as mentors, colleagues, and any other professional title you can think of adding to the list, but I also think of each of you as family. You've each impacted my life in a way that I cannot put in to words. All I can say is that I will do my best to put the things you've taught me in to practice and use them to overcome the many challenges that I will face in the future.

Thank you to my thesis advisor Melina Hale. Melina Hale is the most extraordinary person I have ever met. Melina taught through both speech and action, and always followed through with anything that was asked of her. Fear not, Melina, I will always remember the importance of: a topic sentence, figuring out what the broad question is, generating a testable hypothesis, a simple experimental design, and showing why it is important rather than simply saying it's important. That list can go on for a mile. However, the countless things Melina taught me about the scientific process, writing, and experimental design are miniscule in comparison to the lessons she taught about me about life. I believe that Melina's mission to help me become a better scientist was always second to her mission to teach me life lessons that can be applied both in and out of science. Melina certainly succeeded in this goal. As mentioned above, Melina constantly explained to me the value of teamwork and collaboration. Most importantly, Melina taught me through her own actions that if you consistently work hard work, be selfless, helpful, and kind to others, use the disappointments to motivate you, and be humble in times of achievement that things will work out for you and you will be able to accomplish great things. I found that graduate school was a rollercoaster of highs and lows, but I also found out that having Melina Hale by your side makes dealing with the lows a lot easier and celebrating the highs a lot more fun. Thank you, Melina.

Thank you to the rest of my committee for not only mentoring me, but also treating me as your own student. Thank you to Callum Ross for the countless hours you spent talking to me

about science and life, thank you for teaching me the value of learning human anatomy, and thank you for giving me the opportunity to TA human anatomy. It was the trust and freedom you provided me when teaching the lab for multiple MSTP classes that allowed my teaching ability and experience to grow exponentially. While I will certainly recall many of the countless lessons you taught me over the years, I am looking forward continuing our friendship and seeing you at future meetings for years to come. Thank you to Sliman Bensmaia for the tough love you showed me on numerous occasions. You mentorship style was amazing and I appreciated knowing that nothing was left unsaid in any meeting we ever had. You also showed me the joys of programming and you were there to patiently teach me new data analysis routines over the period of months. Finally, thank you to Mark Westneat for certainly spending just as much time with me as any primary advisor. I thought were meant to work together since we were both from Ohio, but we disagreed on our respective allegiances in nearly every sport we both followed. In all seriousness, your positivity and encouragement were without hesitation. Our ideas together were always big, and our experimental design was always simple. Above all, you taught me how to sit back and enjoy science, which is something I found to be extremely helpful when navigating the ups and downs of graduate school. I will always look back at your approach to both science and life and try to establish that same approach in my future endeavors.

Finally, thank you to both my family and Wenli Dai for your constant love and support. I'd especially like to thank my father, Ronald, who taught me the value of hard work through the actions (never through lecture) of his own life.

B.R.A

July 2017

Chicago

ABSTRACT

From insect wings to tetrapod limbs, the appendages of animals have diversified with the functional demands associated with different behaviors and the invasion of new habitats. In addition to their roles as propulsors, the locomotor appendages of animals also act as sensors that provide critical mechanosensory feedback for the motor performance of animals. This thesis examines the role of sensory feedback in animal locomotion, and then, through an integrative approach, studies limb diversification by assessing the correlated evolution of limb mechanics, morphology, and mechanosensation. I focus on a diverse group of fishes, the wrasses (Labridae), which exhibit a continuum of pectoral fin-based swimming behaviors that range from drag-based rowing to lift-based flapping. While rowers are exceptional at acceleration and maneuverability, flappers are highly efficient and can reach higher cruising speeds. In chapter two, I show that mechanosensory feedback from the fin rays of the pectoral fin is necessary for effective labriform swimming in a parrotfish, *Scarus quoyi*. In control fish, fin beat frequency and the duration of muscle activity relative to total cycle duration both increase with increasing swimming speed. The loss of sensory feedback results in increased fin beat frequency, a transition to the body-caudal fin gait at slower speeds, and an increase in the duration of muscle activity. In chapter three, I examine the relationship between fin mechanics, swimming behavior, and hydrodynamic capability in two species of Labridae that employ different swimming behaviors, the flapping *Gomphosus varius* and the rowing *Halichoeres bivittatus*. I find that in both species, pectoral fin ray stiffness decreases along the proximo-distal axis of the fin, and that fin ray stiffness decreases along the chord of the fin from the leading to trailing edge. Comparing between species, I find that the pectoral fin rays of the flapper, *G. varius*, are nearly an order of magnitude and significantly stiffer than those of the rower, *H. bivittatus*. In chapter four, I assess

how variation in fin ray geometry (second moment of area, *I*), material properties (*E*), fin ray segmentation and fin ray branching patterns explain the multiple levels of variation in fin ray stiffness (within a single ray and between rays, individuals, and species) and also combine to produce the overall stiffness field across the pectoral fin surface. Fin ray segmentation patterns and *E* were similar between species, measurements of *I* and the number of branch nodes were greater in *G. varius* in comparison to *H. bivittatus*, *I* was always significantly correlated with fin ray flexural stiffness, and variation in *I* always explained the majority of the variation in flexural stiffness. In chapter five, I build upon these previous chapters by examining the correlated evolution of pectoral fin shape, mechanics, and mechanosensation across the wrasse phylogeny. Character mapping demonstrates that stiff wing-like pectoral fins evolved multiple times in this group. Afferent nerve activity was recorded during fin bending, and across multiple independent evolutions of stiff fins, the afferents of stiffer fins were more sensitive at lower displacement amplitudes. These results demonstrate mechanosensory tuning to fin mechanics, and a consistent pattern of correlated evolution. Finally, in chapter six, I evaluate the results of earlier chapters in a broader context by outlining the use of integrative data in the design of bioinspired robotic vehicles and summarizing future research directions that will rely on the collaboration between biologists and engineers.

CHAPTER ONE: INTRODUCTION

The origin of paired appendages and their subsequent diversification has shaped the functional capabilities of bilaterians. The evolution and adaptation of appendage morphology is fundamental for the ability of an animal to inhabit a new ecology (Losos, 1990; Wainwright, 1994; Norberg, 1994; Gillis and Blob, 2001; Higham et al., 2014), and conversely, the physical disparities between different habitats are just as likely to drive the evolution of the functional morphology of an animal (Dejours et al., 1987; Denny, 1993; Vogel, 1994; Gillis and Blob, 2001). Extreme examples of morphological adaptation can be seen in vertebrate and invertebrate water to land transitions and multiple secondary transitions of vertebrate clades back into water; morphological diversification has allowed animals to move in new ways, invade new niches, and led to rapid speciation and ecological specialization. More subtly, within a single clade of fish, interspecific variation of locomotor appendage biomechanics and behavior has led to differences in locomotor performance and efficiency (Walker and Westneat, 2000, 2002; Thorsen and Westneat, 2005), which ultimately shaped patterns of niche occupation (Fulton et al., 2001; Bellwood and Wainwright, 2001). In addition to the specialization of appendage biomechanics, the successful locomotion, and ultimately the survival of an animal, also relies on rapid sensory feedback and sensorimotor integration to help control and modulate the complex three-dimensional movements that enable animals to navigate unstable and unpredictable environments (Sainburg et al., 1995; Sane et al., 2007; Mongeau et al., 2015; Williams and Hale, 2015).

The locomotor appendages of animals perform dual roles as sensors and propulsors, and mechanosensory feedback has been shown to be critical to the motor performance of animals. Mechanosensory feedback modulates the motor output of a central pattern generator (CPG)

(Grillner and Zangger, 1984) to maintain normal movement in the event of an unexpected perturbation during locomotion (e.g. Grillner and Zangger, 1984; Giuliani and Smith, 1987; Sainberg et al., 1993). After the loss of sensory feedback, CPG driven movement occurs with atypical kinematics (e.g. Gettrup and Wilson, 1964; Polit and Bizzi, 1978, 1979; Peason and Wolf, 1987; Bosco and Poppele, 2001; Williams and Hale, 2015), reduced accuracy and adaptability (e.g. Grillner, 1975; Sanes et al., 1985; Nathan et al., 1986), and other sensory modalities, like vision, are needed to provide compensatory feedback on appendage movements (e.g. Sanes et al., 1985). The disruption of behavioral output due to the loss of sensory feedback ultimately arises from the impact mechanosensation has on the motor patterns of muscles actuating locomotor appendages. Therefore, it is not surprising that muscle activity patterns became more variable and that a consistent order of activation among a synergistic suite of muscles is not always retained after the loss of sensory feedback (Wilson and Gettrup, 1963; Székely et al., 1969; Kutsch 1974; Grillner and Zangger, 1984; Pearson and Wolf, 1987).

Similar to the appendages found in other animals, the fins of fish are also mechanosensitive. For example, the pectoral fins of the bluegill sunfish (*Lepomis macrochirus*) (Williams et al., 2013) and a catfish (*Pimelodus pictus*) (Hardy et al., 2016) and the adipose fin of a catfish (*Corydoras aeneus*) (Aiello et al., 2016) are all highly innervated and sensitive to bending. In complex environments, several species of fish have been observed using their pectoral fins as mechanosensors to aid in navigation (Sharma et al., 2009; Flammang and Lauder, 2013), which provides behavioral evidence to support the role of fins as sensors. Additionally, in hovering bluegills, the deafferentiation of the pectoral fin resulted in atypical kinematics, increased fin beat frequency, and decreased fin ray bending throughout the fin stroke (Williams and Hale, 2015). However, *it is still unclear how sensory feedback from the pectoral*

fins is used to modulate fin movement during pectoral fin-based swimming. Further, while locomotor appendages have been widely studied for both their role as propulsors and as sensors, it is clear that the sensory and motor components of locomotor appendages act as a single neuromechanical system. This suggests that a change in one component will elicit a change in the other, and vice versa. The well-documented diversification of limb biomechanics across taxa leads to the question of *how the sensory system evolves in coordination with locomotor appendage mechanics across taxa.*

In this thesis, I use the wrasses (Labridae) to take an integrative approach to studying the form, function, and evolution of the pectoral fin neuromechanical system. The wrasses are a morphologically and behaviorally diverse group of fishes with a well-resolved phylogeny (Westneat and Alfaro, 2005). Within wrasses, a continuum of pectoral fin-based swimming (labriform) behavior exists that ranges from the movement of broad low aspect ratio fins in an anterior-posterior direction for drag-based rowing to high aspect ratio wing-like fins moved dorso-ventrally for lift-based flapping (Blake, 1983; Walker and Westneat, 1997). Rowers generate thrust primarily during their posteriorly directed power stroke, generate greater thrust at slow speeds, and are more maneuverable in comparison to flappers (Walker and Westneat, 2000; 2002a;b). Conversely, flappers generate thrust during both the upstroke (adduction) and downstrokes (abduction) and generate greater thrust at high speeds and greater mechanical efficiency at all speeds in comparison to rowers (Walker and Westneat, 2000; 2002a;b). Within Labridae there is a relationship between swimming behavior and habitat use. Rowing species are typically found at greater depths close to the reef surface with calmer water flow patters and flappers are typically found at shallower depths away from the reef bottom with greater exposure to wave-swept environments (Fulton et al., 2001; Bellwood and Wainwright, 2001).

In chapter two of this thesis, I examine the impact of sensory feedback on labriform locomotion in fishes. The propulsive capabilities of a flexible membranous locomotor appendage are largely dependent on the kinematics and three-dimensional deformation of the system (Daniel and Combes, 2002). Fish are said to be able to finely control the position, movement, stiffness and curvature of individual fin rays (Geerlink and Videler, 1987; Standen and Lauder, 2005; Alben et al., 2007; Lauder et al., 2011). As the loss of mechanosensation significantly impairs the ability to complete complex and precise movements (Cooper et al., 1993), the fine control of fin ray movement needed to produce efficient propulsion suggests that sensory feedback will play a large role in producing the dynamic shape of a fin throughout its stroke. In this chapter, I use high-resolution three-dimensional fin reconstructions and electromyography to compare pectoral fin motor patterns and kinematics before and after the loss of sensory feedback in the Quoyi parrotfish, *Scarus quoyi*. In control fish, fin beat frequency and the duration of muscle activity relative to total cycle duration both increase with increasing swimming speed. While pectoral fin rhythmicity remained unchanged after the loss of sensory feedback, fin beat frequency increased and fish transitioned to the body-caudal fin gait at slower speeds. In general, the order of muscle activation during the fin stroke did not change after transection, but the activity in each muscle began earlier and stayed on longer after the loss of sensory feedback.

In chapter three, I examine the relationship between fin mechanics and swimming behavior in two closely related species of Labridae that employ divergent swimming behaviors, the flapping *Gomphosus varius* and the rowing *Halichoeres bivittatus*. The functional capabilities of flexible propulsive appendages are directly influenced by their mechanical properties. As these two species have diverged in their swimming capacity as well as their habitat, it raises questions of how fin mechanics relate to swimming behavior. To determine the

spatial distribution of flexural stiffness across the fin, I performed three-point bending tests at the center of the proximal, middle, and distal regions of four equally spaced fin rays. Pectoral fin ray flexural stiffness for the proximal regions of *G. varius* fin rays was nearly an order of magnitude stiffer than those of *H. bivittatus*. In both species, fin ray flexural stiffness decreased exponentially along the proximo-distal span of fin rays, and flexural stiffness decreased along the fin chord from the leading to trailing edge. I found that differences in the percentage of the fin occupied by skeleton rather than membrane likely contribute to interspecific differences in fin stiffness. The interspecific differences in fin stiffness provide a mechanical explanation for the differences in hydrodynamic capability associated with the different swimming behaviors employed by the flapping *G. varius* and the rowing *H. bivittatus*, which ultimately allow these species to utilize different habitats.

In chapter four, I build upon the work in chapter three by measuring the impact of morphology on the mechanics of fin rays. I examine the impact of fin ray morphology (The effective modulus in bending (E), second moment of area (I), segmentation and branching patterns) on stiffness in the flapping *G. varius* and the rowing *H. bivittatus*. While segmentation patterns and E were similar between species, measurements of I and the number of branch nodes were greater in *G. varius* in comparison to *H. bivittatus*. Further, I find that while most of the morphological variables quantified in this study correlate with fin ray flexural stiffness, variation in fin ray geometry (second moment of area) explains the majority of the variation in fin ray flexural stiffness.

In chapter five, I integrate biomechanics, neurobiology, and a new 340 species phylogeny to examine the correlated evolution of pectoral fin shape, mechanics, and mechanosensation across Labridae. Character mapping demonstrates that wing-like pectoral fins evolved multiple

times in this group, and enabled the identification of four independently evolving pairs of species where one species employs the plesieomorphic paddle-like fin and the other employs an independently evolved wing-like fin. Consistent with chapter 3, in each species pair, the wing-like fin used for flapping was always stiffer in comparison to the paddle-like fin used for rowing. Further, I found that in multiple independent evolutions of stiff fins there was concurrent evolution of increased mechanosensory afferent sensitivity to low amplitude bends, compared to the nerve responses of more flexible fins. Although evolution of limb morphology and movement has been deeply studied, this chapter demonstrates that mechanosensation is also rapidly changing during limb evolution. As mechanosensation is a universal feature of organisms, correlated changes in the mechanics and sensation of an appendage is likely a general feature during the evolution of a neuromechanical system.

Finally, in chapter six, I evaluate the results of earlier chapters in a broader evolutionary and applied context. I outline the importance of taking an integrative approach to understanding the evolution of animal locomotion and the different variables that need to be considered when investigating the effective locomotion of animals. I then apply this outline to set forth a new framework for the use of integrative animal locomotion data in the design of bioinspired robotic vehicles. While engineers often look to biology for inspiration on how animals have evolved solutions to problems experienced in robotic movement, biologists too must proactively engage with engineers to apply interdisciplinary approaches to help answer biological questions. Therefore, I end by summarizing future research directions that will rely on the collaboration between biologists and engineers.

CHAPTER 2: FIN RAY MECHANOSENSATION IMPACTS PECTORAL FIN KINEMATICS AND MOTOR PATTERNS DURING STEADY SWIMMING IN *SCARUS QUOYI*.

Abstract

Proprioceptive feedback, the sense of movement and position of one's body elements in space, is critical to the motor performance of many animals. The pectoral fins of fishes are highly innervated by the sensory system and perform dual roles as propulsors and sensors. Fish control the shape of their fins to maintain efficient propulsion in an unstable environment, which suggests that proprioceptive feedback is needed to complete these complex and precise movements. The objective of this study is to examine pectoral fin motor control across speeds and how the loss of proprioception impacts pectoral fin muscle activity patterns and kinematics during labriform swimming. We focus on a parrotfish, *Scarus quoyi*, which uses its pectoral fins for propulsion. In control trials, both fin beat frequency and the duration of muscle activity relative to total cycle duration increase with increasing swimming speed. After bilateral transections of all sensory nerves that innervate the pectoral fins, the loss of sensory feedback resulted in atypical fin movement, increased fin beat frequency, and a transition to the body-caudal fin gait at lower speeds. However, pectoral fin rhythmicity remained the same or increased after the loss of sensory feedback. In general, the order of muscle activation during the fin stroke did not change after transection. The duration of muscle activity relative to fin cycle duration increased and the lag between the onsets of activity among muscles decreased after transection, which resulted in the overlap of activity between antagonistic muscles. After the loss of sensory feedback, increase in the overlap of activity between antagonistic muscles may

enhance control and stability after sensory loss. These results indicate that proprioceptive feedback is critical for the performance of typical pectoral fin motor patterns and kinematics.

Introduction

The pectoral fins of fish, tetrapod forelimb homologs, perform dual roles as both sensors and motors. As motors, the pectoral fins are used during posture maintenance, maneuvering, braking (Higham et al., 2005), and serve as the primary source of propulsion in many species (Walker and Westneat, 1997; 2000; 2002a, b). As sensors, the pectoral fins respond to fin ray bending, and afferents encode fin ray movement, speed of movement, and position (Williams et al., 2013; Hardy et al., 2016; Aiello et al., 2017b). In bluegill sunfish (*Lepomis macrochirus*), pectoral fin sensory feedback is necessary for generating normal hovering behavior, and the loss of feedback results in atypical kinematics, higher fin beat frequencies, and reduced pectoral fin ray curvature throughout the fin stroke (Williams and Hale, 2015). Further, a behavioral analysis of bluegill sunfish navigating a complex environment found that fish use their pectoral fins to touch obstacles and, in the absence of other sensory modalities (e.g. lateral line and vision), the frequency of pectoral fin tapping increases (Flammang and Lauder, 2013). Together, these studies suggest that pectoral fin ray sensory feedback is important for the successful motor control of other swimming behaviors.

The propulsive capabilities of a flexible membranous appendage are largely dependent on their kinematics and three-dimensional deformation (Daniel and Combes, 2002). In comparison to rigid structures, the deformation of a flexible propulsor increases locomotor efficiency (Yamamoto et al., 1995; Zhu and Shoele, 2008; Young et al., 2009) and maneuverability (Tangorra et al., 2010; Lauder et al., 2011; Flammang et al., 2013). In fishes, muscles attaching

to the proximal portion of each fin ray allow independent control of their movement, and thus, the fin as a whole (Geerlink and Videler, 1987; Lauder et al., 2011). Fish are suggested to be capable of actively controlling the stiffness and curvature of individual fin rays through the differential activity of proximal antagonistic muscles (Geerlink and Videler, 1987; Alben et al., 2007; Lauder et al., 2011), and are capable of independently actuating adjacent fin rays (Standen and Lauder, 2005). As the loss of mechanosensation significantly impairs the ability to complete complex and precise movements in other animals (Cooper et al., 1993), the fine control of fin ray movement needed to produce efficient propulsion suggests that sensory feedback will play a large role in producing the dynamic shape of a fin during the fin stroke.

The loss of sensory feedback is detrimental to locomotor performance in vertebrates. Mechanosensory feedback is used to modulate central pattern generator (CPG) motor output (Grillner and Zangger, 1984) to maintain normal movement when an animal encounters an unexpected perturbation during locomotion (Grillner and Zangger, 1984; Giuliani and Smith, 1987; Sainburg et al., 1995). While typical limb rhythms are still observed after the loss of sensory feedback in vertebrates (Brown and Sherrington, 1912; Sherrington, 1913; Williams and Hale, 2015), CPG driven movement occurs with atypical kinematics (Polit and Bizzi, 1978; 1979; Bosco and Poppele, 2001; Williams and Hale, 2015) and reduced accuracy and adaptability (Grillner, 1975; Sanes et al., 1985; Nathan et al., 1986). For example, in human patients with large fiber neuropathy, multi-joint coordination and movement accuracy is significantly impaired (Sanes et al., 1985; Sainburg et al., 1993; Gordon et al., 1995; Sainburg et al., 1995), and other sensory modalities, like vision, are needed to provide compensatory feedback on limb movements (e.g. Sanes et al., 1985).

The loss of sensory feedback is also detrimental to locomotion in flying insects. Insect wings are another example of a flexible membranous appendage that rhythmically oscillates to locomote and maneuver. The wings of insects are outfitted with rapidly and slowly adapting mechanosensors (Dickinson, 1990a; 1990b; Dickerson et al., 2014) that exhibit firing properties similar to the sensors innervating the fins of fishes (Williams et al., 2013; Aiello et al., 2016; Hardy et al., 2016; Aiello et al., 2017b). Insect wing sensory feedback is important for the performance of normal wing kinematics and the maintenance of body stability in response to perturbations (Gettrup, 1966; Dickerson et al., 2014; Eberle et al., 2015). The loss of sensory feedback from insect wings results in the disruption of wing kinematics and motor patterns (Gettrup and Wilson, 1964; Pearson and Wolf, 1987) decreased wing beat frequency (Pearson and Wolf, 1987), reduced wing stroke amplitude (Frye, 2001), and the inability to regulate wing twisting (Gettrup, 1965; 1966), which, together, reduce lift and thrust production (Gettrup and Wilson, 1964; Gettrup, 1965; 1966; Heide, 1979).

The disruption of behavioral output due to the loss of sensory feedback ultimately arises from the impact mechanosensation has on the motor patterns of muscles actuating locomotor appendages. Surprisingly, there has been little work on the influence of proprioceptive feedback on the motor patterns of limbs in any system (Wilson, 1961; Pearson and Wolf, 1987; Thoumie and Do, 1996). In general, despite the presence of atypical kinematics, the basic motor pattern among limb muscles does not significantly change after the loss of sensory feedback (Székely et al., 1969; Hnik et al., 1982; Thoumie and Do, 1996). While most studies relied on simple qualitative analyses of EMG data, several authors note that the onset, amplitude, and duration of muscle activity patterns became more variable and that the consistent order of activation among a synergistic suite of muscles is not always retained after the loss of sensory feedback (Székely et

al., 1969; Grillner and Zangger, 1984). Studies in tetrapods also note that the activity in some muscles increases in both intensity and duration after the loss of sensory feedback (Székely et al., 1969; Grillner and Zangger, 1975; Perret and Cabelguen, 1976; 1980). Similar results have been found in other systems. For example, after the loss of sensory feedback form the wings of insects, the activity in elevator muscles increased in intensity and became more variable (Wilson and Gettrup, 1963; Pearson and Wolf, 1987), and elevators fired later in the wing phase and overlapped with the subsequent firing of depressors (Pearson and Wolf, 1987).

The few studies on fish fin mechanosensation and motor control provide a foundation and, as limb mechanosensation and motor control are both well studied in tetrapods and insects, begin to fill a major gap in our understanding of sensorimotor control in animals. Here, we build upon this foundation by studying pectoral fin motor control and the role of pectoral fin ray mechanosensory feedback during labriform locomotion. As only two previous studies have recorded the motor patterns responsible for pectoral fin movement during labriform swimming (Drucker and Jensen, 1997; Westneat and Walker, 1997), the first objective of this study was to describe pectoral fin motor control and address fundamental questions about the system, in particular: What is the order of onset among synergistic muscles (adductor vs. abductor groups)? How do muscle activity onset order, onset timing, and duration change across speeds? Given the theoretical basis for fin stiffening through the co-contraction of antagonistic muscles (Alben et al., 2007) and that the propulsive capability of a flexible propuslor increases with increasing propulsor stiffness (Tangorra et al., 2010), is co-contraction of antagonistic muscles observed during steady-state pectoral fin-based swimming and, if so, does duration of co-contraction increase with increasing speed? To answer these questions, electromyograms of the six major fin muscles and

synchronized three-dimensional kinematics were recorded from the pectoral fin of the Quoyi parrotfish (*Scarus quoyi*) at a range of swimming speeds.

The second objective of this study is to examine how the loss of proprioception impacts pectoral fin muscle activity patterns and kinematics during labriform swimming. Based on work in other systems, we hypothesized that, after the loss of sensory feedback, fin beat frequency would increase, fin kinematics and muscle activity patterns would become more variable, pectoral fin ray curvature would decrease, but rhythmicity would not change. To test these hypotheses, we performed bilateral transections of all sensory nerves that innervate the pectoral fins of the same parrotfish used in the control experiments and examined the effects on three dimensional fin kinematics and the activity patterns of the muscles used to actuate the fin.

This study examines the effects of sensory loss on the three dimensional kinematics and motor activity patterns during swimming, and is one of the few to examine pectoral fin kinematics and muscle activity patterns during labriform swimming (see Drucker and Jensen, 1997; Westneat and Walker, 1997). Different from previous sensory afferent transection studies, we sample nearly the entire suite of muscles responsible for actuating a given appendage, which will provide a more holistic view of how sensory feedback impacts the complex interaction among the firing patterns of different muscles. In addition to building our understanding of sensorimotor control, principles from this study can be incorporated into control algorithms to be used in the development of sensory-enabled, bioinspired autonomous robotic vehicles.

Materials and methods

Fish specimens and experimental overview. Six parrotfish, *Scarus quoyi*, were used in this study (standard length: 11.5 – 15.5 cm; average ± stdev = 13.15 ± 1.67 cm). Parrotfish were obtained commercially and housed in aquaria equipped with recirculating water filters. Water temperature was maintained at ~23°C and the fish were exposed to a 12 hour light/dark cycle. Before each experiment, each fish was anesthetized in a solution of MS-222 (0.25 g l^{-1}). Bilateral incisions were made through the skin and the connective tissue overlaying the medial side of the most proximal portion of the left and right pectoral fins to expose the sensory nerves innervating the pectoral fin rays. The performance of an incision prior to the control swimming ensured that all differences in kinematics and motor patterns between trials before and after the loss of sensory feedback (nerve transection) were due to the loss of sensory feedback and not from the effects of surgery. A single bipolar electrode was then inserted into each of the muscles actuating the left pectoral fin. Fish were allowed to recover, placed in a flow tank, and then swam at three different speeds (1, 2, and 3 BL/s). After each fish completed its control swimming trials, the fish was lightly anesthetized and the already exposed sensory nerves were transected. The fish was allowed to recover and was then placed back in to the flow tank to repeat the swimming procedure at a single speed of 2 BL/s. Finally, the speed at which each fish transitioned from the pectoral fin to body-caudal-fin (BCF) gait was also measured before and after afferent nerve transection. Flow speed was increased in a step-wise manner where speed was increased by 0.5 BL/s, stabilized for one minute, and increased again 0.5 BL/s. Flow speed was increased in this manner until the fish transitioned to the BCF gait. All experimental procedures were carried out under University of Chicago Institutional Animal Care and Use Committee guidelines (protocol 72365 to M.W.W.; protocol 71589 to M.E.H.)

Surgical procedures and electrode implantation. Surgery and electromyography (EMG) electrode implantation followed published methods (Westneat and Walker, 1997). Electrodes were made using 0.005 mm diameter insulated stainless steel wire (California Fine Wire, Grover Beach, CA USA). After approximately 0.5 mm of insulation was stripped from the tip of each wire, the wire was fed through a 26 gauge needle and formed into a twist hook (Loeb and Gans, 1986). A single electrode was placed in six different muscles (three lateral muscles: arrector ventralis, abductor profundus, abductor superficialis; three medial muscles: arrector dorsalis, adductor profundus, adductor superficialis). Hot glue was then used to bind the six wires together into a single cable, which was subsequently run dorsally and sutured to the base of the first ray of the dorsal fin. These six electrodes were left in throughout the duration of the experiment and were the same electrodes used for EMG recordings after nerve transection. Upon completion of the experiment, animals were euthanized in a high concentration of MS-222 and electrode implantation was confirmed post mortem.

Data acquisition. EMG and kinematic recordings took place after the fish had recovered for approximately 1-2 hours after surgery. EMG signals were amplified by a factor of 10,000, bandpass filtered from 30 Hz to 6kHz, and notch filtered at 60 Hz using a Grass amplifier (Model 15LT, Grass Technologies, Astro-MED Inc, West Warwick, RI, USA). Signals were then acquired and saved to a computer at 5,000 Hz using the PolyVIEW16 software (Grass Technologies) after being passed through a Grass PVA-16 A/D converter (Grass Technologies).

EMG recordings were collected while each fish was filmed swimming in a flow tank (Vogel and Labarbera, 1978) with a total volume of 360 L and working volume dimensions of 30 cm x 30 cm x 60 cm. Prior to transection, each control fish swam at three different speeds (1, 2,

and 3 BL/s), and after transection each fish swam at 2 BLs^{-1}. Fish were filmed at 500 frames s^{-1} with three synchronized Photron high-speed digital video cameras at 1024 x 1024 pixel spatial resolution (Models: FASTCAM APX-RS, FASTCAM SA7, and Mini UX 100; Photron, San Diego, CA, USA). Two cameras with lateral views were placed with slightly offset angles and the third camera was placed at an equal distance from the tank and filmed the ventral view of the fish using a mirror placed below the flow tank working area at an angle of 45 degrees. EMG and video data were synchronized with the application of a timestamp on the EMG record.

Electromyography and kinematic analysis. For each trial, video and EMG data were analyzed for five continuous fin stroke cycles. Basic kinematic data (abduction onset and duration, adduction onset and duration, and the lag time between consecutive fin strokes) was collected for each fin stroke. EMG data were analyzed using a custom MATLAB (MathWorks, Natick, MA, USA) routine (Jose Iriarte-Diaz, University of Illinois-Chicago). For each EMG burst, the onset (EMG_{on}), offset (EMG_{off}), duration (EMG_{dur} = EMG_{off} - EMG_{on}), time of peak amplitude (EMG_{peak}), and rectified integrated area (RIA) were calculated. Variables were calculated in absolute time (seconds) and converted to percentage of the fin stroke cycle relative to the start of pectoral fin abduction.

In a subset of the individuals (N=4; standard length: 12.2 – 15.5 cm; average ± stdev = 13.80 ± 1.69 cm), three-dimensional pectoral fin kinematics were digitized using the StereoMorph package (Olsen and Westneat, 2015) in R (R Development Core Team, 2011). In at least two views for every other video frame, the tip and base of the leading edge fin ray were digitized as landmarks and a curve (described by 50 evenly spaced points or semilandmarks) was fit along the length of the leading edge fin ray. Several body landmarks were also digitized in at

least two views for every ten video frames: the rostral tip of the dorsal beak, the left eye, the base of the left and right pelvic fins, the most rostral attachment of the anal fin, the most rostral intersection of the left and right operculum, and several midline natural skin coloration markings that were unique to each fish. Custom code (Aaron Olsen, Brown University) was then used to track several variables over the length of each fin stroke: the fin angle relative to the fully adducted position, leading edge fin ray curvature, and the three-dimensional path of the leading edge fin ray tip.

Statistical analyses were performed on the data in R 3.2.1 (R Development Core Team, 2011) and JMP 9.0.1 (SAS, Cary, NC, USA). The rhythmicity of the fin stroke cycle (relative variance in the cycle period) was calculated as the coefficient of variation (Ross et al., 2013). The coefficient of variation (CV) was calculated as CV = (s/m)*100 where s = the standard deviation of the sample and m = the mean of the sample (Sokal and Braumann, 1980). The CV was also calculated for fin beat frequency, EMGon, EMGdur, EMGpeak, and RIA before and after the loss of sensory feedback (transection) as a standardized measure of variation in the data. Student's *t*-tests were also used to test for significant differences between the control and transection trials for several variables: fin beat frequency, EMG_{on}, EMG_{dur}, EMGpeak, RIA, and the CV of fin stroke duration, EMG_{on}, EMG_{dur}, EMG_{peak}, and RIA.

Results

Fin cycle variables

The pectoral fin cycle can be divided into three main components: the downstroke during abduction, the upstroke during adduction, and a transition period where the fin is held against the body wall before the start of the subsequent fin stroke. In both control and transection trials, the proportions of the fin stroke devoted to abduction and adduction are similar across speeds (Table 2.1). In control trials, the abduction and adduction cycles ranged from 45.61 ± 10.78 – 47.39 ± 5.13 and 44.45 ± 9.10 – 46.36 ± 4.68 % fin cycle, respectively. After transection, the abduction and adduction cycles ranged from 45.12 ± 4.10 – 51.68 ± 8.11 and 45.58 ± 6.90 – 48.70 ± 4.35 % fin cycle, respectively. There were no significant differences in the proportion of the fin cycle dedicated to either abduction or adduction between control and transected trials at any speed (p>0.05). The proportion of the fin stroke dedicated to the transition period between subsequent fin strokes decreased with increasing swimming speed. In control trials, transition period decreased from 9.47 ± 10.37 to 6.49 ± 3.45 % fin cycle at 1 and 3 BL/s, respectively. In transection trials, the transition period decreased from 5.14 ± 3.10 to 2.74 ± 2.01 % fin cycle at 1 and 3 BL/s,

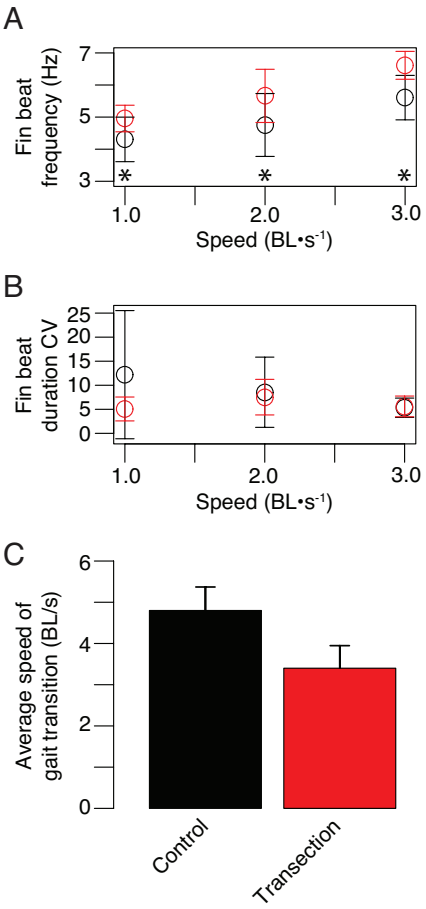

Figure 2.1. Pectoral fin kinematics before and after the loss of sensory feedback.
(A) Fin beat frequency increases with increasing swimming speed, and frequency is significantly greater after the loss of sensory feedback in comparison to control trials. (B) There is no relationship between the coefficient of variation (CV) for fin beat duration and speed, and duration CV does not change after the loss of sensory feedback. (C) In control trials, the transition between the pectoral fin and the body-caudal-fin gait occurs between 4 and 5 BLs-1, and occurs at a significantly slower speed after the loss of sensory feedback.

respectively (Table 2.1). At all three speeds, the average duration of the transition period was shorter in the transection trials than in the control trials, and these differences were significant at both 2 and 3 BL/s (p<0.05).

Fin beat frequency and fin beat rhythmicity were measured across all three speeds, and the speed at which each fish transitioned from the pectoral to body-caudal-fin (BCF) gait was also recorded. In control and transection trials, fin beat frequency increased with increasing swimming speed (control trials: r^2=0.306, slope = 0.652, F-value=36.08, p=<0.0001; transection trials: r^2=0.417, slope = 0.799, F-value=48.63, p=<0.0001), and ranged from 4.31 ± 0.69 to 5.61 ± 0.69 and 4.96 ± 0.41 to 6.61 ± 0.43 in control and transection trials, respectively (Table 2.1; Figure 2.1a). At each speed, the fin beat frequency was significantly greater in transection trials in comparison to control trials (p<0.0001). Fin beat rhythmicity was measured by calculating the coefficient of variation (CV) of fin beat duration (Table 2.1; Figure 2.1b). In control trials, average CV of fin beat duration was 12.20 ± 12.23, 8.55 ± 7.30, and 5.32 ± 2.01 at 1, 2, and 3 BL/s, respectively. A regression analysis revealed that there was no significant relationship between the CV of fin beat duration and swimming speed (r^2 = 0.1065, F-value = 1.6688, p = 0.2173). There was no trend between the CV of fin beat duration and swimming speed in transection trials, and CV was 5.07 ± 2.48, 7.52 ± 3.70, and 5.60 ± 2.15 at 1, 2, and 3 BL/s, respectively. There were no significant differences in fin beat rhythmicity between control and transection trials at any speed (p>0.05). Finally, the average speed at which the transition between the pectoral fin and BCF gait occurred was significantly slower in transection trials in comparison to control trials (control = 4.8 ± 0.57 BL/s; transection = 3.4 ± 0.55 BL/s; p=0.004; Figure 2.1c; Table S2.1).

Table 2.1. Control and transection summary kinematics across speeds.

		Control					
Speed		**% ABD.**	**% ADD.**	**% Tr.**	**Frequency**	**Dur. CV**	**N**
1	Avg ± sd.	46.18 ± 10.78	44.45 ± 9.10	9.37 ± 10.37	4.31 ± 0.69	12.20 ± 13.32	5
	p	0.497	0.243	0.051	0.0001	0.273	
2	Avg ± sd.	45.61 ± 5.32	46.36 ± 4.68	8.03 ± 3.78	4.75 ± 0.98	8.55 ± 7.30	6
	p	0.684	0.044	0.040	0.0001	0.766	
3	Avg ± sd.	47.39 ± 5.13	46.12 ± 4.74	6.49 ± 3.45	5.61 ± 0.69	5.32 ± 2.01	5
	p	0.061	0.785	0.003	0.0001	0.875	
		Transection					
1	Avg ± sd.	47.85 ± 6.33	47.01 ± 6.43	5.14 ± 3.10	4.96 ± 0.41	5.07 ± 2.48	5
2	Avg ± sd.	45.12 ± 4.10	48.70 ± 4.35	6.18 ± 3.24	5.66 ± 0.83	7.53 ± 3.70	6
3	Avg ± sd.	51.68 ± 8.11	45.58 ± 6.90	2.74 ± 2.01	6.61 ± 0.43	5.60 ± 2.15	2

Speed is presented in BLs^{-1}.
N=2 at 3 BLs^{-1} in the transection group because the other individuals transition from the pectoral fin to body-caudal-fin gait at this speed.

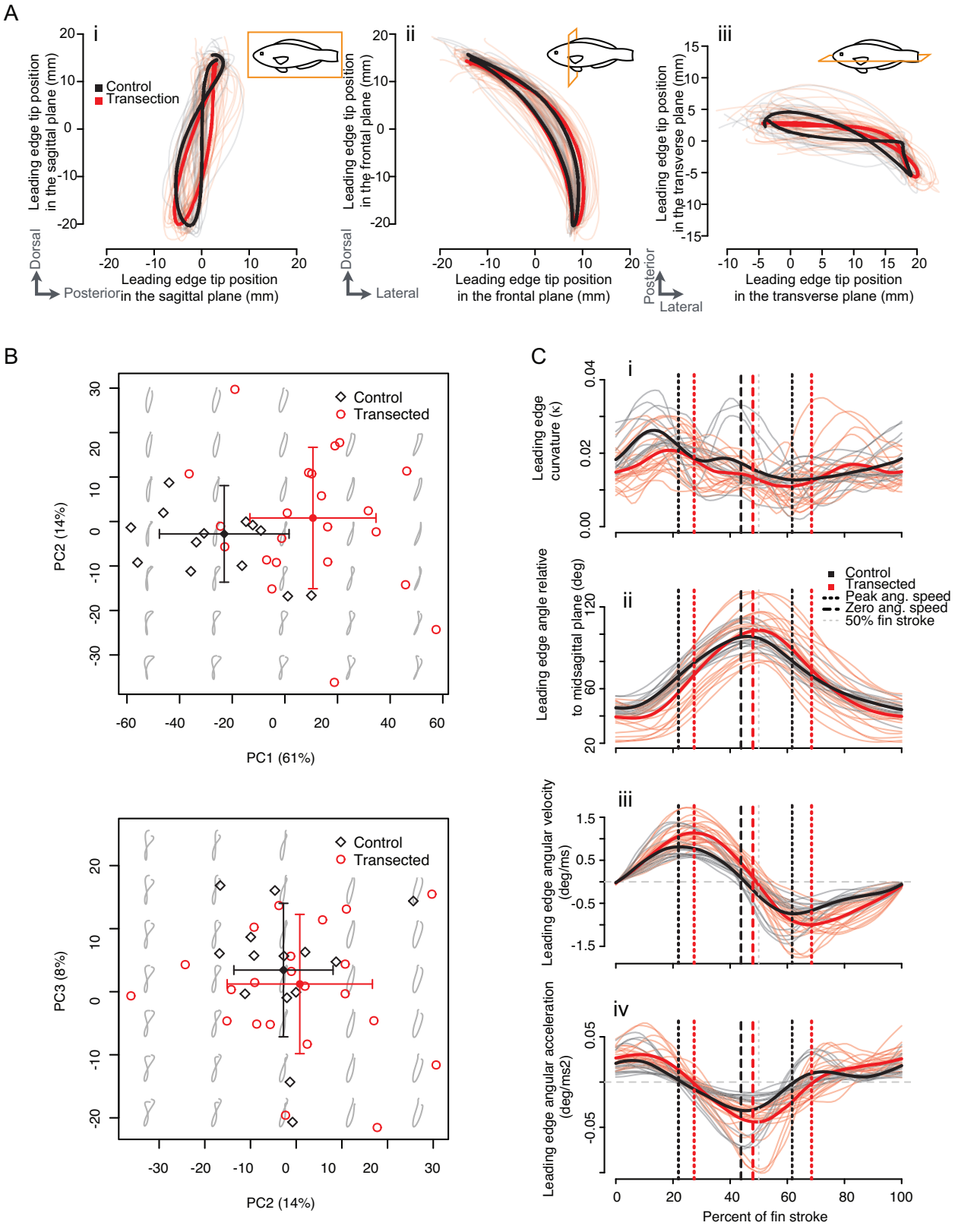

Figure 2.2 continued-on page 21.

Figure 2.2. Leading edge pectoral fin ray kinematics at $2BLs^{-1}$.
(A) The tip of the leading edge fin ray was traced in control (black) and transection (red) trials. In control trials, fin tip trajectory exhibits a figure-eight pattern, and after transection, the trajectory resembles more of a teardrop shape. (B) A PCA of the three-dimensional leading edge tip trajectory (only the saggital view is projected in 'morphospace'); a significant difference in PC1 scores was found between the control and transection groups (p = 0.000359). This suggests that the A-P axis of the fin stroke is the major axis of variation as well as the axis that separates control from transection strokes. (C) The leading edge fin ray curvature (i), fin stroke amplitude (ii), angular velocity (iii), and angular acceleration (iv) are similar throughout the fin stroke between control and transection trials.

Three-dimensional kinematics

An analysis of three-dimensional pectoral fin kinematics was also conducted before and after the loss sensory feedback at a speed of $2BLs^{-1}$. A three-dimensional outline of the leading edge fin ray tip reveals a figure-eight pattern when viewed laterally (Figure 2.2a). The leading edge tip kinematics of deafferented fins appears more like a tear-drop shape (Figure 2.2b). The amplitude of the fin stroke was measured as the angle between the body and the leading edge fin ray ranged between zero and 80 degrees, and there was no significant difference in fin angle between control and transection trials (Figure 2.2c, d). Leading edge fin ray curvature was measured throughout the fin stroke and has two main peaks that occur at approximately the middle of the downstroke and the middle of the upstroke, respectively. Curvature values in both control and transection trials ranged from 0 to 0.02 during the downstroke and peaked at approximately 0.025 during the upstroke (Figure 2.2c, d; Table S2.2).

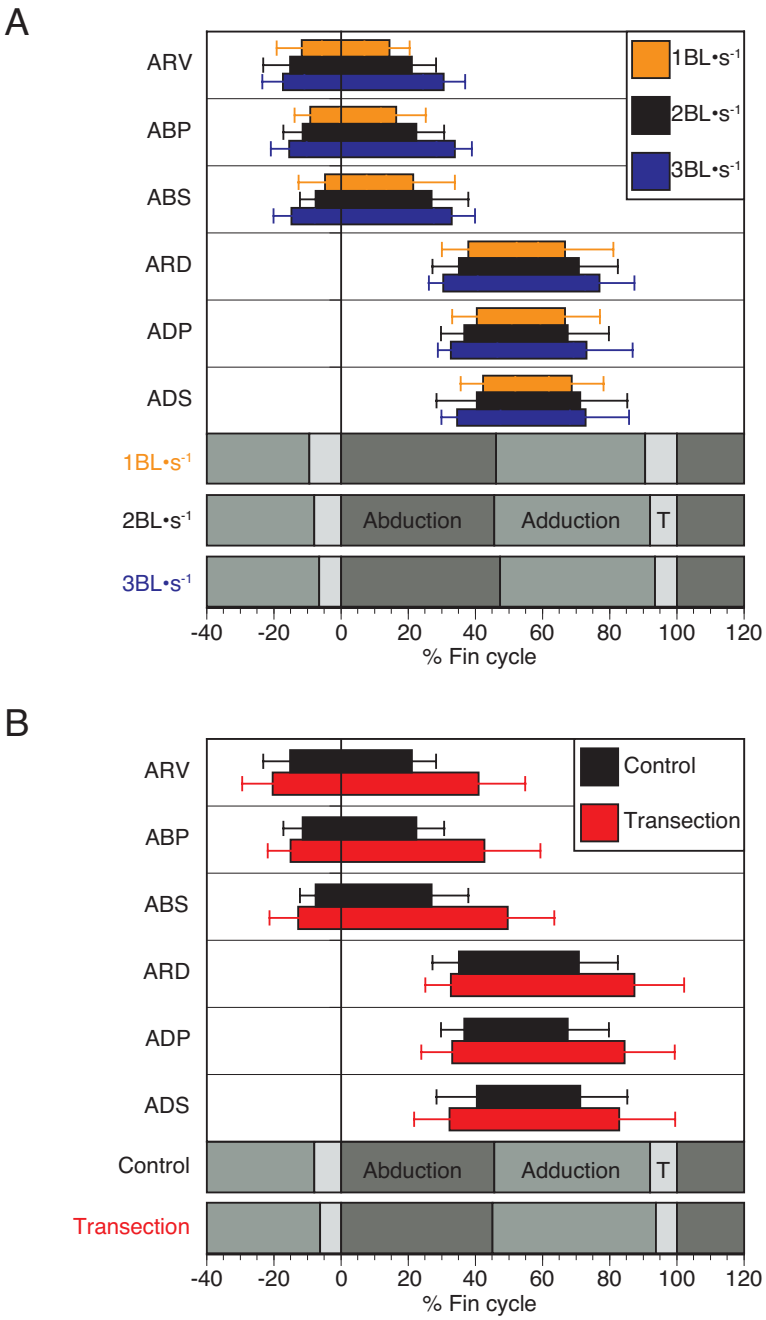

Figure 2.3. Pectoral fin motor patterns across speeds.
(A) The activity patterns for each muscle change with speed in control trials. In transection trials (B), the onset of activity is earlier and the duration is prolonged in comparison to control activity patterns at the same speed.

Muscle activity patterns – control trials

Muscle activity onset, duration, and time of peak amplitude were calculated for six muscles that actuate the pectoral fin. Briefly, activity in the three muscles of the abductor complex, arrector ventralis (ARV), abductor profundus (ABP), and abductor superficialis (ABS) onset at similar times (no greater than 7.54% fin cycle between the onset of any muscles in this group), but were always activated in the consistent order of ARV, ABP, and ABS (Figure 2.3a; Table S2.3). For all three muscles in the abductor complex, activity began before fin abduction; at 1 BL/s, ARV onset at -11.75 ± 7.36 % fin cycle and ABS onset at -4.75 ± 7.95 % fin cycle. Similar trends were found for the adductor muscle complex (Figure 2.3a; Table S2.3). The three muscles of adductor complex consistently activated in the following order: ARD, ADP, and ADS (Figure 3a). At 1BL/s, ARD and ADS onset approximately 10% and 4% fin cycle, respectively, before the start of adduction. Activity in all three muscles of both the abductor and adductor complex began earlier and remained active longer with increasing swimming speed (Figure 2.3; Table S2.4). Similarly, the rectified integrated area (RIA) of the activity for each muscle increased with increasing speed (Figure S2.1; Table S2.3, S2.4). Finally, variation in the onset and duration of muscle activity was measured by calculating the coefficient of variation (CV). In general, for both activity onset and duration across all muscles, CV decreased with increasing speed (Figure S2.2, Table S2.3).

The time of peak EMG amplitude showed a slightly different trend than onset order for the abductor complex, and there was no consistent trend in time of peak amplitude for the adductor complex (Figure S2.1, Table S2.3, S2.4). On average, the time of peak amplitude for each muscle in the abductor complex was in the following order: ABS, ARV, ABP. Different than activity onset, the time of peak amplitude for ARV and ADP became later in the fin cycle

with increasing swimming speed, but there was no trend between time of peak amplitude and speed for ABS (Table S2.4). For the adductor complex, the time of peak amplitude was nearly coincident for each muscle, and, on average, ranged from 51.51 ± 7.82 to 56.22 ± 9.65 % fin cycle among all three muscles and across all three speeds.

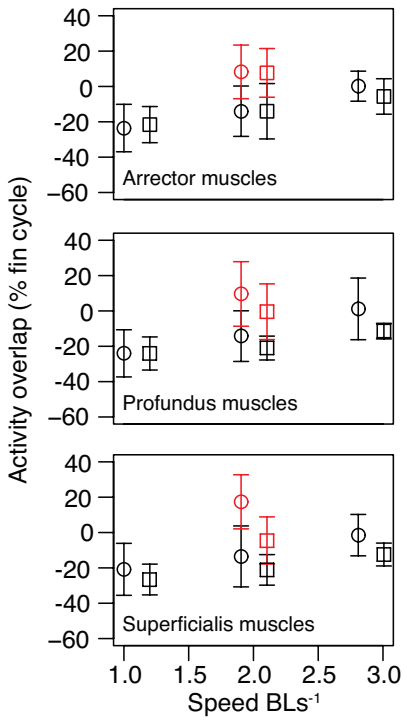

Figure 2.4. The relative overlap in activity between pairs of antagonistic muscles across speeds and between control and transection trials. Overlap in activity between antagonistic muscles is negative at speeds of 1 and 2 BLs^{-1}, and averages a positive number at $3BLs^{-1}$ for the arrector and profundus paris around the time of peak abduction (circles). A similar trend is observed across the period of peak adduction (squares), but the average overlap across peak adduction is always negative across all three speeds. After the loss of sensory feedback, activity overlap between antagonistic muscles significantly increases (red). Black represents control trials, red represents transection trials, circles represent overlap spanning the period of peak abduction, and squares represent overlap spanning the period of peak adduction.

The overlap in activity between antagonistic muscle pairs (ARV – ARD, ABP – ADP, and ABS – ADS) was calculated across the midpoint of the fin cycle between the end of abduction and the start of adduction and also between consecutive strokes during the transition period. For each pair, on average, there is no overlap in activity between antagonistic muscles at speeds of 1 and 2 BLs^{-1} (Figure 2.4; Table S2.5). For the arrector and profundus muscle pairs, there is, on average, 0.12 ± 8.49 and 1.13 ± 17. 44 % fin cycle overlap, respectively, at a speed of 3 BLs^{-1}. The overlap in activity between antagonistic muscles at the transition between consecutive fin beats showed similar trends to those seen at the midpoint of each fin beat, but was lower in magnitude.

Muscle activity patterns – transection trials

Muscle activity patterns were also recorded at a speed of 2 BLs^{-1} after pectoral fin afferents were transected (Figure 3b; Table S3). For the abductor complex, the order of activity onset among the

three muscles was consistent with control trials. For the adductor complex, the average activity onset was nearly coincident among the three muscles and was 32.74 ± 7.69, 33.12 ± 9.23, and 32.20 ± 10.55 % fin cycle for ARD, ADP, and ADS, respectively. In comparison to control trials, the loss of sensory feedback resulted in earlier average activity onset, later, average offset,, and thus an overall increase in activity duration (Figure 2.3b, Table S2.3). Differences in activity offset time and duration between control and transection trials were significant ($p<0.05$) for all six muscles, and activity onset was significantly ($p<0.05$) earlier in the fin cycle in transection trials in comparison to control trials for ARV, ABP, ABS, and ADS. The time of peak EMG amplitude was only significantly different for two of six muscles between control and transection trials (Figure S2.1; Table S2.3); the average time of peak amplitude occurred earlier after transection in the ARV muscle ($p = 0.009$) and later for the ABS ($p = 0.018$). In transection trials, the average RIA for each muscle was approximately double the RIA of control trials, and these differences were significant for each muscle ($p<0.01$; Figure S2.1b; Table S2.3). The overlap in activity between antagonistic muscles also significantly increased for all three antagonistic pairs ($p<0.0001$; Figure 2.4; Table S2.5). Prior to transection, control trials showed no overlap at 2BL/s; after transection, overlap between antagonists averaged 8.24 ± 15.18, 9.61 ± 18.26, and 17.38 ± 15.31 % fin cycle for the arrector, profundus, and superficialis pairs, respectively. Similar patterns were found for the overlap in activity occurring between subsequent fin beats (Table S2.5). Finally, the variation surrounding the onset and duration of activity in each muscle was on average greater for seven of twelve comparisons after transection, but there were never any significant differences in onset or duration CV between control and transection trials ($p>0.05$; Table S2.3).

Discussion

Control kinematic data and its comparison to other underwater flyers

The kinematics of *S. quoyi* resembled kinematic data that have previously been collected in three other species of labriform swimmers. *S. quoyi* exclusively uses its pectoral fins for propulsion between speeds of approximately 1 and 5 BLs^{-1} and fin beat frequency increased with increasing swimming speed (Figure 2.1a), which is similar to trends in the bird wrasse, *Gomphosus varius*, (Walker and Westneat, 1997). The average fin beat frequency was higher for any given speed in *S. quoyi* in comparison to either *G. varius* or the shiner seaperch (*Cymatogaster aggregata*), which peak at approximately 4.2 and 5 Hz, respectively (Webb, 1973; Walker and Westneat, 1997). In *S. quoyi*, the proportion of the fin cycle occupied by adduction and abduction were nearly equal (~45% each) and the proportion of both slightly increased with increasing speed as the transition period (referred to as refractory period by Webb, 1973) decreased with increasing speed (Table 2.1). While the seaperch exhibits a similar pattern of a decreasing transition period with increasing speed (Webb, 1973), the proportion of the fin cycle occupied in the bird wrasse was more variable, ranging from 23-46 %, and a transition period was not mentioned (Walker and Westnear, 1997).

Interspecific differences exist in the speed at which the transition from the pectoral fin to the BCF gait occurs. Three groups of different sized striped surfperch (*Embiotoca lateralis*), transition to a BCF-based "burst-and-coast" swimming mode between 1.8 and 3.4 SLs^{-1} (Drucker and Jensen, 1996). Webb (1973) reports that pectoral fin swimming in the shiner seaperch was augmented by caudal fin beats above speeds of 3.4 TLs^{-1}, and the bird wrasse transitions to a BCF gait between 6-7 TLs^{-1} (Walker and Westneat, 1997). Differently, *S. quoyi* transitions between speeds of 4 and 5.5 TLs^{-1} from an entirely pectoral-fin based gait to the burst-and-coast

swimming mode, where a short burst of BCF swimming occurs and the pectoral fins are redeployed as the fish drifts backwards in the flow. While the bird wrasse and *S. quoyi* belong to the same family, Labridae, these species each belong to an independent evolution of the lift-based flapping swimming behavior (Aiello et al., 2017b), and should not be expected to have identical kinematic parameters. Further, Drucker and Jensen (1996) note a complex relationship between swimming speed, stroke amplitude, and fin beat frequency as well as the effects body size can have on the relationship between these variables and speed. Additional work will need to be done to more accurately compare interspecific results and interpret the hydrodynamic impact of different kinematic variables in fish of different body sizes.

Interspecific comparison of pectoral fin motor control

EMG were recorded from the six major muscles that control pectoral fin movement in *S. quoyi*. In general, alternating activity of the abductor and adductor complexes produced rhythmic pectoral fin oscillation. The order of activation in the abductor group always occurred ARV, ABP, and then ABS (Figure 2.3). The onset of activity in each muscle always preceded the start of abduction and began during the transition phase of the fin cycle at slow speeds and became increasing earlier in the fin cycle with increasing speed so that at $3BLs^{-1}$, all three muscles were likely performing negative work before the start of abduction. The three muscles of the adductor group followed the consistent onset order of ARD, ADP, and then ADS. The onset of activity in each adductor muscle always preceded the start of adduction, and, similar to the abductor group, onset earlier in the fin cycle with increasing speed, which again implies the performance of negative work. Finally, the duration of activity and the RIA of all six muscles had a significant and positive relationship with swimming speed (Table S2.4).

Comparison of motor patterns between *S. quoyi* and the confamilial bird wrasse (*Gomphosus varius*) reveals several similarities and differences. Similar to the results presented here, the activity patterns of the same six muscles in the bird wrasse yield increasing RIA with increasing speed, the onset of ARV and ARD prior to the onset of other muscles in the abductor and adductor groups, respectively, and the cessation of activity in the all three abductors and all three adductors occurred before their respective portions of the fin cycle were complete (Westneat and Walker, 1997). Different from *S. quoyi*, the absolute muscle activity duration of all six muscles decreased with increasing speed and led to a constant duty factor (duration expressed in % fin cycle) across speeds in the bird wrasse. Further, in the bird wrasse, the onset time of all six muscles, when expressed as a percentage of the fin cycle, remained relative constant across speeds, the abductor muscles typically fired after the time of peak adduction, and the adductor muscles typically fired after the time of peak abduction (Westneat and Walker, 1997). In the bird wrasse, no muscles examined exhibited any activity while the fin was held against the side of the body and protracted. The presence of ARV activity occurring before the start of abduction while the pectoral fin is slightly protracted, could suggest that ARV in *S. quoyi* has additional functions.

The differences in motor patterns between *S. quoyi* and *G. varius* likely represent the evolution of different strategies to increase force generation with increasing speed. In the bird wrasse, the onset of activity in all muscles relative to the start of the fin cycle and the duty factor of each muscle remained consistent across speed, leading to the suggestion that the increased force requirement needed as speed increases is met by recruitment of additional muscle fibers (Westneat and Walker, 1997). In *S. quoyi*, the RIA of each muscle increases with increasing speed (Figure S2.1), which also suggests increased muscle recruitment with increasing speed. In

S. quoyi, the onset of activity in each muscle becomes earlier with increasing swimming speed (Figure 2.3a; Table S2.4). The likely active lengthening that occurs in the abductors and adductors before the start of abdudction and adduction, respectively, and that the duration of active lengthening increases with increasing speed suggests these muscles are undergoing active stretch-shorten cycles, which are known to increase the force generation of a muscle (Katz, 1939; Abbott and Aubert, 1952). Stretch-shorten cycles have been observed in muscles actuating the fins of other fish (Flammang and Lauder, 2008; Aiello et al., 2014) and are common feature of tetrapod locomotion (Nelson and Jayne, 2001; Gillis and Biewener, 2002; Daley and Biewener, 2003; Aiello et al., 2013). We suggest, in addition to increasing muscle fiber recruitment, that *S. quoyi* also actively lengthens (eccentrically contracts) its muscles prior to the start of abduction and adduction as an additional means of increasing force generation. Finally, we find that the time of peak muscle activity is generally constant across speeds in *S. quoyi* (Figure S2.1; Table S2.4). The consistency in peak activity time across speeds suggests that the architecture of each muscle (the line of action) is ideally positioned at a certain point in the fin cycle to achieve maximum mechanical advantage.

The impact of sensory feedback

Kinematics

The loss of sensory feedback impacts the kinematic variables differently. The pectoral fin continued to beat rhythmically at slow swimming speeds (Figure 2.1). In comparison to control trials, there was no change in the amplitude of the fin beat at $2BLs^{-1}$, but fin beat frequency increased significantly across all three speeds examined (Figure 2.1). The pectoral fin of flapping fish, when viewed laterally, produces a figure-eight pattern with its tip (Webb, 1973; Walker and

Westneat, 1997), and this is also seen in the control trials of this study. After the loss of sensory feedback, the figure eight pattern is generally lost and the leading edge path resembles a teardrop shape with a small twist near peak adduction (Figure 2.2). Finally, the loss of sensory feedback results in the transition from the pectoral fin to the BCF gait occurring a significantly slower speed (Figure 2.1c).

Changes in limb amplitude after the loss of sensory feedback have been reported in other systems. Pectoral fin ray deafferentiation in the bluegill during hovering resulted in a reduction of fin beat amplitude by increasing the minimum angle of abduction (Williams and Hale, 2015), which is consistent with results of decreased limb excursion in tetrapods following the loss of sensory feedback (Gray and Lissmann, 1940; Miller et al., 1975; Goldberger, 1988). In this study, *S. quoyi* maintained normal fin beat angles after the loss of sensory feedback (Figure 2.2). While a more splayed fin posture may lead to more stability, decreased fin beat amplitude would result in decreased thrust production, which would inhibit the fish from keeping up with the speed of water flow. Alternatively, hovering is a behavior that functions to maintain the stability and the position of a fish in a water column. Other underwater flyers have been reported to not utilize a hovering behavior (Walker and Westneat, 1997), and pectoral fin-based hovering was never observed in *S. quoyi*. The differences in pectoral fin function and behavioral repertoire between bluegills and *S. quoyi* suggests that pectoral fin ray sensory feedback impacts these behaviors differently.

The loss of sensory feedback impacts frequency of limb movement differently across systems. In the locust, the loss of sensory feedback from the wing results in decreased wing beat frequency (Pearson and Wolf, 1987; Wolf and Pearson, 1987). In tetrapods, bilateral deafferentation of limbs reduced the frequency of limb movements in a newt (Székely et al.,

1969) and reduced the frequency (Bickel, 1897) and coordination of limb movements in a frog (Hering, 1983). In contrast, another study found that deafferentation of neonatal rats resulted in increased hindlimb frequency (Yakhnitsa et al., 1987). Finally, in the most similar system to this study, deafferentation of the bluegill pectoral fin resulted in increased fin beat frequency during the hovering behavior (Williams and Hale, 2015), which is consistent with the finding in this study that fin beat frequency increased after pectoral fin deafferentation during steady-state swimming in *S. quoyi*.

It is not currently clear why pectoral fin beat frequency increases after the loss of sensory feedback. One possibility is that because increased fin beat frequency increases the force production per stroke (Kahn et al., 2012), fish can use this as a mechanism for increased stability. A second possibility is that after the loss of sensory feedback, which is known to help maintain limb rhythms (Fuchs et al., 2012), the central pattern generator runs at a naturally higher frequency. The third possibility is that changes in the fin stroke or fin ray deformation pattern after the loss of sensory feedback decreased the hydrodynamic output (lift, thrust, force, etc) per fin stroke, and a higher fin beat frequency was needed to maintain position in the flow tank at each speed. While it is likely a combination of factors, changes in the fin stroke pattern suggest that lowered hydrodynamic efficiency is certainly one factor leading to increased fin beat frequency.

S. quoyi transitioned from the pectoral fin to the body-caudal fin gait at slower speeds after the loss of sensory feedback. We can generate three likely hypotheses to explain the early gait transition (between 3-4 BLs^{-1}) after the loss of sensory feedback. First, deafferentation of pectoral fin ray nerves resulted in increased pectoral fin beat frequency, which averaged 6.61 ± 0.43 Hz at $3BLs^{-1}$. Frequencies of this range may be reaching the biomechanical limit for fish of

this size of this species, and a gait transition might be necessary in order for *S. quoyi* to keep up with the flow speed. Second, there is likely an increased energy requirement needed to support the increased fin beat frequency after deafferentation in *S. quoyi*. In both humans (Margaria, 1938) and horses (Hoyt and Taylor, 1987), it is suggested that gait changes occur in order to minimize energy consumption with changing speeds. If gait changes in fish are related to energy consumption, then our data fit this hypothesis. A third alternative is that deafferented fish change gait in order to achieve more stability by using a locomotor mode with an intact sensory system. In this study, only the pectoral fin ray afferents were transected. A transition to a BCF gait might be aided by sensory feedback from the lateral line system and any potential proprioceptive sensors innervating the body axis or the caudal fin.

S. quoyi might no longer be able to regulate fin twisting after the loss of sensory feedback. Pectoral fin counterclockwise twisting (long axis rotation) is a key feature of the fin stroke in other underwater flappers (Walker and Westneat, 1997), and is involved in the generation of the figure-eight patterned fin stroke. While *S. quoyi* exhibits a well-established figure-eight fin stroke in control trials (Figure 2.2), deafferented fins perform a tear-drop shaped fin stroke, which suggests the loss of fin twisting throughout the fin stroke. Wing twisting is also a key feature in the forewing stroke of the locust (Weis-Fogh, 1956; Gettrup and Wilson, 1964; Gettrup, 1966), and is controlled by muscles proximal to the articulation of the wing with the body (Gettrup, 1966). The deafferentation of the locust flight system (fore- and hindwings) results in the inability of proximal muscles to regulate wing twisting (Gettrup, 1965). The similarities between the insect flight system and the fish pectoral fin (a flexible propulsor outfitted with sensors and the lack of any intrinsic muscles) suggests that pectoral fin ray sensory feedback in *S. quoyi* might be necessary for the regulation of fin twisting.

Motor patterns

The general motor patterns after the loss of sensory feedback were similar to those recorded in control trials. After deafferentation, the onset order among abductors remained the same, but the adductors fired nearly coincidentally with less than one percent fin cycle difference in their onset time (Figure 3B, Table S3). The most consistent difference after deafferentation was the significantly earlier onset and increased duration of activity in each muscle (Figure 3B). The earlier onset and increased duration in activity patterns led to the overlap of activity between antagonistic muscles (Figure 4). The RIA of each muscle increased significantly, but the time of peak amplitude remained consistent after deafferentation. Finally, there were no significant differences in the relative variance surrounding the onset, duration, time of peak amplitude, or RIA for any muscle between control and transection trials.

Consistent with this study, the basic motor pattern is relatively unchanged after deafferentation in other systems. While increases in activity amplitude or RIA were fairly common after deafferentation in some muscles in the limbs of newts (Székely et al., 1969) and cats (Grillner and Zangger, 1984)(Grillner and Zangger, 1984) and the wings of locusts (Pearson and Wolf, 1987), some muscles were not affected. In this study, an increase in the RIA of activity was found for each muscle (Table S1). The activity patterns of the six pectoral fin muscles in *S. quoyi* did not change in variability (Figure S2). In contrast to the results of this study, deafferentation often leads to increased variability in the onset and offset of activity in some of the limb muscles of the cat (Grillner and Zangger, 1984), and to a lesser extent, the newt (Székely et al., 1969). Further, Székely et al. (1969) comments that the amphibian limb is much less sensitive to limb deafferentation in comparison to the mammal limb. Only a single study

reports the presence of a muscle spindle in a salmon jaw muscle (Maeda et al., 1983), and this has never been confirmed or reported in other muscles of fish. Mammalian muscle spindles are innervated by gamma motor neurons and large myelinated Ia afferents (Matthews, 1972; Prochazka et al., 2002; Romanovsky et al., 2007), which do not innervate amphibian spindles. Taken together, differences in activity variability after deafferentation among these groups might be a result of differences in the sensory system among mammals, amphibians, and fishes.

The most common result of limb deafferentation across systems is an increase in the duration of muscle activity and the overlap of activity between antagonistic muscles. The overlap of activity between antagonistic muscles after deafferentation is seen in the flight system of the locust (Pearson and Wolf, 1987), the limbs of newts (Székely et al., 1969), and the limbs of mammals (Grillner and Zangger, 1975; Perret and Cabelguen, 1976; 1980; Grillner and Zangger, 1984). Prolonged muscle activity and the presence of overlapping antagonistic muscle activity after deafferentation is also prominent in the pectoral fin of *S. quoyi* (Figure 4). In animals with intact sensory systems, the co-contraction of functionally anatagonistic muscles commonly occurs during the completion of fine motor tasks, skilled movements, and elaborate movements (Paillard, 1960). The co-contraction of anatagonistic muscles is a significant feature of grading movements, joint fixation, and general limb stability (Paillard, 1960; Székely et al., 1969). Limb stiffening by the co-contraction of antagonistic muscles is also a predominant strategy used by humans when learning novel motor tasks (Bernstein, 1967; Milner and Cloutier, 1993). In *S. quoyi*, the tendons of the pectoral fin muscles cross the joint between the fin and the body, and the co-contraction of antagonists likely results in increased joint stiffness. Therefore, we suggest that increased muscle activity duration and the occurrence of overlapping activity between

antagonistic muscles at both extremes of the fin stroke is a strategy to increase stability of the pectoral fin system after the loss of sensory feedback.

Pectoral fin beat rhythmicity

Pectoral fin beat rhythmicity (relative variance in fin beat cycle duration) was found to be relatively high (low variance was observed). We found no significant relationship between fin beat duration CV and speed. Average fin beat duration CV was consistent across all three speeds. The lack of a significant relationship between rhythmicity and speed is consistent with data from locomotion in tetrapods (Ross et al., 2013). Values of pectoral fin beat duration CV are well within the ranges reported for highly rhythmic tetrapods (birds and mammals), which range from averages of 5.5 to 11.01 depending on substrate type, and are below (less variable) the average CV reported for less rhythmic tetrapods (reptiles and amphibians), which range from 19.2 to 20 (Ross et al., 2013). Interestingly, in control trials, the average variation associated with the onset and duration of activity in all six muscles was generally higher than the variability associated with fin beat cycle duration across all three speeds. This suggests that the underlying variability in neuromuscular control of the pectoral fin system might be used to maintain low variability in the total output (behavior) of the system, which leads to highly rhythmic pectoral fin movement.

The high rhythmicity of the pectoral fin system cannot be explained by the same hypothesis used to explain high rhythmicity in mammals and birds. Ross et al. (2013) suggests that, in comparison to reptiles and amphibians, high rhythmicity in mammals and birds is related to the convergent evolution of muscle spindle innervation by gamma-motorneurons (Bilo et al., 1980; Maier, 1992a; b; Romanovsky et al., 2007) and large Ia afferents (Matthews, 1972; Prochazka et al., 2002; Romanovsky et al., 2007) in these two groups. It is likely that the muscles

of fishes do not possess muscle spindles. Even after the loss of pectoral fin ray sensory feedback in *S. quoyi*, rhythmicity is never significantly different and, in two of three cases, increases (Figure 1B). Taken together, this leads to several alternative hypotheses. One possibility is that the pectoral fin system is inherently more rhythmic because of external variables, perhaps the influence of an aquatic, rather than terrestrial, environment. Another possibility is that no mechanosensory feedback from the limbs themselves is needed for the generation of limb rhythms, which has been seen in in mammals (Brown and Sherrington, 1912; Sherrington, 1913) and the locust flight system (Stevenson and Kutsch, 1986; Stevenson and Kutsch, 1987; Stevenson and Kutsch, 1988). While some evidence suggests that the fundamental rhythm of phasic movement is not always dependent on sensory feedback, mechanosensation does provide feedback to modulate (Katz and Harris-Warrick, 1990) and reinforce rhythmicity (Fuchs et al., 2012) in central pattern generating circuits. In this study and a previous study on the loss of pectoral fin ray sensory feedback in fish (Williams and Hale, 2015), sensory feedback was only removed from the pectoral fin rays, and more proximal sensory structures may still exist. Therefore, a third alternative, is that fish have independently evolved a different sensorimotor solution to allow for increased rhythmicity, and that rhythmic pectoral fin movements are not entrained by sensory feedback from the fin rays. In the locust, and likely all flying insects, a stretch receptor near the joint between the base of the wing and the body encodes wing stroke variables (Möhl, 1985; Frye, 2001) and is used to entrain the flight rhythm (Reye and Pearson, 1988). Putative sensors have been suggested to be present in the tendons attached to the base of fin rays (Pansini, 1888; Fessard and Sand, 1937; Ono, 1979) and in the joints and muscles associated with fins in chondrichthyans (Wunderer, 1908; Fessard and Sand, 1937; Lowenstein,

1956). Proximal mechanosensation might have a large role in the maintenance of pectoral fin rhythms.

The co-contraction of antagonistic muscles

The fin rays of fish are bilaterally symmetric structures, and differential activity or co-contraction of antagonistic muscles is suggested to actively curve or stiffen the ray (Alben et al., 2007). The hypothesis that antagonistic muscle co-contraction will be presented during steady state swimming is supported by work on robotic fins that found that increasing the stiffness of a flexible propulsor increases its propulsive capability (Tangorra et al., 2010). While the active stiffening and curvature of fin rays is certainly possible, it does not appear to occur in the pectoral fin of *S. quoyi* during steady state swimming across a range of speeds. Only at the highest speed is overlap in activity even seen during the fin stroke (near peak abduction) and overlap is never seen during the period of peak adduction between consecutive strokes (Figure 4). While antagonistic muscle activity overlap within the fin stroke significantly increases after the loss of sensory feedback at 2BLs-1 (Figure 2.4), there is no significant difference in leading edge fin ray curvature throughout the fin stroke between control and transection trials (Figure 2). In this case, the overlap in activity between antagonists is caused by the increasingly early activity onset and prolonged activity duration that occurs with increasing speed, which we believe is used to increase the force generation of each muscle through a stretch-shorten cycle. Further, we find that overlap in activity is centered around peak abduction when the fin is in the process of completing its down-stroke, flipping, and beginning the upstroke. We suggest that active stiffening would need to occur midway through either the down-stroke or the upstroke during peak velocity and fin curvature to make a significant hydrodynamic contribution.

Therefore, we suggest, at least in *S. quoyi*, that the active stiffening and curvature of fin rays is reserved for other fin behaviors such as maneuvering, posture control, and braking. Future studies should continue to integrate three-dimensional kinematics and electromyography to study fin control and deformation during other behaviors.

CHAPTER 3: THE RELATIONSHIP BETWEEN PECTORAL FIN STIFFNESS AND SWIMMING BEHAVIOR IN LABRIDAE: INSIGHTS INTO DESIGN, PERFORMANCE, AND ECOLOGY

Abstract

The functional capabilities of flexible propulsive appendages are directly influenced by their mechanical properties. The fins of fishes have undergone extraordinary evolutionary diversification in structure and function, which raises questions of how fin mechanics relate to swimming behavior. In the fish family Labridae, pectoral fin swimming behavior ranges from rowing to flapping. Rowers are more maneuverable than flappers, but flappers generate greater thrust at high speeds and achieve greater mechanical efficiency at all speeds. Interspecific differences in hydrodynamic capability are largely dependent on fin kinematics and deformation, and are expected to correlate with fin stiffness. Here we examine fin ray stiffness in two closely related species that employ divergent swimming behaviors, the flapping *Gomphosus varius* and the rowing *Halichoeres bivittatus*. To determine the spatial distribution of flexural stiffness across the fin, we performed three-point bending tests at the center of the proximal, middle, and distal regions of four equally spaced fin rays. Pectoral fin ray flexural stiffness ranged from 0.0001- 1.5109 microNewtons•m^2, and the proximal regions of *G. varius* fin rays were nearly an order of magnitude stiffer than those of *H. bivittatus*. In both species, fin ray flexural stiffness decreased exponentially along the proximo-distal span of fin rays, and flexural stiffness decreased along the fin chord from the leading to trailing edge. Further, the proportion of fin area occupied by fin rays was significantly greater in *G. varius* than in *H. bivittatus*, suggesting that the proportion of fin ray to fin area contributes to differences in fin mechanics.

Introduction

The form and function of propulsive appendages are fundamental to the ecology of a wide range of organisms (Liem, 1990; Losos, 1990; Wainwright and Reilly, 1994; Gillis and Blob, 2001; Taft and Taft, 2012; Higham et al., 2014). In coral reef fishes, interspecific variation of fin form and function strongly impacts hydrodynamic capability in fishes (Walker and Westneat, 2000b; 2002a; b; Thorsen and Westneat, 2005), and has ultimately shaped patterns of niche occupation (Bellwood and Wainwright, 2001; Fulton et al., 2001; Wainwright et al., 2002). Combes and Daniel (2002) explored the flexural stiffness of insect wings, and suggested that because of the complex relationship existing between the form and function of a propulsor, predictions of functional capabilities in propulsors based on shape alone are valid only under limited circumstances. The mechanics of insect wings (Newman and Wootton, 1986; Ennos, 1988a; Steppan, 2000; Combes and Daniel, 2003b; a), bird wings (Macleod, 1980; Bonser and Purslow, 1995; Bachmann et al., 2012), and bat wings (Swartz et al., 1996; Swartz and Middleton, 2008) share characteristics of their stiffness fields (the spatial distribution of flexural stiffness across an appendage), including a stiffened leading edge, a more flexible trailing edge, and a structure that tapers along its span. Together, these common features of stiffness profiles lead to the convergence of similar propulsor bending regimes across a highly diverse group of taxa (Lucas et al., 2014). Yet, fin ray stiffness is rarely considered in the discussion of fin design and hydrodynamic capability in fishes; this leads to questions of how the distribution of mechanical properties across the fins of fish relates to swimming behavior, whether the distribution of fin mechanics leads to the passive production of an advantageous bending regime across the surface of a fin, and how pectoral fin mechanics compare to the mechanics of flexible propulsors found in other systems. Our understanding of fish fin biomechanics, hydrodynamic capability and

evolutionary diversification may thus benefit through efforts to document associated changes in the fin's mechanical properties.

The pectoral fin is a flexible propulsor with a composite structure typically composed of a membrane supported by multiple fin rays (Goodrich, 1904). Fin rays, or lepidotrichia, are bilaminar composite structures made up of two crescent –shaped acellular bony hemitrichia (Geerlink and Videler, 1987) that surround a core of collagen gel (Goodrich, 1904). In pelagic fishes, the proximal portion of each hemitrich is typically unsegmented and the distal portion is segmented (Goodrich, 1904). Up to four muscles attach via tendons to the proximal base of each fin ray control the movement of individual rays as well as the fin as a whole (Geerlink and Videler, 1987; Lauder et al., 2011). While many animals (e.g. birds, bats, and fishes) are capable of actively tuning the shape or mechanics of their flexible propulsor (Geerlink and Videler, 1987; Kent and Carr, 2001; Lauder et al., 2006; Alben et al., 2007; Cheney et al., 2014), the flexural stiffness of a structure, or its resistance to bending, will largely determine its shape change in response to the application of locomotor forces (Gordon, 1978; Vogel, 2003b). The propulsive and maneuverability capabilities of animals with flexible propulsors are largely dependent on the kinematics and three-dimensional deformation of their appendages (Yamamoto et al., 1995; Daniel and Combes, 2002; Zhu and Shoele, 2008; Young et al., 2009; Tangorra et al., 2010; Flammang et al., 2013; Mistick et al., 2016). Therefore, swimming performance in fishes using labriform locomotion will largely be a consequence of the spatial distribution of spanwise (along the length of the fin from proximal to distal) and chordwise (across the width of the fin from its leading edge to trailing edge) fin ray flexural stiffness.

The spatial distribution of intrinsic pectoral fin ray flexural stiffness has been explored in the bluegill sunfish (*Lepomis macrochirus*) (Tangorra et al., 2010; Lauder et al., 2011). In the

bluegill pectoral fin, the stiffness of a given ray decreases from proximal to distal, and, across the chord, the central rays are stiffer than the dorsal and ventral rays(Tangorra et al., 2010; Lauder et al., 2011). Beyond bluegill, our understanding of fin ray stiffness is inferred from differences in fin ray geometry in specialized benthic species (Taft, 2011; Taft and Taft, 2012). Aiello et al. (2017) also reported the comparative stiffness of a single ray in eight labrid species and found that flexural stiffness decreases exponentially long the length of the third fin ray and that stiffness was generally related to swimming behavior. A larger body of comparative work on fin stiffness is necessary to address questions regarding the features of pectoral fin ray stiffness that are general to actinopterygians, how the spatial distribution of flexural stiffness across a fin varies among species, and associations among pectoral fin stiffness profile, swimming behavior, hydrodynamic capability, and the ecology of fishes. Differences in swimming behavior and trade-offs between maneuverability and propulsive efficiency would be expected to drive the evolution of different pectoral fin flexural stiffness spatial profiles among species.

Here we explore these questions in the wrasses (Labridae), a clade that employs pectoral fin-based propulsion with kinematics ranging from drag-based rowing to lift-based flapping (Walker and Westneat, 2000b; 2002a; b). Rowers generate thrust primarily during their posteriorly directed power stroke, generate greater thrust at slow speeds, and are more maneuverable in comparison to flappers (Walker and Westneat, 2000b; 2002a; b). Conversely, flappers generate thrust during both the upstroke and downstrokes and generate greater thrust at high speeds and greater mechanical efficiency at all speeds in comparison to rowers (Walker and Westneat, 2000b; 2002a; b). While a flexible propulsor will typically generate more thrust in comparison to a rigid propulsor (Yamamoto et al., 1995; Zhu and Shoele, 2008; Young et al., 2009), excessive flexibility reduces propulsive efficiency (Liu and Bose, 1997; Heathcote et al.,

2008). Additionally, modeling studies have found that a biorobotic fin with stiff and tapered fin rays exhibits greater propulsive capabilities than a fin with relatively more flexible and uniformly designed rays (Tangorra et al., 2010). Therefore, we hypothesized that fin ray stiffness would decrease along the span of the fin ray from proximal to distal in both flappers and rowers, and flappers would have stiffer fins in comparison to rowers, which might allow flappers increased efficiency and rowers increased maneuverability.

To address these hypotheses we assessed intrinsic/passive (uninfluenced by muscle activity) pectoral fin ray flexural stiffness in two closely related and size-matched species, the flapping *Gomphosus varius* and the rowing *Halichoeres bivittatus*. To determine the spatial distribution of flexural stiffness, we performed three-point bending tests at the center of the proximal, middle, and distal one-third of four equally spaced fin rays across the chord of each fin. We compared the spatial distribution of *G. varius* and *H. bivittatus* pectoral fin flexural stiffness with published data from other species to begin to explore how different stiffness profiles relate to the swimming behavior, hydrodynamic capability, and the niche of a species. Additionally, because fin shape (aspect ratio) is correlated with swimming behavior (Wainwright et al., 2002; Walker and Westneat, 2002b) and we have observed interspecific differences in the number of fin rays per fin, we also quantified the area of a fin covered by ray versus membrane to probe the morphological underpinning of variation in fin stiffness.

A comparative analysis of the spatial distribution of pectoral fin flexural stiffness and how it relates to fin morphology provides new insights into fin function and build upon recent work (Tangorra et al., 2010; Lauder et al., 2011; Taft, 2011). In addition, this study broadens our understanding of the diversity of fin ray mechanical properties, providing a foundation for

comparative and phylogenetic studies of pectoral fin function that include the mechanical properties of fin tissues.

Materials and methods

Fish specimens. We collected data on the mechanical properties of the pectoral fin rays from seven *Gomphosus varius* individuals (mass ranged between 7.8 – 39.8 grams; mean ± stdev = 22.44 ± 13.19 grams) and eight *Halichoeres bivittatus* individuals (mass ranged between 6.0 – 64.6 grams; mean ± stdev = 22.03 ± 19.05). Fish were obtained commercially and maintained in 200L marine aquaria (34.51 ppt) under natural day:night light cycles with a mean water temperature of 24°C. After fish were euthanized in a .05g/l- solution of MS-222 (Tricaine methanesulfonate, Sigma-Aldrich, St. Louis, MO), the right pectoral fins were excised from the body and placed in extracellular solution to maintain cell survival and structural integrity. All experimental procedures, housing, and euthanasia methods were carried out under University of Chicago Institutional Animal Care and Use Committee guidelines (protocol 72365 to M.W.W.).

Three-point bending tests. In order to determine the spatial distribution of intrinsic pectoral fin ray stiffness we performed three-point bending tests on the fin rays of *Gomphosus varius* and *Halichoeres bivittatus* using a material testing machine (LS1, Lloyd Instruments, Fareham, UK) with a 50N load cell (minimum load resolution = 0.0001N). Data was acquired using the Nexygen Plus software (Lloyd Instruments, Fareham, Hants, UK).

Flexural stiffness (EI) is a measurement of a structure's resistance to bending and depends upon its material properties (E, Young's modulus of elasticity) and cross-sectional geometry (I, second moment of area) (Gordon, 1978; Vogel, 2003b). The conditions to measure E and I independently are rarely met for biological materials, as the material must be homogenous, isotropic, and linearly elastic (Vogel, 2003, Young et al., 2012). Furthermore, fin

rays are composite structures (i.e. crescent–shaped hemitrichia that surround a core of collagen gel), making accurate and reliable measurements of I difficult. Therefore, we measured EI as a single variable using beam theory as in Vogel, 2003:

$$\mathbf{EI = F(d^3)/48Y}$$

where F is applied force (N), d is the distance between (m), and Y is fin ray displacement (m) at the location of the force application (Fig. 1). This equation is only valid however, for small displacements where Y ≤ 10% of L because a material can experience shear as well as bending at larger displacements (Blob and LaBarbera, 2001; Young et al., 2012). Therefore, we recorded the force exerted when fin ray displacement (Y) equaled 10% of L.

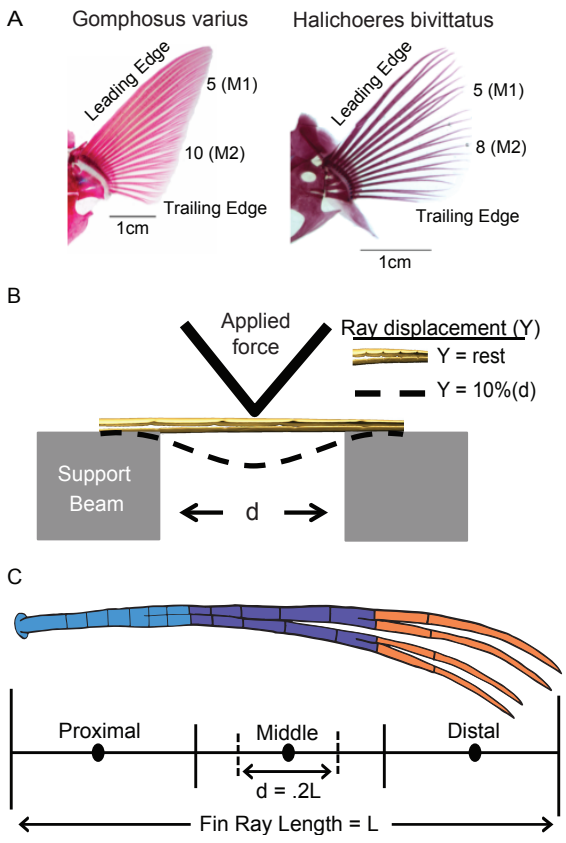

Figure 3.1. Schematic of methodology used in this study. The leading edge ray, trailing edge ray, and two middle fin rays equidistant from each other and from the leading and trailing rays were dissected from fresh fins and used for mechanical property testing (A). The fins pictured in A are cleared and stained versions for morphological reference. Fin rays were isolated and placed on a three-point bending apparatus (B). Individual tests occurred at three different locations per fin ray, the middle of the proximal third (16.65 % fin ray length), the middle of the middle third (50.00 % fin ray length), and the middle of the distal third (83.34 % fin ray length) (C).

Pectoral fin rays 1 (leading edge), 5, 10, and 14 (trailing edge) of *Gomphosus varius* and 1, 5, 8, 12 of *Halichoeres bivittatus* were individually dissected from the pectoral fin (Fig. 1a). Fin rays were placed across adjustable support beams so that flexural stiffness was measured at the center of the proximal (16.67% ray length), middle (50% ray length), and distal (83.25% ray length) third of each fin ray (Fig. 3.1). To standardize measurements across species, the distance between supports (d) was set to 20% of fin ray length

(L) and force was applied at a rate of 0.1mm/sec. Fin rays were kept moist with 4°C PBS solution throughout the duration of the experiment.

To ensure the most accurate measurement of fin ray flexural stiffness, local three point bending tests were conducted at proximal, middle, and distal locations along the fin's length. The gradual change in fin ray cross section that occurs locally within these small regions allows the three point bending equation to be applied with sufficient accuracy (Young et al., 2012). Furthermore, in the proximal bending location, force was always applied to a section that was unsegmented. This method can accurately measure flexural stiffness at multiple locations along a single fin ray, and when done on multiple fin rays, can reveal the spatial distribution of flexural stiffness across a fin.

A single value of flexural stiffness per fin ray could be obtained by conducting cantilever-bending tests (Vogel, 2003). However, cantilever-bending tests have several assumptions that are not met by fin rays. Fin rays are continuously tapered structures. While equations have been developed to deal with continuously tapered structures to varying success (Young et al., 2012), these methods require knowledge of the variation in second moment of area along the beam's length. Attempts have been made to measure second moment of area in fin rays (Taft, 2011). However, the complex bilaminar structure of two independent hemitrichs surrounding a core of collagen and the unknown contributions of these materials to fin ray stiffness makes it difficult to accurately measure the second moment of area. Finally, fin rays are typically unsegmented proximally and segmented distally. While equations have been developed to measure the flexural stiffness of slotted uniform beams during cantilever bending (Young et al., 2012), no equations exist, to the best of our knowledge, to account for a tapered beam that abruptly becomes segmented.

Skeletal area. In order to test how differences in the area of a fin occupied by ray skeleton impacts flexural stiffness across the pectoral fin and between individuals we measured skeletal area: the percent of fin surface area occupied by fin ray skeleton (as opposed to the area occupied by only fin membrane). For each species, five cleared and stained specimens were acquired from the Field Museum of Natural History (Chicago, IL). *G. varius*: FMNH 124858, 111975, 111976, and 101280 (N=2); *H. bivittatus*: FMNH 101276 (N=2) and MW-NC92 (N=3). The cleared and stained individuals of each species fell within the same size range of the experimental individuals used in this study. The length of the leading edge fin ray ranged between 1.269 and 2.953 centimeters in *G. varius* (mean ± stdev = 2.146 ± 0.619) and 1.287 and 2.383 centimeters in *H. bivittatus* (mean ± stdev = 2.036 ± 0.438). Leading edge fin ray length was not significantly different between species (p=0.754). Excised fins were placed on a white light board with fin rays in a splayed position. Digital images were captured using an Olympus DP72 camera (Olympus Camera, Center Valley, PA). Images were imported into Adobe Photoshop CS5 (Adobe System, Inc., San Jose, CA, USA) and converted to black and white images by isolating the pixels of the fin rays from the white background. Black and white images were saved and converted into binary files in NIH ImageJ 1.62 (NIH, Bethesda, MD, USA). We then used ImageJ to calculate fin area and the percentage of that area composed of black pixels (fin rays) and white pixels (membrane).

Statistical Analysis. We performed Student's t-tests to determine if there were significant differences in fin ray flexural stiffness and skeletal area within and across species. Linear regressions were also performed to determine if leading edge flexural stiffness correlates with measurements of fin ray length, body mass, and standard body length and if skeletal area correlates with fin area. ANCOVA models were fit to test for significant differences between the

slope and y-intercept of the leading edge stiffness by body mass regressions between both species. In the ANCOVA models, stiffness was the dependent variable, species was a factor, and mass was the covariate. All statistical analyses were conducted using the program JMP v. 5.0 (JMP, 2002) or the R statistical environment (R Development Core Team, 2017).

Results

Pectoral fin ray flexural stiffness ranged from 0.0001 - 1.5109 $\mu N \bullet m^2$. We found similar trends in the fin's span-wise and chord-wise spatial distribution of ray stiffness in *G. varius* and *H. bivitattus* (Fig. 3.2). Stiffness decreased exponentially along the proximo-distal span of a given ray (Table 3.1). Of the 60 rays examined (four rays per individual) between the two species, 25 of 28 and 24 of 32 showed a significant ($p<0.05$) exponential relationship between stiffness and proximo-distal position in *G. varius* and *H. bivitattus*, respectively (Fig. 3.3A; Table S3.1). To account for the low number of data points per fin ray and to increase statistical power, within each species, data were pooled by position for each fin ray. An analysis of the pooled data of each fin ray for each species always found a significant ($p<0.01$) exponential relationship between stiffness and position along the ray's length of a given

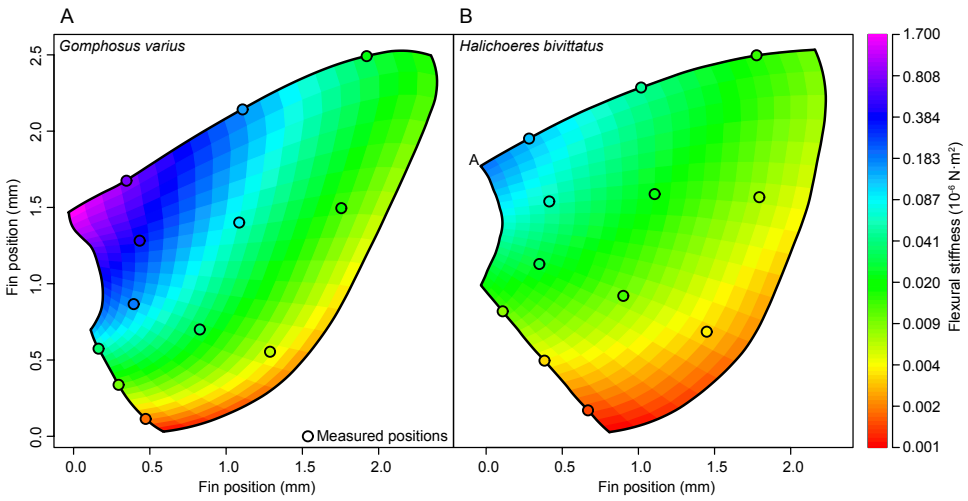

Figure 3.2. The average spatial distribution of flexural stiffness across the pectoral fins of *G. varius* (A) and *H. bivittatus* (B). In both species, flexural stiffness decreased in the span-wise direction and along the chord from the leading to trailing edge. Flexural stiffness was approximately an order of magnitude greater in *G. varius* in comparison to *H. bivittatus*. Each black circle represents the locations across the fin where three-point bending tests were conducted.

ray (Table S3.2). Furthermore, both species showed trends of decreasing ray stiffness along the fin's chord from the leading to trailing edge (Fig. 3.3A; Table 3.1). The comparison of y-intercepts between different regressions can also reveal differences in flexural stiffness between fin rays or species. Since no significant difference was detected in the exponential regression slope between any fin ray combinations within a given species (Table S3.3), differences in the y-intercept imply shifts in the magnitude of the exponential relationship between flexural stiffness and fin ray position. Within each species, an analysis of the regressions between stiffness and ray position on the pooled data for each ray reveal significant differences ($p<0.001$) between the y-intercepts for the leading and trailing edge as well as middle ray 1 and the trailing edge (Table S3.3). For *G. varius*, the leading edge and middle ray 2 also exhibited a significant difference ($p<0.01$) in the y-intercept of a regression between stiffness and the position along the fin ray. These results, together with the lack of significant differences between the y-intercepts of adjacent rays, suggest that fin ray stiffness gradually decreases along the fin's chord, from leading to trailing edge, in both species.

A comparison between species reveals significant differences in fin stiffness (Fig. 3.2). For the leading edge, the average flexural stiffness of the proximal and middle portion of the ray was significantly greater ($p<0.05$) in *G. varius* than in *H. bivitattus* (Fig. 3.3B), and averaged 0.8899 ± 0.4587 and 0.1588 ± 0.0613 $\mu N \bullet m^2$ in *G. varius* and 0.1671 ± 0.1496 and 0.0676 ± 0.0762 $\mu N \bullet m^2$ in *H. bivitattus* (Table 3.1). A comparison of stiffness at the distal tip of the leading edge fin ray between *G. varius* and *H. bivitattus* revealed no significant difference (Table 3.1; Fig. 3.4). Similar trends in fin ray stiffness between *G. varius* and *H. bivitattus* were also found for middle ray 1, middle ray 2, and the trailing edge ray (Table 3.1). To further test differences in flexural stiffness between species we compared y-intercepts of exponential

regressions for each fin ray between species. For each fin ray, the y-intercept was significantly greater in *G. varius* than in *H. bivitattus* (Table S3.2).

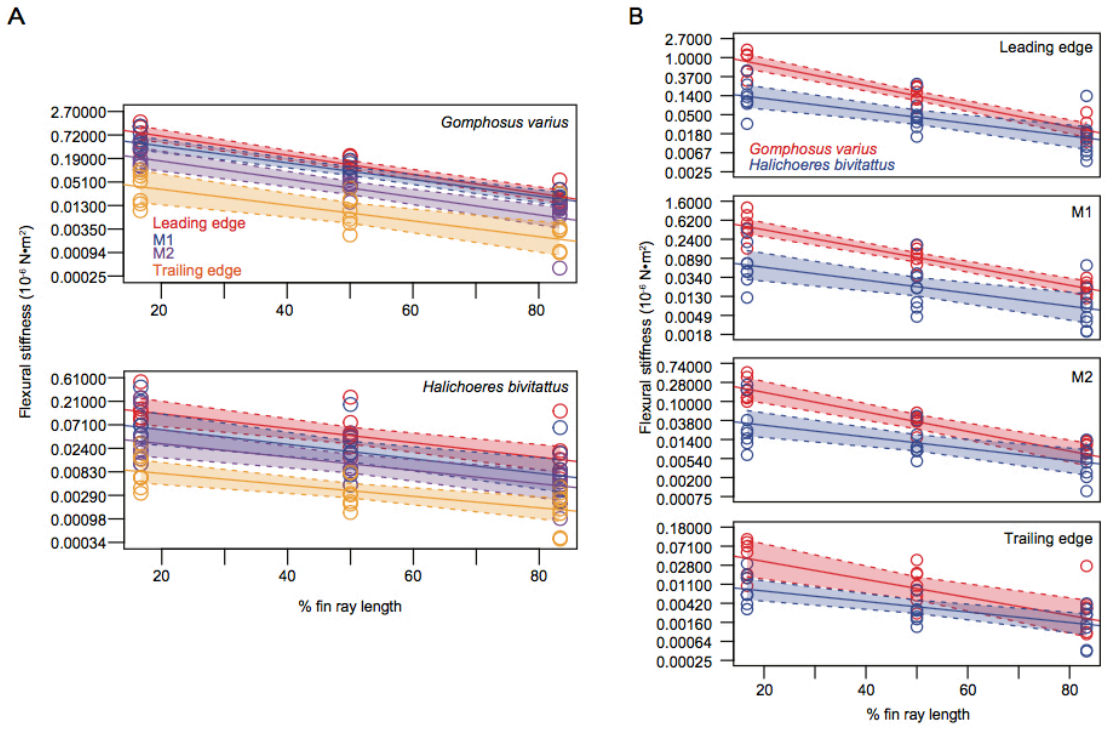

Figure 3.3. Flexural stiffness along the length of each fin ray for each species.
(A) Flexural stiffness decreases exponentially along the length of each fin ray in the span-wise direction. Red, blue, purple, and orange shading represent the confidence interval of the flexural stiffness data for the leading edge, M1, M2, and trailing edge fin rays, respectively. (B) Significant differences in flexural stiffness of each fin ray at 16.65 and 50.00 % fin ray length exist between species. However, there were no significant differences between species in fin ray flexural stiffness at the distal tip (83.34% fin ray length). The red and blue shading represents *G. varius* and *H. bivitattus*, respectively. In both panels (A and B), the shaded region of each fit represents a 99% confidence interval of the linear regression.

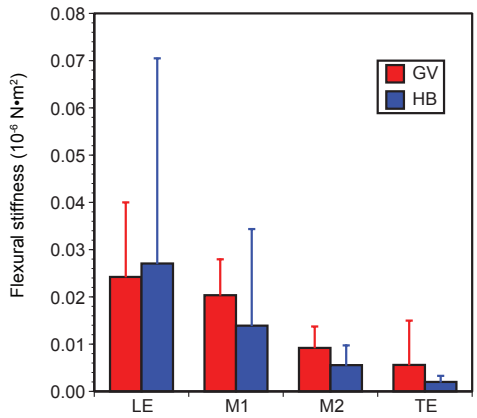

Figure 3.4. An interspecific comparison fin ray distal flexural stiffness.
In all four fin rays examined, there was no significant difference in a fin ray's distal flexural stiffness (83.34 % fin ray length) between species (p>0.05).

Fin ray stiffness is correlated with size in both *G. varius* and *H. bivitattus* (Fig. 3.5). In both species, there was a significant and positive relationship between fin ray stiffness at 50% ray length and total ray length (Table S3.4). Similarly, there was a significant and positive relationship between stiffness of the leading edge ray at 50% ray length and body mass (Table

S3.4). Further, ANCOVA models were fit to the *G. varius* and *H. bivitattus* leading edge ray stiffness by body mass regressions. An ANCOVA model where stiffness is modeled as the dependent variable, species as a factor, and mass as the covariate reveals no significant interaction between mass and species (p=0.38, F-value = 0.838), which means that the slope of the regression between mass and stiffness are statistically the same between *G. varius* and *H. bivitattus*. A second ANCOVA model found a significant difference in the y-intercepts of the leading edge by mass regressions between *G. varius* and *H. bivitattus* (p=7.52x10^{-7}, F-value = 87.08), indicating that the two species had significantly different stiffness regressions.

The percentage of total fin ray area occupied by fin ray versus membrane (fin ray area) was also quantified in five individuals of each species (Fig. 3.6). Fin rays occupied 55.35 ± 8.12 % and 37.96 ± 3.50 % of the total fin area (Fig. 3.6c) in *G. varius and H. bivittatus*, respectively. A t-test revealed that fin ray area was significantly greater in *G. varius* in comparison to *H. bivittatus* (p<0.01). There were no significant trends between skeletal area and fin area, which scales with body size, for either species (Fig. 3.6d).

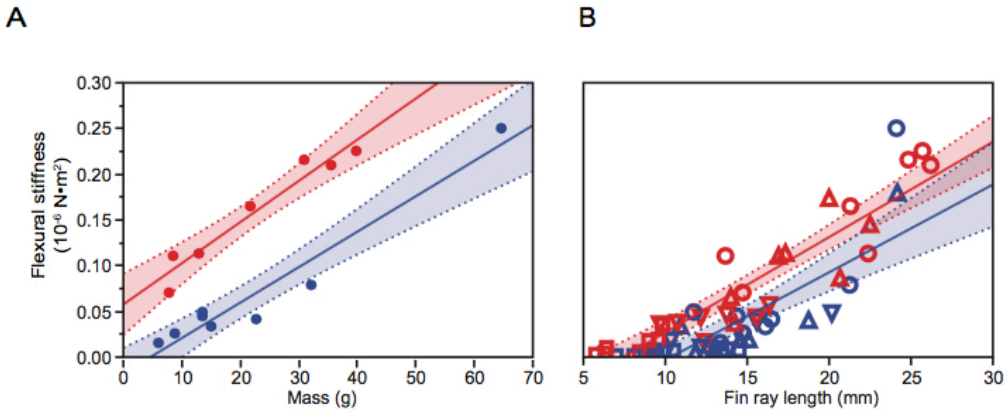

Figure 3.5. The relationship between body size and flexural stiffness.
Leading edge flexural stiffness at 50% fin ray length is positively and significantly correlated with both body mass (A) and fin ray length (B) in both species. In both cases there were no significant differences in the regression slope between species. The red and blue shading represents *G. varius* and *H. bivitattus*, respectively.

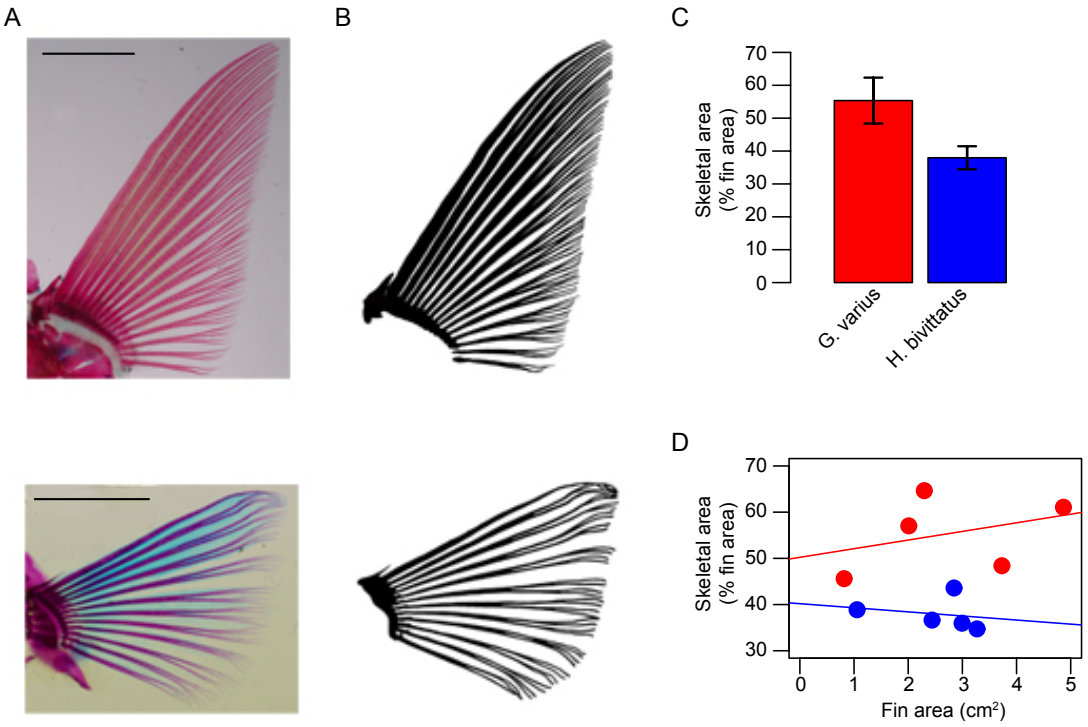

Figure 3.6. A comparison of skeletal area between *G. varius* and *H. bivitattus*.
Pectoral fins were cleared, stained, and photographed (A), and converted into black and white binary images (B) for analysis. Scale bar = 1cm. Pectoral fin skeletal area (the percentage of the fin area occupied by fin rays versus membrane) was significantly greater in *G. varius* in comparison to *H. bivitattus* (C). There was no significant relationship between fin area and skeletal area in either species (D). *G. varius* *p*-value = 0.5487, r^2=0.1315, F-ratio = 0.454; *H. bivitattus* *p*-value = 0.7211, r^2 = 0.04878, F-ratio = 0.1538.

Table 3.1. Raw data, mean and s.d. of fin ray flexural stiffness for each region of each ray per individual.

	LE			M1			M2			TE		
Indiv.	**Prox.**	**Mid.**	**Distal**	**Prox.**	**Mid.**	**Distal**	**Prox.**	**Mid.**	**Distal**	**Prox.**	**Mid.**	**Distal**
1	1.1701	0.2256	0.0566	0.8054	0.1459	0.0261	0.1832	0.0577	0.0128	0.0709	0.0188	0.0039
2	1.1202	0.1134	0.0197	0.4194	0.1103	0.0220	0.1223	0.0438	0.0137	0.0148	0.0062	0.0032
3	1.5109	0.2159	0.0180	1.1901	0.1733	0.0150	0.3655	0.0161	0.0004	0.1008	0.0178	0.0034
4	1.1550	0.2100	0.0327	0.5434	0.0865	0.0204	0.1829	0.0432	0.0106	0.0524	0.0359	0.0266
5	0.4891	0.1651	0.0166	0.3264	0.1140	0.0333	0.4662	0.0467	0.0072	0.0869	0.0100	0.0001
6	0.4884	0.1108	0.0140	0.3370	0.0653	0.0140	0.1287	0.0362	0.0083	0.0178	0.0049	0.0010
7	0.2956	0.0705	0.0120	0.1474	0.0373	0.0117	0.1018	0.0375	0.0113	0.0099	0.0025	0.0009
AVG	**0.8899**	**0.1588**	**0.0242**	**0.5385**	**0.1047**	**0.0203**	**0.2215**	**0.0402**	**0.0092**	**0.0505**	**0.0137**	**0.0056**
STDEV	**0.4587**	**0.0613**	**0.0158**	**0.3532**	**0.0465**	**0.0076**	**0.1393**	**0.0127**	**0.0045**	**0.0371**	**0.0116**	**0.0094**
T-test P-value	***0.0010***	***0.0252***	0.8732	***0.0068***	***0.0335***	0.4457	***0.0254***	***0.0137***	0.1267	***0.0118***	***0.0475***	0.2968
1	0.0979	0.0337	0.0092	0.0456	0.0095	0.0035	0.0201	0.0083	0.0021	0.0065	0.0031	0.0013
2	0.0308	0.0157	0.0073	0.0120	0.0046	0.0021	0.0065	0.0047	0.0010	0.0064	0.0019	0.0004
3	0.0884	0.0260	0.0060	0.0304	0.0072	0.0022	0.0232	0.0098	0.0026	0.0064	0.0013	0.0004
4	0.0992	0.0493	0.0148	0.0448	0.0194	0.0075	0.0118	0.0096	0.0078	0.0169	0.0081	0.0032
5	0.1264	0.0449	0.0196	0.0683	0.0344	0.0195	0.0393	0.0185	0.0069	0.0040	0.0029	0.0023
6	0.1461	0.0416	0.0044	0.0693	0.0199	0.0044	0.0152	0.0079	0.0044	0.0031	0.0021	0.0015
7	0.2421	0.0791	0.0218	0.2053	0.0412	0.0091	0.1891	0.0389	0.0052	0.0146	0.0081	0.0042
8	0.5058	0.2504	0.1333	0.3966	0.1795	0.0626	0.2458	0.0486	0.0142	0.0299	0.0081	0.0025
AVG	**0.1671**	**0.0676**	**0.0271**	**0.1090**	**0.0395**	**0.0139**	**0.0689**	**0.0183**	**0.0055**	**0.0110**	**0.0045**	**0.0020**
STDEV	**0.1496**	**0.0762**	**0.0434**	**0.1304**	**0.0580**	**0.0205**	**0.0934**	**0.0164**	**0.0042**	**0.0091**	**0.0031**	**0.0013**

p-values italicized and bolded are significant.

Discussion

The movement and deformation pattern of pectoral fins impact their hydrodynamic capabilities (Walker and Westneat, 2000, 2002; Yamamoto et al., 1995; Zhu and Shoele, 2008). The distribution of mechanical properties across fin surfaces will strongly influence fin deformation in response to inertial and hydrodynamic forces during the fin stroke. The purpose of this study was to test our hypotheses by examining the relationship between swimming behavior (e.g. rowing and flapping) and the distribution of flexural stiffness across the pectoral fin (stiffness field). We examined this relationship in two closely related species of wrasse, the flapping *G. varius* and the rowing *H. bivittatus*; the wealth of data published on the ecology, kinematics, motor patterns, and hydrodynamic capabilities of these species allows us to better infer the

effects of different pectoral fin stiffness fields. In both species, fin ray flexural stiffness decreased exponentially along the length of any given fin ray (Figs. 3.2, 3.3), and fin ray stiffness decreased along the chord from the leading to trailing edge of each fin (Figs. 3.2, 3.3). Fin ray flexural stiffness throughout the proximal 70% of each fin ray was nearly an order of magnitude greater in the flapping *G. varius* than in the rowing *H. bivittatus* (Figs. 3.2, 3.3), and these interspecific differences in fin ray stiffness are consistent over a range of body sizes (Fig. 3.5). While fin ray stiffness was significantly different between species, the slope of the regression between leading edge flexural stiffness and body mass is similar between species (Fig. 3.5). Therefore, the scaling relationship that likely exists between body size fin ray stiffness will also be similar between species. Further, we examined how the portion of fin surface area occupied by fin ray skeleton (skeletal area), as opposed to membrane, effects fin stiffness. We found that skeletal area is significantly greater in *G. varius* than in *H. bivittatus* (Fig. 3.6), which suggests that the distribution of fin skeleton strongly impacts the flexural stiffness of fins.

Design principles of a flexible propulsor. A key feature of an efficient propulsor is the reduction in flexural stiffness along its span through a structure that tapers resulting in a finer tip than base. In a study using biorobotic pectoral fins, fins with tapered rays had greater propulsive capabilities in comparison to fins outfitted with rays of uniform dimensions (Tangorra et al., 2010). Multiple examples of this principle exist in nature. The shafts of bird feathers (Bachmann et al., 2012) and the wings of insects (Combes and Daniel, 2001; 2003b) both decrease in stiffness along their proximo-distal span. This can also be seen in the pectoral fins of bluegill sunfish, which employ rays with a proximal portion that is two to six times stiffer in comparison to its distal tip (Tangorra et al., 2010; Lauder et al., 2011). Similarly, this study and previous work on labrid pectoral fin ray stiffness (Aiello et al., 2017) found that fin ray stiffness decreases

exponentially along the span of fin rays. In both engineered and biological systems, the spanwise tapering of a propulsor will reduce the energy needed for oscillation as well as increase tip flexibility, which can reduce damage from the application of unexpected forces or impacts (Wootton, 1992; Flammang et al., 2013). Furthermore, Lucas et al. (2014) found that, across a diverse range of animals, the inflexion point of maximal bending typically occurs within the distal 35% along the span of propulsors. Our data provides mechanical evidence to support the findings of Lucas et al. (2014) in fishes, and supports hypotheses that animals employing flexible propulsive appendages have convergently evolved structures that decrease in stiffness along their spans.

The highly flexible distal tips of fin rays employed by flappers might also be advantageous for minimizing induced drag from wing tip vortices. The flapping swimming behavior utilizes lift-based propulsion that relies on the generation of circulating vortices and dorso-ventral pressure gradients (Spedding, 1992; Vogel, 1994). The shedding of vortices from wing tips and local flow from the dorso-ventral pressure gradient across the wing results in induced drag and a lower lift to drag ratio (Vogel, 1994). However, animals have evolved traits to reduce the effect of wing tip vortices. For example, birds have evolved slotted wing tips that minimize induced drag during flight (Tucker, 1993). Similarly, aerodynamic wing theory has been inspired by biology and engineers have implemented vertically oriented wing tips, also known as winglets, to reduce the shedding of wing tip vortices and minimize induced drag (Hossain et al., 2011). Despite *G. varius* having significantly stiffer fin rays throughout the proximal 66% of each ray in comparison to *H. bivittatus*, there were no significant differences in distal fin ray flexural stiffness between these species (Fig. 3.4). Flexural stiffness measurements from the third fin ray of three additional flapping labrids (all representing independent evolutions

of the flapping behavior) also yields highly flexible distal tips (Aiello et al., 2017), and suggests highly flexible distal fin ray tips is a common feature that has convergently evolved in lift-based flexible propulsors. We suggest the reduced flexural stiffness of the distal tips in flapping species will localize and maximize spanwise bending within the distal third of fins, which might help minimize induced drag and maximize lift-to-drag ratios.

Interspecific differences in the spatial variations in stiffness, or stiffness fields, across the fins will produce different bending regimes during swimming. In both *G. varius* and *H. bivittatus* flexural stiffness was greatest at the leading edge and decreased posteriorly along the fin chord (Fig. 3.2). A stiffened leading edge is not unique to fish fins and can be found in other flexible propulsors. For example, insect wings have a stiffened leading edge due to increased vein density in this region (Wootton, 1992), and the shafts of leading edge feathers in bird wings are also stiffer in comparison to more trailing edge feathers (Purslow and Vincent, 1978). A stiffened leading edge is advantageous to resist bending caused by the large inertial and fluid dynamic forces associated with the onset of movement and propulsor reversal between the down and upstrokes. Furthermore, a propulsor with a stiffened leading edge and a more flexible trailing edge will produce a propeller-blade-like twist in response to torsional forces (Wootton, 1981; 1992). Wing twisting is prominent across insect species and is suggested to automatically and passively generate camber across the wing (Ennos, 1988a; b; Wootton, 1992). The generation of camber in a propulsor can increase fluid-dynamic efficiency as well as increase the resistance to spanwise bending (Jensen, 1956; Vogel, 1967; Ellington, 1984; Wootton, 1992). The pectoral fins of *G. varius* also experience a propeller-like twist throughout their fin stroke (Walker and Westneat, 1997). The data presented here provide a mechanical basis for this kinematic feature

of lift-based labriform locomotion and suggest that the propeller-blade-like twist, and therefore camber, of the fin could be generated passively.

The pattern of relative fin ray flexural stiffness across fins is similar between *G. varius* and *H. bivittatus*, but different from that of the bluegill sunfish (*Lepomis macrochirus*). In the bluegill sunfish, the central rays are stiffer than the dorsal and ventral rays (Lauder et al., 2011) leading to a bell-shaped curve of stiffness along the fin chord. While *G. varius* and *H. bivittatus* exclusively employ the pectoral fin lift-based and drag-based swimming behaviors, respectively (Walker and Westneat, 2000, 2002), the bluegill primarily uses its pectoral fins for hovering and low-speed swimming before switching to a body-caudal fin gait (Gibb et al., 1994). Bluegill also employ both the most dorsal and most ventral fin ray as its leading edge at different points of the fin stroke (Gibb et al., 1994; Lauder and Madden, 2007), which allows them to perform both lift-based and drag-based propulsion (Gibb et al., 1994; Lauder and Madden, 2007). A study using biorobotic fins found that the spatial distribution of flexural stiffness across a fin could be tuned for directing propulsive forces along different axes (Tangorra et al., 2006). Bluegill sunfish have been the primary source of data when designing bioinspired pectoral fin-based propulsors for underwater autonomous vehicles (e.g. Sitorus et al., 2009; Phelan et al., 2010; Tangorra et al., 2012). Data from this study can be used to produce alternative robotic fin shapes, stiffness fields, and informs how the relationship between fin shape and stiffness could be tuned to meet the demands of drag- versus lift-based propulsion (maneuverability versus high thrust production and efficiency).

The functional morphology of labriform locomotion. Despite performance differences, the evolutionary persistence of the extreme swimming behaviors of rowing and flapping suggests that these swimming modes are ecologically advantageous (Fish, 1996; Walker and Westneat,

2000, 2002; Wainwright et al., 2002). Indeed, there is a relationship between labrid swimming behavior and habitat use. Flapping species, which achieve high mechanical efficiency, generate greater thrust at high speeds, and generally swim at higher cruising speeds in comparison to rowers (Walker and Westneat, 2002; Wainwright et al., 2002) and are typically found at shallower depths away from the reef bottom with greater exposure to high energy wave-swept environments (Fulton et al., 2001; Bellwood and Wainwright, 2001). In comparison to rigid propulsors (no flexibility), a flexible propulsor will typically generate more thrust (Yamamoto et al., 1995; Zhu and Shoele, 2008; Young et al., 2009). Yet, high degrees of propulsor flexibility that result in extreme bending magnitudes can reduce thrust production and propulsive efficiency (Liu and Bose, 1997; Heathcote et al., 2008). Within this window of advantageous propulsor flexibility, Tangorra et al. (2010) showed in a biorobotic pectoral fin model that propulsive forces increase with increasing fin ray stiffness. Our result, that flappers employ pectoral fins nearly an order of magnitude stiffer than rowers, suggests that increased fin stiffness is one trait that flapping species have evolved to help increase thrust production and mechanical efficiency in comparison to rowing species (Walker and Westneat, 2000, 2002). In comparison to more flexible finned species, the stiff fins of flapping species provide the increased efficiency and propulsive force necessary to cruise through high-energy wave swept environments.

In contrast to flapping species, rowing species are capable of higher acceleration and thrust production at low speeds, hypothesized to achieve greater maneuverability (Walker and Westneat, 2002; Wainwright, 2002), and are typically found at greater depths close to the reef surface with calmer water flow patterns (Fulton et al., 2001; Bellwood and Wainwright, 2001). Fishes are capable of actively controlling the shape and curvature of their fins (Videler, 1977; Geerlink and Videler, 1987; Alben et al., 2007). We suggest that the greater pectoral fin

flexibility of rowers in comparison to flapping species will allow them to generate three-dimensional fin topographies to maximize their drag coefficient, and have finer control over a wide range of the thrust vectors generated during the powerstroke, thus allowing them greater maneuverability. It is not surprising that species employing flexible pectoral fins are found close to the reef bottom where they can take advantage of high accelerations and maneuverability as they traverse the complex substrate to avoid predators and feed. Interspecific variation in fin ray stiffness is thus associated with interspecific variation in swimming performance and exemplifies the impact morphological variation can play in driving niche occupation.

Conclusion. These results broaden our understanding of fin diversification, and highlight the critical role of fin stiffness in the transmission of forces externally to the water. In combination with previous comparative work on fin ray flexural stiffness in the Labridae (Aiello et al., 2017b), the results presented here show that interspecific differences in pectoral fin flexural stiffness broadly correspond to the behavioral phenotypes of rowing and flapping swimming (Fig. 1a, 6a) and provide a mechanical explanation for the performance tradeoffs in thrust production and maneuverability. Future work should focus on measuring the fin stiffness fields of species using intermediate swimming behaviors as well as rowers and flappers known to be exceptions to the typical habitats occupied by these swimming modes (Fulton et al., 2001; Bellwood and Wainwright, 2001); this future work may reveal additional morphological features that enable fish to maintain both high efficiency and maneuverability. The existence of many extant species employing different degrees of intermediate swimming modes along the rowing-flapping swimming behavior continuum could help shed light on the complex selective pressures and evolutionary dynamics that drive correlated changes in fin shape and mechanical properties.

CHAPTER 4: A COMPARISON OF PECTORAL FIN RAY MORPHOLOGY AND ITS IMPACT ON FIN FLEXURAL STIFFNESS IN LABRIFORM SWIMMERS

Abstract

The propulsive capabilities of appendages used in aquatic locomotion are influenced by the mechanical properties of the tissues forming the appendage. In the fish family Labridae, pectoral fin flexural stiffness is tuned to swimming behavior, where fins range on a continuum from stiff wing-like fins to relatively flexible broad fins. In species on both ends of the spectrum, pectoral fin flexural stiffness decreases exponentially along the length of any given fin ray, and ray stiffness decreases along the fin's chord from the leading to trailing edge. In this study, we examine the impact of fin ray morphological parameters such as The effective modulus in bending (E), second moment of area (I), segmentation and branching patterns on fin stiffness. We quantify intrinsic pectoral fin ray stiffness in similarly sized fins of two closely related species that employ fins of divergent mechanics, the flapping *Gomphosus varius* and the rowing *Halichoeres bivittatus*. While segmentation patterns and E were similar between species, measurements of I and the number of fin ray branch nodes were greater in *G. varius* in comparison to *H. bivittatus*. A multiple regression model found that of these variables, I was always significantly correlated with fin ray flexural stiffness and that variation in I always explained the majority of the variation in flexural stiffness. This study examines the relationship between fin ray form and function and finds that while most of the morphological variables quantified in this study correlate with a fin ray's flexural stiffness, second moment of area is the greatest factor contributing to variation in flexural stiffness. The comparison of these results to

other systems begins to unveil fundamental morphological features of biological beams and yields insight into the role of mechanical properties in fin deformation for aquatic locomotion.

Introduction

The ability of a flexible locomotor appendage to deform in response to a load greatly impacts its propulsive capabilities. In the large morphologically and behaviorally diverse group of coral reef fishes, the family Labridae, pectoral fin flexural stiffness is tuned to swimming behavior (Aiello et al., 2017a; Aiello et al., 2017b). Labrids employ pectoral fin-based propulsion ranging from rowing to flapping, where rowing species use relatively flexible broad fins to perform drag-based propulsion for high maneuverability and flapping species use stiff wing-like fins to perform lift-based propulsion that maximizes thrust and mechanical efficiency. While flappers employ stiffer fins than rowers, a common spatial distribution of flexural stiffness along the fin ray and across the fin chord exists among species belonging to both behavioral groups. Fin ray flexural stiffness decreases exponentially along the length of any given fin ray, and ray stiffness decreases along the fin chord from the leading to trailing edge. The existence of multiple levels of variation in fin stiffness (within a single ray and between rays, individuals, and species) (Tangorra et al., 2010; Lauder et al., 2011; Aiello et al., 2017a; Aiello et al., 2017b) raises questions of how differences in fin stiffness are achieved through the variation and distribution in fin ray geometry, material properties, segmentation and branching throughout the fin.

The fin rays of fishes can be thought of as biological beams, and principles from engineering can be used to study biological systems. For a continuous beam composed of a homogeneous material, flexural stiffness, or resistance to bending, is quantified as the product of

Young's modulus (E) and second moment of area (I) (Vogel, 2003b; Young et al., 2012). However, the conditions in which to measure flexural stiffness (i.e. material must be homogeneous, isotropic, linearly elastic) are rarely met for biological materials, and other variables must be taken into account to provide a better understanding of how the underlying morphological features of a biological structure impact its flexural stiffness. Pectoral fin rays are made of two convex shaped hemitrichia that surround a core of collagen gel (Goodrich, 1904; Geerlink and Videler, 1987). Fin rays of active labriform swimmers are typically unsegmented along the proximal 40-60 % of their length and become both segmented and branched distally (Goodrich, 1904). Further, fin rays typically taper, decreasing in thickness along their proximodistal axis. Therefore, to get a more complete representation of the variables contributing to the multiple levels of fin stiffness variation discussed above, in addition to E and I, fin ray morphology needs to be taken into account.

The relationship between fin ray form and function has rarely focused on the mechanical properties of the system (Taft, 2011; Taft and Taft, 2012). Two studies that have examined this relationship have focused on a fin ray's second moment of area I (Taft and Taft, 2012), or examined the impact of a fin ray's unsegmented length on the magnitude and location of curvature achieved through the active relative displacement of a ray's paired hemitrichia (Taft and Taft, 2012). A different study measured the proximal and distal flexural stiffness, Young's modulus, and second moment of area of multiple fin rays of the bluegill (*Lepomis macrochirus*) pectoral fin (Lauder et al., 2011), but the relationship between these three variables was not described. Very few studies have quantified the percent of a fin ray that is unsegmented (Taft and Taft, 2012; Flammang et al., 2013) or average segment length (Lundberg and Marsh, 1976), and, to our knowledge, the number of segments per unit length and the anatomical branching

patterns of propulsive fins remain to be explored, although their impact on performance has been hypothesized (Marsh, 1977).

In other systems for which stiffness plays an important functional role, the relationship between flexural stiffness and one or more of these morphological features has been investigated. Variation in flexural stiffness along the length of cockroach antennae (Mongeau et al., 2014), bird feather shafts (Bachmann et al., 2012), fish ribs (Horton and Summers, 2009), and rat whiskers (Williams and Kramer, 2010) are all predominantly due to changes in geometry rather than material properties. Additionally, interspecific differences in the material properties of homologous bones (Currey, 2002) and the rachis of feathers (Macleod, 1980) have evolved, presumably to meet the mechanical demands of different species. Further, the Young's modulus of the rachis of feathers (Macleod, 1980) and rat vibrissa (Quist et al., 2011) are reported to increase along their length, which will impact local flexural stiffness.

In serially segmented biological beams, a relationship between the number of joints per unit length (joint density) and flexural stiffness has not been found. In crinoid arms, increases in joint density were associated with decreases in flexural stiffness, but there was no significant relationship between these two variables in crustacean antennae, despite the antennae possessing more than two times the number of joints than a crinoid arm of the same length (Etnier, 2001). Interestingly, in both examples, despite the presence of segments, appendage diameter was the strongest influence on its flexural stiffness (Etnier, 2001). To our knowledge, these are the only two systems where the relationship between joint number and flexural stiffness has been explored.

In this study, we examine the relationship between pectoral fin ray morphology and flexural stiffness in a pair of closely related species (within the same subfamily) that employ

different swimming behaviors, the stiff-finned flapper, *Gomphosus varius*, and the flexible-finned rower, *Halichoeres bivittatus*. The central goal of this study is to probe the relationship between the flexural stiffness and morphology of pectoral fin rays across species and swimming behaviors, and to quantify fin ray segmentation and branching patterns in search of associations between morphology, mechanical properties and propulsive function. We set out to assess how variation in *I*, *E*, segmentation and branching patterns combine to produce the overall stiffness field across the pectoral fin surface. The stiffness field of a fin is hypothesized to be a key factor in the mechanism of thrust production for efficient forward locomotion and maneuverability in fishes with varying fin designs. This study broadens our understanding of fin ray design principles and begin to uncover the variation and similarities that exist between species, swimming behaviors, and ecologies. Additionally, a better understanding of the different morphological features that impact a fin's flexural stiffness can be used to inform the design of underwater robotic propulsors.

Materials and Methods

Fish specimens. Fishes were obtained commercially and maintained in 80-200L saltwater (34.51 ppt) aquaria under 12:12 day:night light cycles with a mean water temperature of 23.5°C. Fish were euthanized in a .05g/$^{l-}$ solution of MS-222 ((Tricaine methanesulfonate, Sigma-Aldrich, St. Louis, MO) and their right pectoral fins were excised from their body, immediately placed in extracellular solution to maintain cell survival and structural integrity. Pectoral fin rays 1 (leading edge), 5 (M1), 10 (M2), and 14 (trailing edge) of *Gomphosus varius* and 1 (LE), 5 (M1), 8 (M2), 12 (TE) of *Halichoeres bivittatus* were used in this study for flexural stiffness (see Aiello et al., 2017a,b) and morphology data collection. All experimental procedures, housing,

and euthanasia methods were carried out under University of Chicago Institutional Animal Care and Use Committee guidelines (protocol 72365 to M.W.W.).

Fin ray flexural stiffness. Flexural stiffness data collection followed previously published methods (Aiello et al., 2017a,b). Briefly, flexural stiffness, which is the product of Young's modulus (E) and second moment of area (I), was calculated a single variable using beam theory (Vogel, 2003). Flexural stiffness was calculated using the following equation: $EI = F(d^3)/48Y$ where Y is vertical displacement of the fin ray in response to an applied force, F, and d is the distance between the supports of the three-point bending apparatus. Three-point bending tests were conducted at the center of the proximal (16.67% ray length), middle (50% ray length), and distal (83.25% ray length) one-thirds of each fin ray using a materials testing machine (LS1, Lloyd Instruments, Fareham, UK) equipped with a 50N load cell (minimum load resolution = 0.0001N). Nexygen Plus (Lloyd Instruments, Fareham, UK) software was used to acquire the data

Fin ray morphology. We examined pectoral fin ray morphology in a subset of the individuals used in a previous study on fin mechanics (Aiello et al., 2017a). For the analysis of fin ray second moment of area, five *Gomphosus varius* (mass range 10.7 – 36.8 g; mean = 22.16±11.85 g) and six *Halichoeres bivittatus* (mass range 10.8 – 36.1 g; mean = 17.33±9.62 g) were chosen so there were no significant differences in the size of the fish used in this study (p=0.474). Of these fishes, the four most closely size-matched individuals from each species were chosen for the analysis of fin ray segmentation and branching, and were the individuals used in all bivariate and multivariate amylases (*Gomphosus varius* mass range 10.9 – 36.8 g, mean ± standard

deviation = 25.03±11.51 g; *Halichoeres bivittatus* mass range 12.1 – 36.1 g. mean ±standard deviation = 20.43±10.77 g). There were no significant differences in the size of the fish used in these analyses (p=0.581).

To quantify pectoral fin ray morphology we placed the four excised fin rays from the fin of each individual used for mechanical property testing on a flat plate under a Leica MZFLIII dissecting microscope (Leica Microsystems, Buffalo Grove, IL) mounted with an Olympus DP72 camera (Olympus Camera, Center Valley, PA). Images of each fin ray laid flat on its medio-lateral surface were collected and analyzed to measure its width and laid on its side to measure its depth (thickness).

Fin ray width and depth were measured at the center of the proximal (16.67% ray length), middle (50% ray length), and distal (83.25% ray length) one-thirds of each fin ray using NIH ImageJ 1.62 (NIH, Bethesda, MD, USA). These are the same locations flexural stiffness was measured in the related study (Aiello et al., 2017a). We modeled the fin ray as a rectangular beam, and calculated second moment of area at the proximal, middle, and distal measurement site for each fin ray using the following equation: $I = (\text{width} * (\text{thickness}^3))/12$. These measurements were repeated using digital calipers to ensure accuracy. Since flexural stiffness is a product of its material's Young's modulus (E) and its second moment of area (I) (Gordon, 1978; Vogel, 2003b), we divided each flexural stiffness measurement by I to obtain the effective modulus in bending, E, which is representative of the composite material properties at each location of a given fin ray.

Fin rays were then fixed overnight in 10% buffered formalin, stepped into a 0.3% KOH solution, and mixed with 1-2 drops of 30% hydrogen peroxide per 100millileters of solution to remove skin pigmentation. Fin rays were then stained in calcein solution following published

methods (Haga et al., 2010) or cleared and stained with alizarin red following published methods (Dingerkus and Uhler, 1977; Potthoff, 1984). Each fin ray's medio-lateral surface was photographed under fluorescent light to aid in the visualization of segmentation. Images were imported into NIH ImageJ, and total fin ray length, unsegmented length, the number of

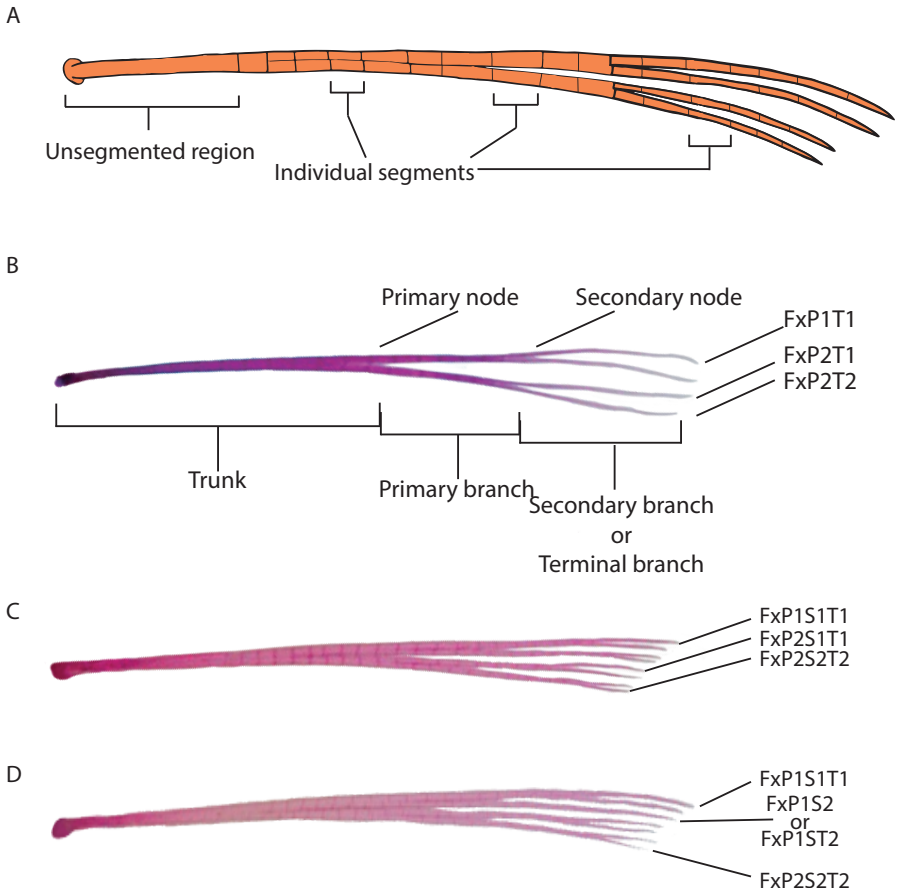

Figure 4.1. Fin ray segmentation and branching methodology.
(A) A fin ray schematic from the pectoral fin of *Gomphosus varius* with the unsegmented region and three individual segments labeled. (B) An image of the fifth fin ray from the pectoral fin of *H. bivittatus* with fin ray trunk, primary branch, and secondary branch labeled. For this particular fin ray, the secondary branch is also the terminal branch. (C) An image of the fifth fin ray from the pectoral fin of *G. varius* with an example of our proposed branch name scheme where F3P1S1T1 represents the first terminal branch from the first secondary branch from the first primary branch of fin ray three. (D) A second example of the proposed fin ray branch naming scheme on a fin ray with a different branching pattern. In general, a comparison of the fin ray presented in (B) with the fin rays presented in (C) and (D) exemplifies the difference in branching patterns between *H. bivittatus* (B) and *G. varius* (C,D).

segments, and the length of each segment were measured (Fig. 1a).

Fin ray branching was then digitized using the StereoMorph package (Olsen and Westneat, 2015) in R (R Core Team, 2012; Vienna, Austria). An additional specimen (beyond

the prior fins tested) per species was added to this analysis to obtain a larger sample size (N=5 for each species). These individuals both fell within the size range of the specimens used in this study (*Gomphosus varius* mass = 20 g; *Halichoeres bivittatus* mass = 25 g). Landmarks were placed at the proximal base of the fin ray, the point of separation for the primary and any secondary and tertiary branching events that occurred, and on the distal tips of each terminal branch (Fig. 4.1b-d). A custom analysis routine (A.M. Olsen) was then used to calculate the number of branch points (nodes), span-wise distance between the base and the primary node, and span-wise distance between each subsequent node. We used this data to find the fin ray branching index, which was calculated for each fin ray by dividing the sum of all branch lengths by mean branch length.

Statistics. Bivariate regressions were conducted to determine whether significant relationships exist between each of the independent variables (*E*, *I*, percent unsegmented, number of segments divided by fin ray length, average segment length, and number of branch point nodes) and the dependent variable, flexural stiffness, at the proximal, middle, and distal measurement locations of the four equally spaced fin rays from each individual of each species. Next, to determine the relative effects of each independent variable on fin ray flexural stiffness at the proximal, middle, and distal measurement location, a multivariate standard least squares regression model was conducted. In each model, all variables were standardized to z-scores and beta coefficients were used to measure the relative effect of each independent variable on flexural stiffness. Further, student t-tests were used to test for interspecific significant differences in the magnitude of independent variables. Multivariate and bivariate analyses were performed in JMP v. 9.0.1 (SAS, Cary, NC, USA) and t-tests were performed in R (R Core Team, 2012; Vienna, Austria).

Results

Second moment of area and The effective modulus in bending . Fin ray second moment of area (*I*) was measured at three points along the span of each fin ray, which correspond to the same locations flexural stiffness was measured in Aiello et al. (2017): the proximal (16.65% fin ray length), middle (50.00% in ray length), and distal (83.34% in ray length) locations. In both *G. varius* and *H. bivittatus*, a significant exponential relationship ($p<0.05$) was found between *I* and fin ray position, where *I* decreased along the proximodistal axis of each fin ray (Fig. 4.2a). *I* ranged from $1.31 \bullet 10^{-17}$ to $1.32 \bullet 10^{-14}$ and $2.21 \bullet 10^{-18}$ to $1.71 \bullet 10^{-15}$ m^4 in *G. varius* and *H. bivittatus*, respectively. *I* was nearly an order of magnitude greater in *G. varius* ($1.32 \bullet 10^{-14} \pm 0.226 \bullet 10^{-14}$ – $1.44 \bullet 10^{-16} \pm 0.802 \bullet 10^{-16}$ m^4) compared to *H. bivittatus* ($0.17 \bullet 10^{-14} \pm 0.0601 \bullet 10^{-14}$ – $0.277 \bullet 0^{-16} \pm 0.102 \bullet 10^{-16}$ m^4) and those differences became smaller with increasing % fin ray length (Fig. 2a). *I* was significantly greater at the proximal location (16.65% fin ray length) in *G. varius* compared to *H. bivittatus* for the leading edge (LE), middle 1 (M1), and trailing edge (TE) fin rays (Table S4.1). Interspecific significant differences in *I* were also found at the middle location (50% fin ray length) for two of four comparisons (LE and TE), but no significant differences in *I* were found at 83.34% fin ray length (Table S4.1).

The effective modulus in bending was also calculated at the proximal (16.65% fin ray length), middle (50.00% in ray length), and distal (83.34% in ray length) measuring points in all four fin rays for each species. Similar ranges of *E* were found across both species (*G. varius*: 0.021 – 0.958 GPa; *H. bivittatus*: 0.046 – 0.980 GPa; Fig. 4.2b) and no significant differences were found between species ($p>0.05$; Table S4.2). In both species, the average *E* was greatest at the distal location (83.34% fin ray length), and *E* was significantly greater at the distal location

(83.34% fin ray length) compared to the proximal location (16.65% fin ray length) in five of eight fin rays across both species (Table S4.2). It is also important to note that are values of *I* are likely small overestimations (<10%) because we modeled the fin ray as a solid beam; hollow beams of the same dimensions will have a smaller *I*. Therefore, our calculations of *E* are likely slightly lower than their actual value, but we estimate that this error is no greater than 10% based on the differences in the equations to calculate *I*.

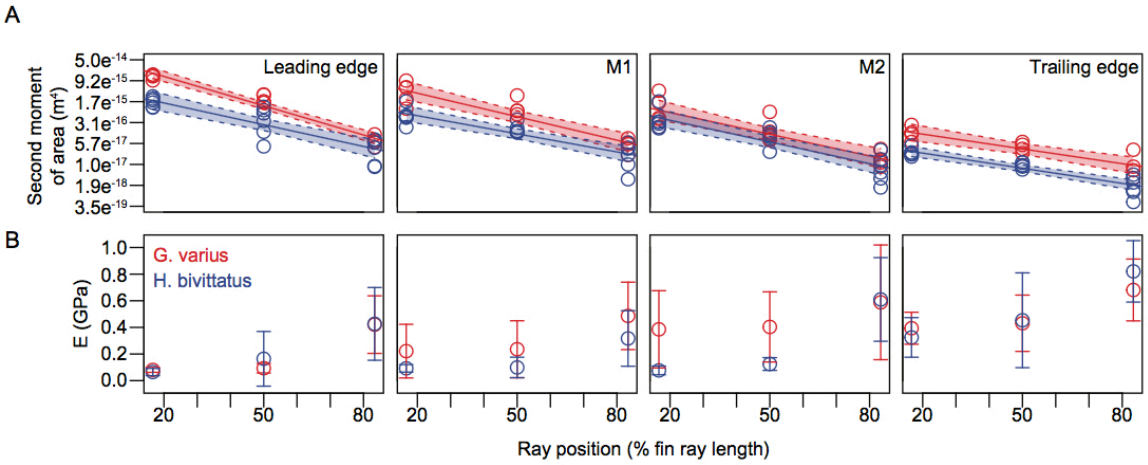

Figure 4.2. The second moment of area and material properties of fin rays along their length.
(A) Second moment of area (I) decreased exponentially along the span of each fin ray in both species. The average I was always greater in *G. varius* in comparison to *H. bivittatus* at each measurement location and was significantly great in five of twelve comparisons. As expected, since flexural stiffness is not significantly different between species at the distal measurement location, second moment of area was also never significantly different at the distal measurement location between species. (B) Fin ray *E* ranged from 0.022 to 0.980 GPa across the two species and there were no significant differences in the absolute range of *E* between fin rays or species. In both species for each fin ray, the average E was greater at the distal measurement in comparison to the proximal measurement and was significant in five of eight comparisons. Red = *G. varius*; blue = *H. bivittatus*.

Fin ray segmentation and branching patterns. The segmentation patterns of the pectoral fin rays were similar in the two species, but the fin ray branching pattern showed major differences between species. In both species, the percentage of the total fin ray length that was unsegmented (unsegmented length) was greatest in the leading edge and least in the trailing edge (Fig. 4.3a; Table S4.3). Across fin rays, unsegmented length ranged from 38.014 ± 15.954 to 18.731 ± 6.977 % fin ray length in *G. varius* and 37.949 ± 1.927 to 28.354 ± 4.581 % fin ray length in *H.*

bivittatus. After alpha was Bonferroni corrected to 0.0125, there were no significant differences in unsegmented length between species for any comparison between the same fin rays.

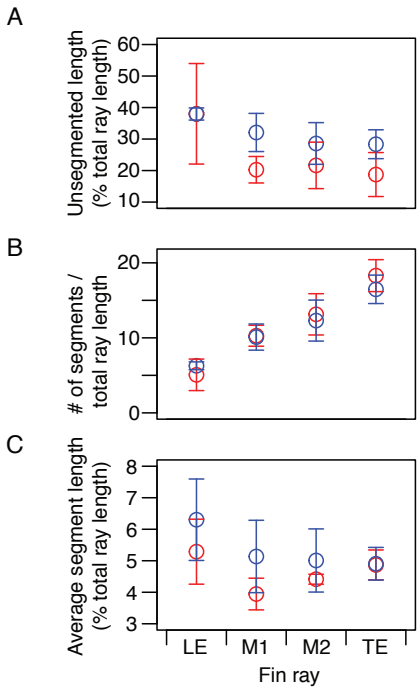

Figure 4.3. Summary of fin ray segmentation. (A) Unsegmented length decreases along the chord of the pectoral fin in both species from the leading to trailing edge. The average unsegmented length of each fin is similar between species, but is significantly greater in *H. bivittatus* in comparison to *G. varius* for the M1 fin ray ($p = 0.018$). (B) The size corrected number of segments per fin ray increased across the chord of the pectoral fin from leading to trailing edge in both species and there we never significant interspecific differences for any fin ray. (C) In *H. bivittatus*, average segment length decreased along the chord from the leading to trailing edge, and in *G. varius*, average segment length decreased between the leading edge and M1 and then increased slight from M1 across the chord to the trailing edge. There were never significant differences between species for any fin ray.

Trends in the size corrected number of segments per fin ray (numbers of segments / fin ray total length) were nearly identical between species for each fin ray (Table S4.3). In each species, the number of segments per centimeter per fin ray increased from the leading to trailing edge (Fig. 4.3b). Across both species, the number of segments divided by fin ray length ranged from 2.290 to 7.393 in the leading edge and 14.069 to 20.238 in the trailing edge. There were no significant differences between species in the number of segments divided by fin ray length of any fin ray.

There were no significant differences between species for any fin ray's average segment length. In both species, the leading edge contained segments of the largest average length: 4.978±0.857 and 6.054±1.221 % fin ray length for *G. varius* and *H. bivittatus*, respectively (Fig. 4.3c; Table S4.3). In *G. varius*, the M1 fin ray had segments of the smallest average length and average segment length increased from the M1 ray (3.890 ± 0.463) to the trailing edge (4.852 ± 0.513). In *H. bivittatus*, average segment length also decreased from the leading edge to the M1 ray, but plateaued from ray M1 (4.939 ± 1.001) to the trailing edge (4.857 ± 0.554).

In contrast to fin ray segmentation, fin ray branching shows a strong species-specific pattern. Fin ray branching patterns were compared intraspecifically (between individuals and fin rays) and between species. In both species, the leading edge fin ray was not branched and there was little variation in branching pattern between non-leading edge fin rays within a single individual or between the individuals of a species. However, there was significant variation in non-leading edge fin ray branching patterns between species. In *H. bivittatus*, all non-leading edge fin rays branched at least one time to form two primary branches. In larger individuals of *H. bivittatus*, both of the primary branches branched again to produce three total branch nodes and a total of four terminal secondary branches (Fig. 4.1b). In one case there were only two branching nodes and the trailing edge primary branch did not branch a second time. In the M1 and M2 fin rays of *G. varius* there was a minimum of three branch nodes (four terminal branches) in all individuals, and larger individuals exhibited six or seven nodes with either seven or eight terminal branches, respectively (Fig. 4.1c). In fin rays with only six nodes, the trailing edge branch from the secondary node of the trailing edge primary branch was usually the secondary branch that remained unbranched (Fig. 4.1d), but in one case the trailing edge branch from the secondary node of the leading edge primary branch

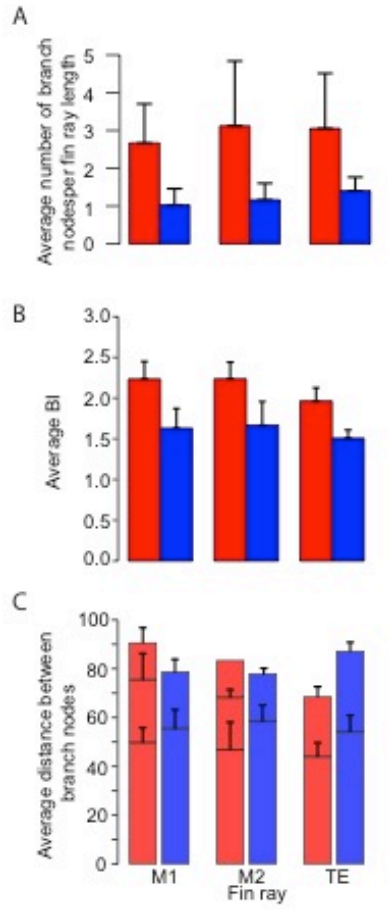

Figure 4.4. Summary of fin ray branching patterns.
In both species, there was no trend between fin ray and the (A) average number of branch nodes per fin ray length or (B) the average branching index (BI). In all cases, the average number of branch nodes per fin ray length and the average BI was significantly greater in *G. varius* in comparison to *H. bivittatus*. (C) The relative distance between the base and the first branch node is not significantly different between species ($p>0.05$), and for fin rays M2 and TE, the secondary branching event occurred significantly more distal along the length of the fin ray in *H. bivittatus* in comparison to *G. varius* ($p<0.05$).

was the secondary branch that remained unbranched. The trailing edge fin ray of *G. varius* always had either two or three branching nodes to produce a total of three or four terminal branches. Finally, while there is a noticeable and predictable increase in the number of branch nodes in larger individuals of each species, the number of branch nodes did not have a correlation with fin ray length or an individual's standard length ($p>0.05$) because of the punctuated relationship between branching events and body size, where new branching events occur at different body size intervals.

To summarize and quantify differences in branching patterns between species, we calculated the number of branch nodes and a branching index (BI), which is calculated as the sum of all branch lengths divided by mean branch length, for each fin ray (Table S4.4). There were always a significantly greater number of branching nodes per fin ray in *G. varius* in comparison to *H. bivittatus* (Fig. 4.4a). The number of branch nodes per fin ray length slightly increased from the M1 to trailing edge fin ray in both species. The number of branch nodes per fin ray length ranged from 2.667 ± 1.038 to 3.05 ± 1.460 in *G. varius* and from 1.028 ± 0.431 to 1.402 ± 0.362 in *H. bivittatus*. We also measured a fin ray's degree of branching through the calculation of a branching index, which is a unitless number that can be a minimum of one (no branching) and has no maximum. A fin ray that branches but only near the tip would have a BI just greater than one because it is mostly a single path. A fin ray that frequently branches along its length would have a higher BI. Similar to the number of branching nodes per ray, each ray also had a significantly larger BI in *G. varius* in comparison to *H. bivittatus* (Fig. 4.4b). BI ranged from 1.964 ± 0.163 to 2.234 ± 0.216 in *G. varius* and from 1.507 ± 0.102 to 1.630 ± 0.242 in *H. bivittatus* (Table S4.4).

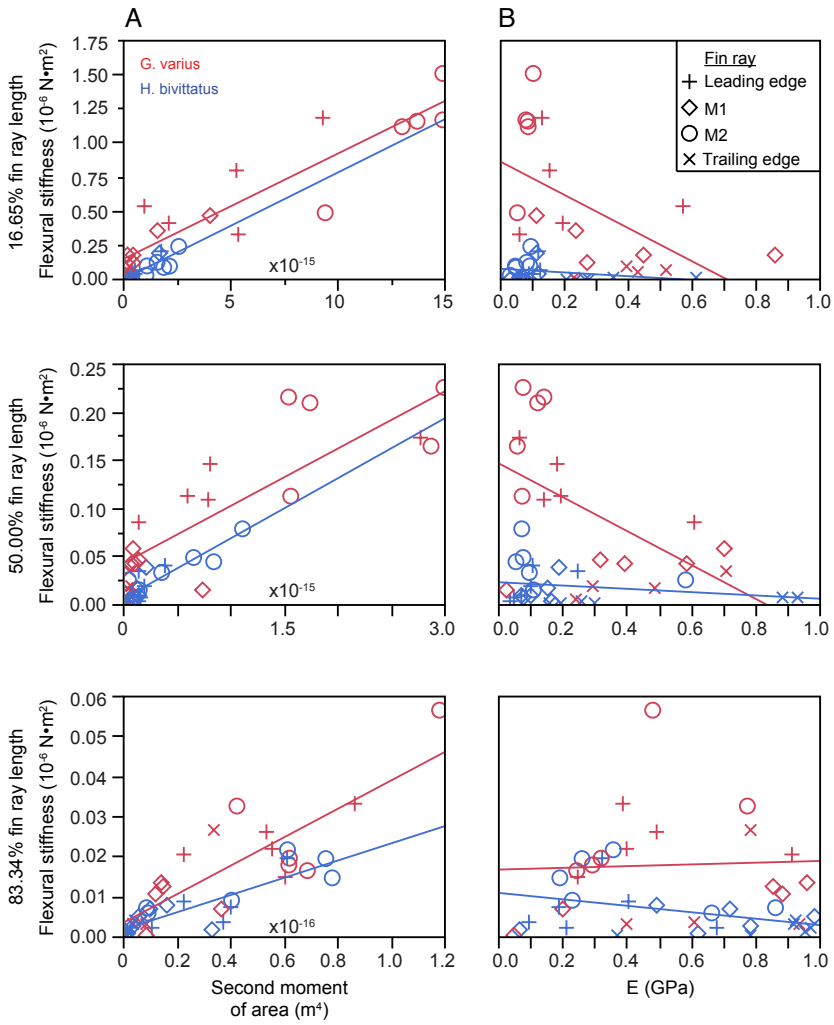

Figure 4.5. The bivariate relationships between flexural stiffness and second moment of area (A) and material properties (B). Second moment of area (I) was significantly correlated with flexural stiffness at all three measurement locations in both species (p<0.0001). The effective modulus in bending (E) was only significantly correlated with flexural stiffness in *G. varius* at the proximal (p=0.3177) and middle (p=0.2150) measurement locations.

The distance to the first branching point and distances between all subsequent branching points were measured for all four fin rays of interest in each species. In *G. varius*, the average distance between the base and the first branch node was 49.74 ± 5.89, 46.75 ± 11.12, and 43.98 ± 5.52 % fin ray length for fin ray M1, M2, and TE, respectively. The average distance between branch nodes one and two and two and three for each ray can be seen in Table S4.5. In *H. bivittatus*, any given branching event (node 1 or 2) always occurred more distally along the fin

ray (% fin ray length) in comparison to the same branching event in *G. varius* (Fig. 4.4c). Because branching patterns exhibited consistent intraspecific similarity and interspecific

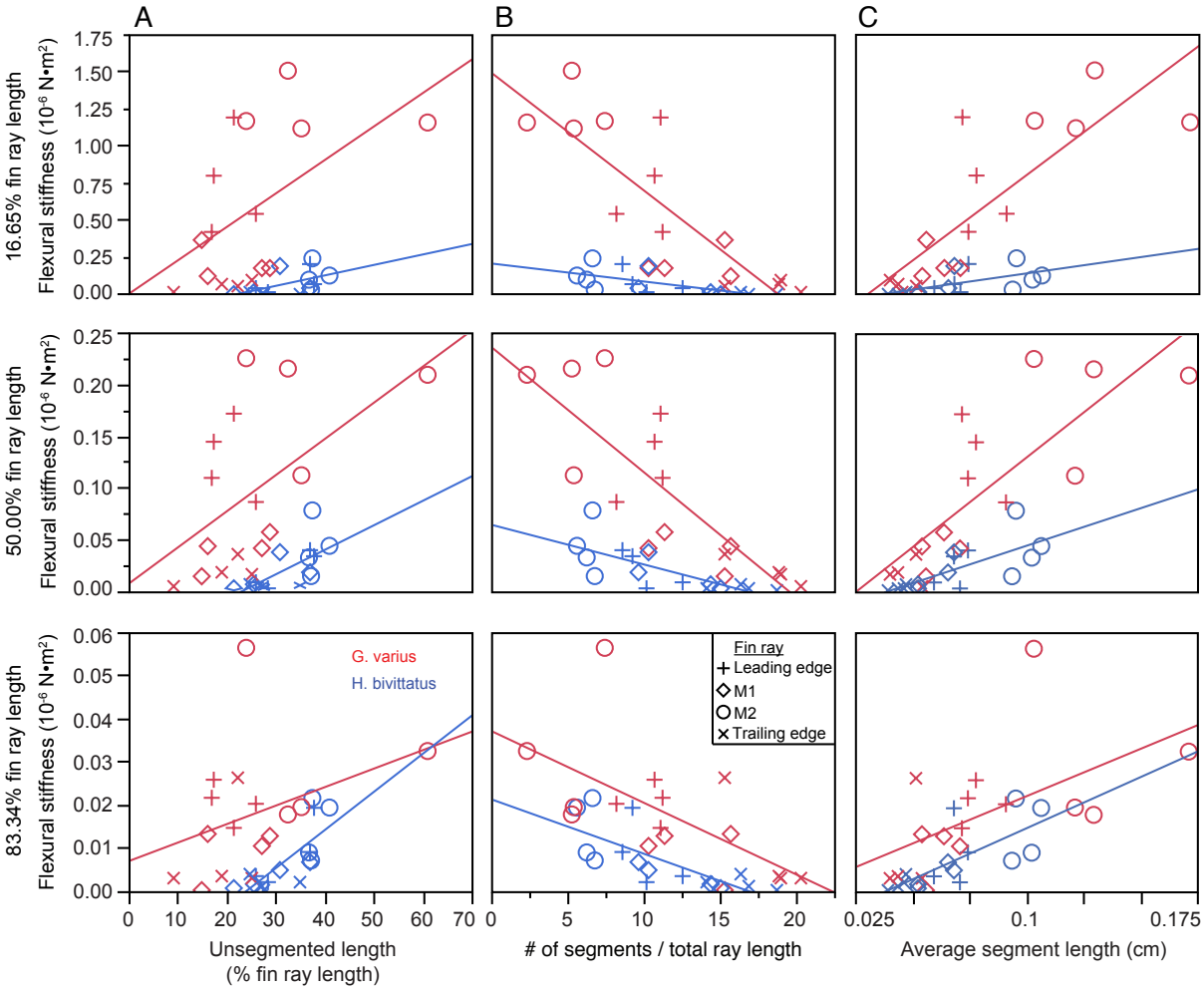

Figure 4.6. The bivariate relationships between flexural stiffness and patterns of segmentation. Each variable was significantly correlated with flexural stiffness at each measurement location (p<0.05) with the exception of the correlation between unsegmented length and flexural stiffness at the distal measurement location in *G. varius* (p=0.1673).

differences, the relationship between branching patterns and fin ray flexural stiffness was not examined in the statistical analyses below.

Bivariate analyses. All measured variables other than E (I, unsegmented length, number of segments / fin ray length, and average segment length) were significantly correlated with flexural

stiffness the proximal and middle measurement locations (Table S4.6). All measured variables other than *E* and unsegmented length were significantly correlated with flexural stiffness at the distal (83.34%) fin ray location (Table S6). For both species, there was a positive and significant relationship between *I* and flexural stiffness ($p<0.0001$, Fig. 4.5a, Table S4.6). There was no consistent relationship between *E* and flexural stiffness (Fig. 4.5b; Table S4.6); however, in two instances for *G. varius* (proximal and middle locations) there was a negative and significant relationship between *E* and flexural stiffness ($p=0.012$ and 0.015, respectively). Furthermore, in both species, the relationship was always positive between flexural stiffness and both unsegmented length and average segment length (Fig. 6), and these relationships were significant ($p<0.05$) in all cases other than for the correlation between unsegmented length and flexural stiffness at the distal location in *G. varius*. Finally, in both species, the relationship between the number of segments divided by fin ray length and flexural stiffness was negative and significant at all fin ray locations ($p<0.01$, Fig. 4.6, Table S4.6).

Multivariate analyses. A multivariate analysis was used to assess the relative influence that each independent variable (morphological traits) has on the dependent variable (flexural stiffness) for each species at all three fin ray locations (proximal, middle and distal). We performed two standard least squares multiple regressions where each model included different parameters. The results were highly consistent across models (Table S4.7). Model one only included the standardized independent variables, and model two included a cross to account for interaction effects between *E* and *I*. Table S4.7 quantifies the results of each model. Across both models, *I* was always significantly correlated with and explained the most variation in flexural stiffness in comparison to all other independent variables. The beta coefficient of *I* was always at

least six times greater than the next largest beta coefficient, which typically (in 11 of 12 instances) corresponded to the variable *E*. In the most basic model, *E* was also significantly correlated with flexural stiffness in both species at distal location (83.34% fin ray length). The addition of the interaction effect in the second model resulted in *E* being significantly correlated with flexural stiffness in both species at each fin ray length, but the *E* beta coefficient always remained less than that of *I*. This means that while *E* does not always have a direct effect on flexural stiffness, through *E*'s interaction with *I*, *E* and flexural stiffness have a positive and significant relationship. Finally, both models found a significant correlation between average segment length and flexural stiffness for *H. bivittatus* proximally, and the second model also found a significant correlation between the number of segments divided by fin ray length and flexural stiffness for *H. bivittatus* at this location. However, the beta coefficients of these variables, and therefore the amount of the variation in flexural stiffness that they explain, were negligible in comparison to *I* (Table S4.7).

Discussion

The purpose of this study was to determine the relationship between features of fin ray morphology and pectoral fin stiffness. As a case study, we compared fin ray morphology and flexural stiffness in two closely related species of Labridae that employ different swimming behaviors and utilize fins of significantly different stiffness. In both the stiff-finned flapper, *G. varius*, and the flexible finned rower, *H. bivittatus*, the second moment of area *I*, the number of segments divided by fin ray length, and average segment length were significantly correlated with flexural stiffness along the fin span from proximal to middle and distal locations. In all cases, multivariate analyses revealed that variation in *I* explained the majority of the variation in

fin ray stiffness in both species. Significant differences in *I* and fin ray branching patterns were found between species, which suggests the importance of these mechanical features for pectoral fin propulsive capability. These results broaden our understanding of fin ray form and function and also inform the design of biologically inspired underwater propulsors.

The material properties of fin rays. The Effective modulus in bending (*E*) of pectoral fin rays was similar between fin rays across the fin, individuals, species, and similar to the properties of biomaterials such as feather and bone in other locomotor systems. Fin ray *E* ranged from 0.022 to 0.980 GPa across the two species. The lack of significant differences in the absolute range of *E* between fin rays or species is consistent with the interspecific ranges of *E* in bird feathers (Bonser and Purslow, 1995). The range of *E* reported here is similar to that of the pectoral fin rays of bluegill sunfish, which had an average and standard deviation of 1.34 ± 1.40 proximally and 0.38 ± 0.28 distally (Lauder et al., 2011), as well as the *E* of tendon, a uniform arrangement of collagen, from a variety of mammal species, which is approximately 1.5 GPa (Bennett et al., 1986). The *E* of the fin rays in this study is lower than values reported for the keratin of a bird feather's rachis (4.14 – 6.93 GPa), rat vibrissae (3.34 ± 1.48 GPa), individual collage fibers (5 – 11.5 GPa), acellular fish bone (3.67 – 8.40 GPa), and vertebrate cellular bone (6.7 – 34.1 GPa) (Currey, 2002; Wenger et al., 2007; Horton and Summers, 2009; Quist et al., 2011; Bachmann et al., 2012).

Fin rays are composite structures made of multiple materials. In addition to the two hemitrichs of a fin ray that are made of acellular bone and surround an inner core of collagen gel, collagen fibrils run perpendicular to the long axis of a fin ray between opposing hemitrichs as well as parallel to the segments (Montes et al., 1982; Becerra et al., 1983), and elastic fibers

connect adjacent segments (Haas, 1962). It is not possible to determine the contribution of each material in a fin ray to the composite *E* calculated in this study. The contribution of multiple materials and the effect of a material's fiber orientation to fin ray *E* and overall flexural stiffness needs to be tested further. Yet, the *E* of fin rays in this study is considerably less that that of a fish's acellular bone (Horton and Summers, 2009), and is more similar to that of tendon (Bennett et al., 1986). This suggests that although fin rays contain acellular bone, their material properties are strongly influenced by the fibrous and collagenous materials of the fin.

The fin rays examined in this study showed trends of a greater *E* at the distal (83.34%) location in comparison to the proximal (16.65%) fin ray location (Fig. 2b, Table S2). Similar results have been found in other systems utilizing tapering, anisotropic, biological beams. In rat vibrissae and the rachis of bird feathers, which both geometrically taper from base to tip, *E* was greatest near the distal tip of vibrissae (Quist et al., 2011) and rachis (Macleod, 1980; Bonser and Purslow, 1995; Bachmann et al., 2012). A distal increase in the *E* of a beam while simultaneously reducing its cross sectional area could function to reduce its mass and size while maintaining greater stiffness; this strategy acts to ultimately reduce energy expenditure during movement, drag, and/or the effects of wear (Rayner, 1993; Bonser and Purslow, 1995; Bachmann et al., 2012).

The morphological and/or histological contribution to the distal increase in fin ray *E* (Table S4.2) is unclear. In rat vibrissae, the distal increase in *E* was associated with an increase in the fractional cross section of the vibrissa occupied by the cuticle (Quist et al., 2011). In fin rays, the distal increase of *E* could similarly be due to an increase in the percentage of the fin ray cross sectional area occupied by hemitrich (bone) relative to non-bone (vessels, nerves, collagen gel core). This could be achieved locally at the distal region of each fin ray, or this could result

as a by-product of fin ray branching producing more bone per total fin ray cross sectional area. The relationships between cross sectional area, branching pattern, and the percentage of a fin ray occupied by bone versus collagen will certainly have large effects on the distribution of stiffness and likely influence fin ray strength, toughness, and resistance to fatigue.

The impact of morphology on fin ray stiffness. The lack of intra- and inter-specific variation in *E* suggests that morphology, rather than intrinsic material properties, has a greater impact on the stiffness of a fin ray. *E* only correlated with flexural stiffness in two of six bivariate analyses (*G. varius* at proximal and middle locations), and the multivariate analysis conducted in each species only found a significant correlation between *E* and fin ray stiffness distally (Table S4.6, S4.7).

The geometry of a fin ray is the largest factor impacting its flexural stiffness. Fin ray *I* was always significantly correlated with fin ray stiffness (Fig. 4.2a, Table S4.7). Fin ray stiffness is significantly different between species at the proximal and middle measurement locations (Aiello et al., 2017b), and, in this study, *I* was significantly greater in *G. varius* at proximal and middle locations (16.65 and 50.00% fin ray length) in the majority of comparisons between species. Since distal flexural stiffness was not significantly different between these species (Aiello et al., 2017b), it is not surprising (rather it is expected) that *I* is not significantly different at this location either. The dominant influence of *I* in determining the flexural stiffness of a structure is consistent with results from other biological systems. Flexural stiffness is predominantly explained by variation in beam geometry (*I*) in cockroach antennae (Mongeau et al., 2014), bird feather shafts (Bachmann et al., 2012), fish ribs (Horton and Summers, 2009), crustacean antennae (Etnier, 2001), crinoid arms (Etnier, 2001), and rat whiskers (Williams and

Kramer, 2010). These results suggest that the modulation of the stiffness of a biological beam through geometric variation is a common theme in biology.

Variation in fin ray segmentation patterns does not necessarily relate to differences in flexural stiffness. While our study found that segmentation patterns are regularly correlated with fin ray stiffness, variation in segmentation patterns did not explain the majority of the variation in fin ray stiffness (Table S4.7). Variation in the number of segments, the length of segments, and the length of the unsegmented proportion of the fin ray has been characterized in different species (Lundberg and Marsh, 1976; Marsh, 1977; Taft and Taft, 2012). Taft and Taft (2012) measured sculpin pectoral fin ray curvature in response to the relative displacement of the two hemitrichia of a fin ray. Taft and Taft (2012) found that when opposing hemitrichs are displaced, the location of maximum bending occurs more distally in fin rays with a longer proximal unsegmented region, and that the *I* of a fin ray influenced fin ray curvature at 50% fin ray length, but not at more proximal or distal locations. Different from previous studies, our study measured passive (intrinsic) flexural stiffness through three-point bending tests. Despite these differences, the results presented here provide further support to Taft and Taft's (2012) hypothesis that variation in segmentation pattern significantly impacts fin ray function. Consistent with this hypothesis, we suggest that variation in fin ray segmentation patterns likely have the biggest impact in determining the magnitude and location of curvature along the length of a fin ray. Further, a serially multi-segmented beam will result in evenly distributed deformation along its length (Etnier, 2001). Therefore, variation in segmentation patterns (unsegmented length, average segment length, and number of segments divided by fin ray length) could have profound effects on the deformation of fin rays in response to actively (through the active displacement of a fin ray's hemitrichs by muscle activity) and passively generated curvature.

The distribution of variable segmentation patterns across a fin will also impact its passive deformation pattern in response to an externally applied force. The application of a force to a cantilever beam causes a bending moment that increases from the beam's tip to its base (Young et al., 2012). In a fin ray, the bending moment would be greatest most proximally where the fin ray articulates with the body. It is not surprising that the unsegmented portion of the fin ray corresponds to the region experiencing the greatest bending moment. The presence of a proximal unsegmented region, in addition to *I* being greatest proximally (Fig. 4.2), likely acts to help reduce the span wise bending of the ray and prevent fracture by increasing stiffness in this region. Additionally, all other variables being equal, an increase in the number of segments per fin ray length will result in a more even (uniform) distribution of deformation along the length of a beam (Etnier, 2001). In both species, we found that the average number of segments per fin ray increases from the leading to trailing edge of the fin (Fig. 4.3b), and the number of segments divided by fin ray length was inversely correlated with fin ray stiffness (Fig. 4.4b). Further, we found that the average percentage of a fin ray that is unsegmented decreases from the leading to trailing edge (Fig. 3a), and the length of the unsegmented region of a fin ray is correlated with fin ray flexural stiffness (Fig. 4a). Together, theory suggests that, in these species, span-wise fin ray deformation will become increasingly more uniform and evenly distributed along the length of a given fin ray across the chord of a fin from the leading to trailing edge.

The propulsive capabilities and maneuverability of a fin-based flapper are largely dependent on the kinematics and three-dimensional deformation of its flexible propulsor (Yamamoto et al., 1995; Daniel and Combes, 2002; Zhu and Shoele, 2008; Tangorra et al., 2010). Interray and interspecific differences in segmentation pattern could combine to ultimately tune deformation patterns across the fin and between species for more efficient locomotor

performance. Future studies will need to aim to combine high-resolution 3D fin topographic deformation patterns, detailed maps of fin ray mechanics and morphology, muscle activity patterns and their contribution to active fin ray curvature or stiffening, and reliable models of inertial and hydrodynamic moments acting on the fin to tease apart the variables responsible for the observed fin deformation patterns.

Fin ray branching patterns. Fin rays and/or spines are the primary structural support in all fins, and have important hydrodynamic functions. The dynamic changes in shape that occur across the surface of a pectoral fin during flapping or rowing locomotion are partly determined by the number of rays and their distribution of across the fin via fin ray branching patterns. We found that pectoral fin ray branching patterns exhibited consistent species-specific phenotypes and significant interspecific differences (Fig, 4; Table S5), leading us to conclude that fin ray branching patterns influence the stiffness field of fins and the apparent stiffness of the membranous webbing between adjacent fin rays and branches. In addition to *G. varius* employing a greater number of fin rays (15) in comparison to *H. bivittatus* (12), the pectoral fin rays of *G. varius* were significantly more branched in comparison to *H. bivittatus*. Previous work found that the percentage of pectoral fin area covered by fin ray (skeletal area), as opposed to fin membrane, is significantly greater in *G. varius* in comparison to *H. bivittatus* (Aiello et al., 2017a). Here we find that fin ray branching is also significantly greater in *G. varius* in comparison to *H. bivittatus* (Fig. 4). We suggest that, in addition to significant interspecific differences in fin ray geometry (*I*), interspecific differences in fin ray branching patterns are also contributing to differences in the pectoral fin stiffness field between these two species.

The evolutionary history and the genetic mechanism of fin ray branching are unknown. One possibility is that fin ray branching evolved as a mechanism to more evenly distribute the structure (fin ray) resisting deformation from the application of forces across the total area of the fin. In both species, and pectoral fins in general, fin area expands along its proximo-distal axis so that the distance between the leading edge and the trailing edge is much greater distally that it is at the proximal attachment of the fin with the body. In order to fill the expanding area along the proximo-distal axis of a fin it would require either the addition of more fin rays, which is limited by the width of the fin at its proximal base, or the branching of fin rays. Fin ray branching allows fin rays to maintain a large second moment of area (*I*) at their proximal end as well as distribute structural support across the expanded distal area of a fin without adding additional rays. In this study we found that the second branching event occurs more distally along the length of the M2 and trailing edge fin rays in *H. bivittatus* in comparison to *G. varius* (Fig. 4.4c). Therefore, we suggest that, because there are fewer branching events per fin ray in *H. bivittatus* in comparison to *G. varius* (Fig. 4.4a), the second branching event in *H. bivittatus* occurs more distally in comparison to *G. varius* in order to efficiently maintain the structural distribution in a fin that has less branching events.

Fin ray branching patterns across the chord of a fin may also be used to help orient the fin rays throughout the fin stroke. The application of force to a biological beam can cause the beam to undergo torsion, which would change its angle of attack (Carruthers et al., 2007; Bachmann et al., 2012). The presence of a stiff, unbranched, leading edge could act to reduce drag and the torque moment placed on the fin ray, and is a common theme amongst pelagic fishes. The presence of branched, non-leading edge, fin rays will cause a greater torque moment on the trunk of a given fin ray in comparison to a fin ray that is not branched. In flapping species that employ

lift-based propulsion, each fin stroke ends as the fin is clapped against the body wall and the subsequent fin stroke begins with the sequential peeling of each fin ray off the body wall one fin ray at a time (Walker and Westneat, 1997; Westneat and Walker, 1997; Walker and Westneat, 2002a). The angle of attack of a fin ray could change throughout the fin stroke based on the magnitude of the torque vector imposed from the direction of the leading edge. Additionally, given the same force, the angle of attack of a fin ray could be modulated by variation in branching width (lateral distance from the trunk's midline), where a wider branching event would produce a greater torque moment on the fin ray. Therefore, variation in branching pattern could be used as a passive mechanism to twist individual fin rays along their span to orient them at an advantageous angle of attack or position to produce an efficient shape of the entire fin over the stroke.

In theory, fin ray branching will modulate the "apparent" flexural stiffness of the webbing (fin membrane) between adjacent branches and fin rays. Beam theory states that in a three point bending test of a structure with homogenous geometry and material properties, the force required to bend that structure a given distance is related to the third power of the length between the supports so that halving the length between supports increases the force necessary to bend a structure a given distance by eight times. Thus, the apparent stiffness of the webbing across the fin surface, and ultimate deformation pattern, can be modulated locally through branching patterns without changing its material properties or geometry in specific locations. The branching patterns observed in this study (Fig. 4.4a; Table S4.4) support the hypothesis that fin ray branching is an effective mechanism to modulate the stiffness of fin webbing. Together, these results suggest that the webbing between fin rays and fin ray branches is *apparently* stiffer in *G. varius* than in *H. bivittatus* because there is less distance between the adjacent supports

(rays or ray branches) in *G. varius* than in *H. bivittatus*. As the stiffness of a flexible propulsor is positively correlated with thrust production (Tangorra et al., 2010), this could be a further mechanism used to enhance propulsor stiffness and generate the higher thrust and mechanical efficiency that is seen in *G. varius* in comparison to *H. bivittatus* (Walker and Westneat, 2000b; 2002a; b). Further, the apparently less stiff webbing in *H. bivittatus* would deform more in response to a given hydrodynamic force. Therefore, increasing the deformation of the fin rays and webbing would create a greater drag coefficient, and allow fish that employ a drag-based swimming behavior, like *H. bivittatus*, to produce more drag-based thrust per fin stroke.

CHAPTER 5: MECHANOSENSATION IS EVOLUTIONARILY TUNED TO LOCOMOTOR MECHANICS

Abstract

The biomechanics of animal limbs has evolved to meet the functional demands for movement associated with different behaviors and environments. Effective movement relies not only on limb mechanics but also on appropriate mechanosensory feedback. By comparing sensory ability and mechanics within a phylogenetic framework, we show that peripheral mechanosensation has evolved with limb biomechanics, evolutionarily tuning the neuromechanical system to its functional demands. We examined sensory physiology and mechanics of the pectoral fins, forelimb homologs, in the fish family Labridae. Labrid fishes exhibit extraordinary morphological and behavioral diversity and employ pectoral fin-based propulsion with fins ranging in shape from high aspect ratio (AR) wing-like fins to low AR paddle-like fins. Phylogenetic character analysis demonstrates that high AR fins evolved independently multiple times in this group. Four pairs of species were examined; each included a pleseiomorphic low AR and a high AR species. Within each species pair, the high AR species demonstrated significantly stiffer fin rays in comparison to the low AR species. Afferent sensory nerve activity was recorded during fin ray bending. In all cases, afferents of stiffer fins were more sensitive at lower displacement amplitudes demonstrating mechanosensory tuning to fin mechanics, and a consistent pattern of correlated evolution. We suggest that this is a clear example of parallel evolution in a complex neuromechanical system, with a strong link between multiple phenotypic characters: pectoral fin shape, swimming behavior, fin ray stiffness, and mechanosensory sensitivity.

Introduction

The appendages of animals, from insect wings to tetrapod limbs, have evolved and diversified with the functional demands associated with a species' behaviors and the environments in which it lives (Losos, 1990; Wootton, 1992; Gillis and Blob, 2001; Higham et al., 2015). While the evolution of appendage structure and movement has been identified as critical, both to key evolutionary innovations and to more subtle taxonomic specialization (Losos, 1990; Bellwood and Wainwright, 2001; Gillis and Blob, 2001; Pierce et al., 2012; Higham et al., 2015), it is clear that mechanosensation, which includes the ability to sense the relative movement and position of one's own body elements, is also critical for effective appendage function and control. For example, people who have lost mechanosensation of their limbs must attend visually to their affected limbs to know where they are in space and to modulate motor output effectively (Sanes et al., 1985; Sainburg et al., 1993). Experimental sensory denervation of limbs (Gray and Lissmann, 1940; Tourtellotte and Milbrandt, 1998; Abelew et al., 2000; Woo et al., 2015) and other appendages (Sane et al., 2007; Hall et al., 2015; Williams and Hale, 2015) in a range of other species has also been shown to result in significant disruption of normal movement. The recent discovery of mechanosensation in the pectoral fins of fishes (Williams et al., 2013; Williams and Hale, 2015; Hardy et al., 2016) provides an opportunity to explore evolutionary patterns of mechanosensation relative to interspecific variation in limb locomotor biomechanics.

Sensory capabilities evolve with behavior to reflect the diverse sensory needs across species (Simoncelli, 2001; Warrant, 2004; Moir et al., 2013). The absolute range of perceptible sensory cues varies among species for a given sensory modality, as seen in the diversity of auditory frequency ranges represented among insects (Cardone, 1981; Moir et al., 2013) and rodents (Webster and Webster, 1971; 1972; Plassmann and Kadel, 1991), and the olfactory detection thresholds among primates (Passe and Walker, 1985; Laska et al., 2000). In addition,

activity in particular regions of a sensory range may be enhanced to reflect biologically relevant inputs. For example, the olfactory system has been highly specialized through evolution to the relevant olfactory cues (Dekker et al., 2006; Andersson et al., 2009; Hansson and Stensmyr, 2011). Appendage mechanosensation is different from these sensory modalities in that the appendages of animals are integrated sensorimotor structures that perform dual roles, acting as both sensory and motor structures during a given behavior (Muniak et al., 2007; Williams et al., 2013). Interspecific variation in appendage mechanics will influence the magnitude of bending and shape change incurred from the application of forces during locomotion (Gordon, 1978; Vogel, 2003b), which will consequently change the range of mechanosensory stimuli relevant to each species. The diversity of pectoral fin shape and behavior among fishes provides a unique opportunity to test whether the mechanosensory system undergoes correlated changes in relation to the mechanical properties of locomotor appendages, which would suggest that limb mechanics and the limb's associated mechanosensory system are major axes of structural and functional variation in neuromechanical systems.

In this study we investigated the correlated evolution of mechanosensation and limb mechanics in fish pectoral fins, the homologs of tetrapod forelimbs. Pectoral fin nerves have recently been shown to provide feedback on fin ray bending amplitude and rate as well as on fin ray position (Williams et al., 2013; Williams and Hale, 2015). Here we examined proprioception in the fish family Labridae (wrasses), a group that demonstrates considerable morphological, biomechanical and movement diversity (Wainwright et al., 2002). Aspect ratio (AR) is a measure of the fin's span squared relative to its surface area, with higher AR indicating relatively longer and narrower, more wing-like fins, and low AR indicating a broader more paddle-like fin shape. Labrids use pectoral fin-based swimming behaviors along a continuum that ranges from drag-

based rowing with broad, low AR fins for high maneuverability, to lift-based flapping driven by high AR, wing-like fins that maximize thrust and mechanical efficiency(Walker and Westneat, 2000b; Wainwright et al., 2002; Walker and Westneat, 2002a; b; Westneat et al., 2004). The central aim of this study is to test the hypothesis that the mechanosensory response to fin ray bending undergoes evolutionary tuning with fin mechanical properties across a diversity of fin shapes and behaviors. First, we hypothesized that high AR pectoral fins have increased overall flexural stiffness due to their propensity to bend less during locomotion in comparison to more flexible low AR fins (Fig. S1). Second, we hypothesized that in comparison to more flexible fins, the reduced bending magnitude that occurs in stiff fins has driven their associated sensory system to evolve increased sensitivity to lower amplitude bending.

We sought to explore broad evolutionary patterns of fin design and function. To test our hypotheses in a phylogenetic framework we performed a phylogenetic analysis of pectoral fin aspect ratio using a new phylogeny of 340 species of Labridae (Fig. 1, S2). Based on this reconstruction, four species pairs were chosen, each pair from a different labrid subfamily. Within each pair, selected species employed fins of divergent shapes, one with high AR fins and one with low AR fins. The four species pairs (*Gomphosus varius* and *Halichoeres bivittatus*, *Halichoeres hortulanus* and *Halichoeres melanurus*, *Scarus taenopterus*, and *Cheilinus fasciatus*, *Clepticus parrae* and *Bodianus rufus,* high AR and low AR respectively) were used to test patterns of correlated evolution between fin ray flexural stiffness and the mechanosensory afferent response to step-and-hold stimuli in our analysis of the evolutionary tuning of neuromechanical systems.

Materials and methods

Sampling of labrid fishes. Species pairs were selected from the phylogenetic topology specifically to be close relatives with divergent fin shapes, representing disparate regions of the tree, while simultaneously satisfying criteria of availability and aquarium husbandry. Four adult *Gomphosus varius* (9.9-12.0 cm), *Halichoeres bivittatus* (8.0-10.9 cm), *Halichoeres hortulanus* (7.3-10.5 cm), *Halichoeres melanurus* (7.5-8.8 cm), *Cheilinus fasciatus* (9.5-13.2 cm), *Scarus taeniopterus* (9.5-11.9 cm), and *Bodianus rufus* (7.8-10.2 cm) and two adult *Clepticus parrae* (8.1 and 8.2 cm) were used in this study. The individuals of each species were sized matched and their standard lengths ranged from 7.3 to 13.2 cm. The average±standard deviation standard length for *G. varius*, *H. bivittatus*, *H. hortulanus*, *H. melanurus*, *C. fasciatus*, *S. taenopterus*, *B. rufus*, and *C. parrae* was 10.62±0.95, 9.025±1.52, 8.70±1.39, 8.1±0.45, 12.30±1.41, 9.88±1.10, 9.45±0.58, and 8.15±0.35cm, respectively. There were no significant differences in size between the individuals of the two species in each pair ($p>0.05$). Two additional *Halichoeres bivittatus* were used in this study to expand the range of body sizes (standard lengths: 5.3 and 16.2 cm). Fish were obtained commercially and housed in aquaria equipped with recirculating water filters. Water temperature was maintained at ~23°C and the fish were exposed to a 12 hour light/dark cycle. For each animal used, we performed mechanical testing in one pectoral fin and the physiological recording of the afferent response to fin bending in its pair. All experimental procedures were carried out under University of Chicago Institutional Animal Care and Use Committee guidelines (protocol 71589 to M.E.H.).

Pectoral fin aspect ratio. Pectoral fin images were collected from museum specimens and mined from FishBase image collections and other sources (see SI Dataset 1 for sources and associated aspect ratio). Images were selected for lateral view of the fin, with fin rays spread in

the standard way for tank photography or a similar degree of fin ray separation, with fish length information recorded if present. Fin aspect ratio was calculated as the square of the longest fin span (usually the leading edge), divided by fin area. Fin length and area were measured in the FIJI version of ImageJ (Schindelin, 2012).

Phylogenetics and ancestral state reconstruction. A phylogenetic analysis of 340 species of labrid fishes was performed, using an aggregated data set of 10 genes used in previous labrid phylogenetics (Westneat and Alfaro, 2005; Smith et al., 2008), new sequences generated for this study and additional genetic data obtained from GenBank (SI Dataset 2). Briefly, a topology of relationships for the Labridae was resolved based on five nuclear markers (*otx1, dlx2, bmp4*, *rag2* and *tmo4c4*) and four mitochondrial regions (*12S*, *16S, cytB*, *COI*). A 10 million generation MrBayes 3.2.2 XSEDE run on the CIPRES Science Gateway was conducted using the concatenated DNA supermatrix as input. Analyses discussed here are based on the topology and branch length data from the maximum posterior-probability tree for the Labridae. The phylogeny used in this study is available on the TreeBASE and OpenTree repositories. Ancestral state reconstruction of pectoral fin aspect ratio was performed on the 340 species phylogeny, and a version of the same tree pruned to 150 species. At least one species from every major labrid clade was represented in the fin character matrix. Aspect ratio was also binned into three discrete characters: low AR (AR: 0.73-1.5), intermediate AR (AR: 1.50-3.0), and high AR (AR: 3.0-4.6). Character states for 340 species were visualized at the tips of the phylogeny and analyzed using likelihood ancestral state reconstructions using the R packages ape (Paradis et al., 2004) and phytools (Revell, 2012). Aspect ratio was examined for phylogenetic convergence using the R package Windex (Arbuckle et al., 2014) in which the Wheatsheaf Index was calculated by

designating all taxa with an AR > 3.2 as focal for the significance test of evolutionary convergence.

Mechanical property testing. Intrinsic pectoral fin ray flexural stiffness was measured through a series of three point bending tests along the ray's span with a material testing machine (LS1, Lloyd Instruments, Fareham, UK) using a 50N load cell. For each individual, mechanical property testing was conducted on the same ray used in the electrophysiology experiment (ray 3) on the fin's pair. Flexural stiffness, a measurement of a material's resistance to bending, is calculated as the product of Young's modulus of elasticity (E) and the second moment of area (I') (Gordon, 1978; Vogel, 2003b). The conditions to measure E and I' independently (i.e. material must be homogenous, isotropic, linearly elastic) are rarely met for biological materials (Vogel, 2003b; Young et al., 2012). Therefore, EI' was measured as a single variable using beam theory (Vogel, 2003b) where F is the applied force (N), L is the distance (mm) between support beams, and Y is the vertical displacement (mm) of the material: $EI'=F(L^3)/48Y$. The Y variable never exceeded 10%(L) because a material can experience shear as well as bending at larger displacements (Blob and LaBarbera, 2001; Young et al., 2012). In order to standardize measurements across individuals and species of different sizes, L was always equal to 20% fin ray length, Y was always equal to 10%(L), and displacement speed was always set 0.1mm/s. Fin rays were stored in extracellular solution at 4°C post mortem and kept moist throughout the duration of the experiment. Mechanical property tests were always conducted within four hours post mortem. Statistical analyses were conducted to test for significant differences in fin ray mechanical properties between the species of each pair. All flexural stiffness data for each species was pooled and fit with a least squares exponential curve and a 99% confidence interval of the regression. Two sided t-tests were conducted on the pooled data for the two species of

each pair to test the null hypothesis that slopes and y-intercepts of the regression lines are the same.

Electrophysiology. We recorded from pectoral fin nerves following published methods (Williams et al., 2013). Fish were euthanized in a $0.5g \bullet L^{-1}$ solution of MS-222 (tricaine methanesulfonate, Sigma-Aldrich, St. Louis, MO). Immediately post mortem, the left pectoral fin was dissected from the body and bathed in an extracellular solution of published ionic concentrations (Masino and Fetcho, 2005). The solution was changed frequently throughout the experiment. The skin was removed to expose the nerves leading into the medial side of each fin, and pins were used to secure the fin the bottom of extracellular dish. An extracellular glass suction electrode was connected to one of the afferent nerve fibers to record multiunit physiological responses to fin ray bending. Borosilicate glass capillaries (GC150F-7.5 1.5mm OD, 0.86ID, Harvard Apparatus, Holliston, MA) were pulled in a P-97 Flaming/Brown micropipette puller (Sutter Instrument Co., Novato, CA) and fire-polished with a microforge (MF-830, Narishige, East Meadow, NY) to make electrodes (tip diameter: 20-40 μm).

In each individual, the third fin ray was bent in order to standardize experiments. The fin rays were clamped at their proximal end and the inter-ray membrane was cut to isolate the individual ray for bending. A fin ray actuator was mounted to the end of a voice coil positioning stage (VCS10-023-BS-01-M, H2W Technologies Inc., Valencia, CA) and controlled by a programmable driver (Intelligent Servo Drive IDM640-8EI, Technosoft, Canton, MI). Randomly ordered series of five step-and-hold stimuli (1.2, 2.4, 3.6, 4.8, and 6.0 mm) and six step-and-hold stimuli (1.2, 2.4, 3.6, 4.8, 6.0, and 7.2 mm) were applied to the rays of stiff-finned species and flexible-finned species, respectively, to assess nerve response to fin ray bending. Exceptions to these stimuli sets includes the addition of a smaller bending amplitude (0.6mm) for *H.*

hortulanus and *H. melanurus*, the addition of larger bending amplitudes (7.2 and 8.4 mm) for *C. fasciatus* (slightly larger fins), and stimuli sets of 1.44, 2.88, 4.32, 5.76, and 7.20 mm for *G. varius* and 1.44, 2.88, 4.32, 5.76, 7.20, 8.64, and 10.08 mm for *H. bivittatus*. Stimuli sets were changed after the *G. varius* and *H. bivittatus* to lower the minimum bending amplitude of the stimuli set and produce a stimuli set with greater resolution. Each stimulus was 5 seconds in duration. This was repeated four times for each specimen. Bending magnitudes greater than 7.20mm could not be applied to stiff fin rays without risking structural damage to the fin ray.

Extracellular voltage was monitored with a MultiClamp 700B amplifier (Molecular Devices, Foster City, CA), digitized by a DigiData 1440A digitizing board (Molecular Devices, Foster City, CA), and acquired using pClamp 10 Clampex software (Molecular Devices, Foster City, CA). Data was sampled at 100kHz and down-sampled to 10kHz. Data was analyzed in MATLAB 7.10.0 (Mathworks, Natick, MA) using a custom routine (R. Williams IV, University of Chicago). The burst duration associated with the stimulus onset (fin movement) and the spike rate over the hold period of the stimulus were calculated. A burst was defined as three or more spikes within 50 ms of each other (Williams et al., 2013). The first action potential after the start of the stimulus was considered the first spike in the burst at the onset of the stimulus, and the burst duration was ongoing so long as 3 or more spikes were recorded within 50 ms of one another. To determine if afferents could encode information on the intensity of ray movement, linear regressions were conducted to test for correlations between ray bending magnitude and burst duration. Additionally, a comparison of the spike rate over the hold period to the spike rate of a 0.5 second prestimulus baseline was conducted to determine if individuals are capable of sensing the static position of their fin rays. Across all individuals, burst duration associated with the onset of the stimulus never exceeded 1.5 seconds. Therefore, the hold period of the stimulus

was from 1.5 to 4.5 seconds after the onset of the stimulus to ensure the exclusion of afferent activity associated with ray movement. One-way ANOVAs were used to test for significant differences between the mean spike rates of baseline and different bending magnitudes, and linear regressions were used to test for correlations between the magnitude of fin ray deflection and spike rate during the hold phase. All statistical analyses were performed on each individual independently because of inevitable differences in the total number of afferents recorded from in each individual. All statistical analyses were performed in RStudio 0.98.484 (RStudio, Inc., Boston, MA, USA) or JMP 9.0.1 (SAS, Cary, NC, USA).

Results

Phylogenetics and ancestral state reconstruction. Our analysis of DNA sequence data for 340 species of labrid fishes yielded a well-resolved phylogeny (Fig. S5.1) to use in exploring phylogenetic patterns of pectoral fin shape. Character optimization and ancestral state reconstruction revealed a most likely ancestral state of low AR fins at the root node of the tree (likelihood probabilities of each fin AR: low = 0.47, intermediate = 0.29, high = 0.24) and at least 22 independent evolutions of high aspect ratio fins associated with the flapping swimming behavior (Fig. 5.1, S5.2, S5.3; Table S5.1). The phylogenetic reconstruction shows a rich history of fin shape evolution, with multiple clades having evolved upward and downward on the fin aspect ratio continuum, producing complex patterns of divergence and parallelism across the tree. High AR fins (AR>3.2) were highly significantly (p<0.01) convergent across the tree. While the character state at the root node is equivocal, ancestral state reconstructions show high likelihood values for character states of low, intermediate or high AR at progressively more distal nodes. Therefore, our interpretation of multiple independent evolutions of high aspect ratio fins is not dependent on the character state at the root node. The probability of representing the

low AR character state at the node of a species pair's most recent common ancestor is 0.872 for *C. parrae* and *B. rufus* (node 27), 0.756 for *G. varius* and *H. bivittatus* (node 206), and 0.750 for *H. melanurus* and *H. hortulanus* (node 296). The node (node 58) of the most recent common ancestor between *C. fasciatus* and *S. taeniopterus* has a 0.491 probability of representing the low AR fin character state. Although this node is equivocal, the parrotfish *Scarus taeniopterus* represents a large clade of high AR flapping species, and a particularly notable independent evolution of high aspect ratio fins from the common ancestor of the cheiline and scarine wrasses.

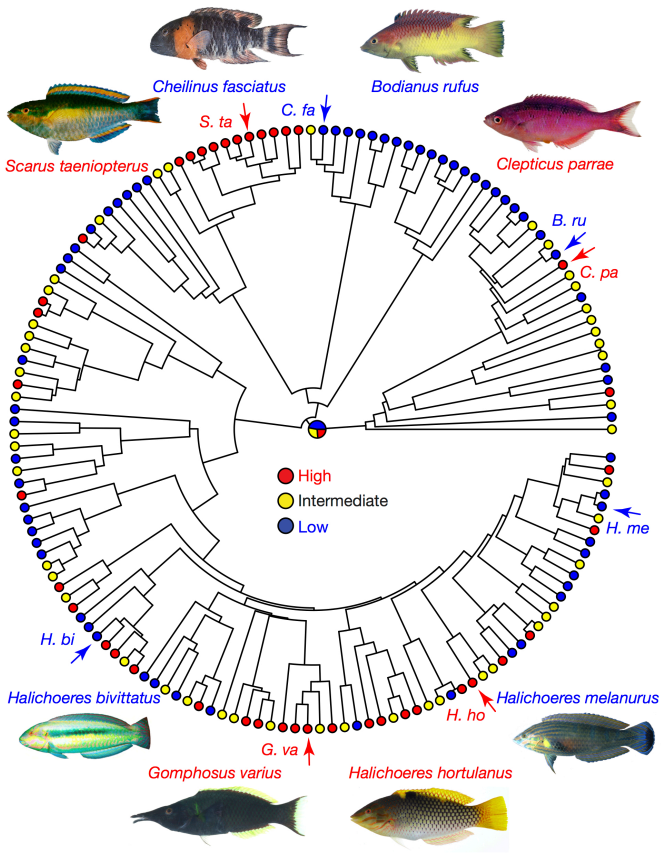

Figure 5.1. The phylogenetic relationships of the Labridae and pectoral fin aspect ratio ancestral state reconstruction. The maximum likelihood reconstruction revealed a most likely ancestral state of low aspect ratio pectoral fins (low = 0.47, intermediate = 0.29, high = 0.24) and at least 22 independent evolutions of high aspect ratio fins. An arrow and the species' initials highlights the phylogenetic position of each species used in this study. The two species of each pair were always located within the same subfamily and each species pair contains an independent evolution of the high AR fin. The phylogeny presented here is pruned from 340 species to 150 species to maximize visualization. The ancestral state of the basal node is taken from the 340 species reconstruction. The full 340 species phylogeny and accompanying 340 species ancestral state reconstruction can be found in Figure S2, and the node labels and the corresponding likelihood of the ancestral state at each node can be found in Figure S3 and Table S1, respectively. Red = high aspect ratio, yellow = intermediate aspect ratio, blue = low aspect ratio. Photo credits: HB – Paul Humann; HH, GV – Jeffrey T. Williams; BR, CP, CF, HM, ST – John E. Randall.

Fin ray mechanics. The morphological phenotypes of low and high AR fins (Fig. 5.2a) corresponded to a strong divergence in fin ray flexural stiffness. The average flexural stiffness, or resistance to bending, at 50% fin ray length was between 190±30 and 210±50 $x10^{-9}$ $N \bullet m^2$ (average±stdev) among the high AR species and

between 20±10 and 40±10 $x10^{-9}$ $N \bullet m^2$ among the low AR species. These data indicate largely consistent trends in flexural stiffness among size-matched individuals in each behavioral phenotype. Within each species pair, the average flexural stiffness at 50% fin ray length of high AR fins was 5.4 – 11.6 times greater and significantly different than that of low AR fins (Fig. 5.2b; t-test p-values < 0.05; Fig. S5.4). Across all eight species, flexural stiffness decreases exponentially along the length of the fin ray, and regressions of stiffness against fin ray position reveal significant differences in the y-intercept between species for all four pairs and significant differences in the regression slope between species for three pairs (*Gomphosus varius*, *Halichoeres bivitattus*; *Clepticus parrae*, *Bodianus rufus; Cheilinus fasciatus*, *Scarus taeniopterus*) (p<0.01; Table S5.2). The significant differences in y-intercept suggest that there is a strong species effect on fin ray stiffness and significant differences in the regression slope suggest that the rate fin ray stiffness changes along the length of the fin ray is different between species.

Mechanosensation. Afferent nerve responses to fin ray bending were recorded for all eight of the species tested and consistent trends were identified among taxa. In response to step-and-hold stimuli, where a single fin ray is bent, held in a bent position, and then returned to rest, a burst of spikes occurred both when the fin was raised from and when it was returned to its resting position. The duration of bursts (three or more spikes within 50 ms of each other) associated with stimulus onset increased significantly with increasing bending amplitude (Fig. 5.3a; Table S5.3). Furthermore, fibers continued to respond during the hold phase of the stimulus (Fig. 5.2c). At high bending amplitudes, the spike rate over the hold period (a 3-s portion of the trace that began 1.5-s after stimulus onset to ensure activity associated with fin movement was not included in this analysis) was significantly greater than the spike rate of a pre-stimulus baseline for each

species used in this study (one-way ANOVAs, $p<0.05$; Table S5.4). At these higher bending amplitudes, a significant and positive relationship was found between hold period spike rate and bend amplitude ($p<0.05$) for all individuals across all species (Fig. S5.5, Table S5.5).

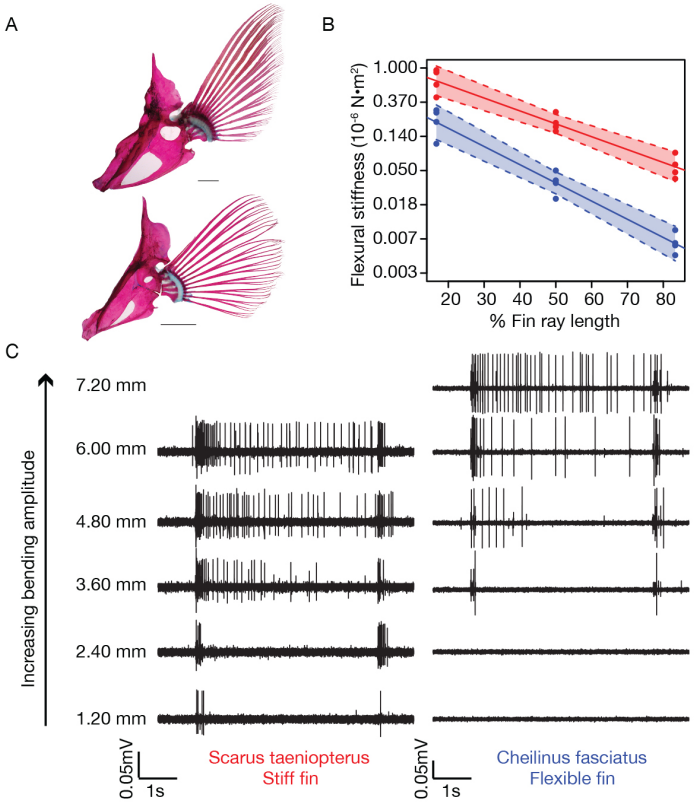

Figure 5.2. Comparative pectoral fin morphology, mechanics, and proprioceptive sensitivity between closely related low AR (*Cheilinus fasciatus*) and high AR (*Scarus taeniopterus*) species. (A) Cleared and stained pectoral fins of *S. taeniopterus* (flapper; top) and *C. fasciatus* (rower; bottom). *S. taeniopterus* employs wing-like high-aspect ratio pectoral fins, while *C. fasciatus* employs broad paddle-like pectoral fins. Scale bar = 1cm. (B) The pectoral fin rays of *S. taeniopterus* (high AR; red) are significantly stiffer than the rays of *C. fasciatus* (low AR; blue). All flexural stiffness data for each species was pooled and fit with an exponential curve ($r^2 = 0.93$, 0.95 for *S. taeniopterus* and *C. fasciatus*, respectively). Correspondingly, the data are presented in a semi-log fashion with a logarithmically scaled y-axis. The shaded region of each fit represents a 99% confidence interval of the linear regression. The y-intercept and slope of the regression line was significantly different between each species ($p<0.05$; Table S2). (C) Representative nerve recordings from one individual of *S. taeniopterus* (left) and *C. fasciatus* (right). A three times larger bending magnitude is needed to elicit a response in the size-matched pectoral fin of the flexible-finned *C. fasciatus* in comparison to the stiff-finned *S. taeniopterus*.

Comparing across the species pairs, stiff finned species consistently demonstrated greater sensitivity in comparison to species employing more flexible fins. The average minimum bending amplitude to elicit a response (response threshold) was between 17.84±0.88 and 30.67±1.03% fin ray length (3.6±0.0 and 6.12±0.72mm) among the low AR species and between 5.91±0.58 and 8.20±3.03% fin ray length (1.05±0.3 and 1.5±0.42 mm) among the high AR species (Table S5.6). Similar to fin stiffness, these data show consistent trends in response threshold among size-matched individuals in each morphological phenotype. Within each

species pair, the average response threshold of the low AR species was 2.39 – 5.19 times greater in percent fin ray length than that of the high AR species (Fig. 35.b). This corresponds to differences in average response threshold between the species of each pair ranging from approximate bending magnitudes of 11 - 25% fin ray length, and significant differences in

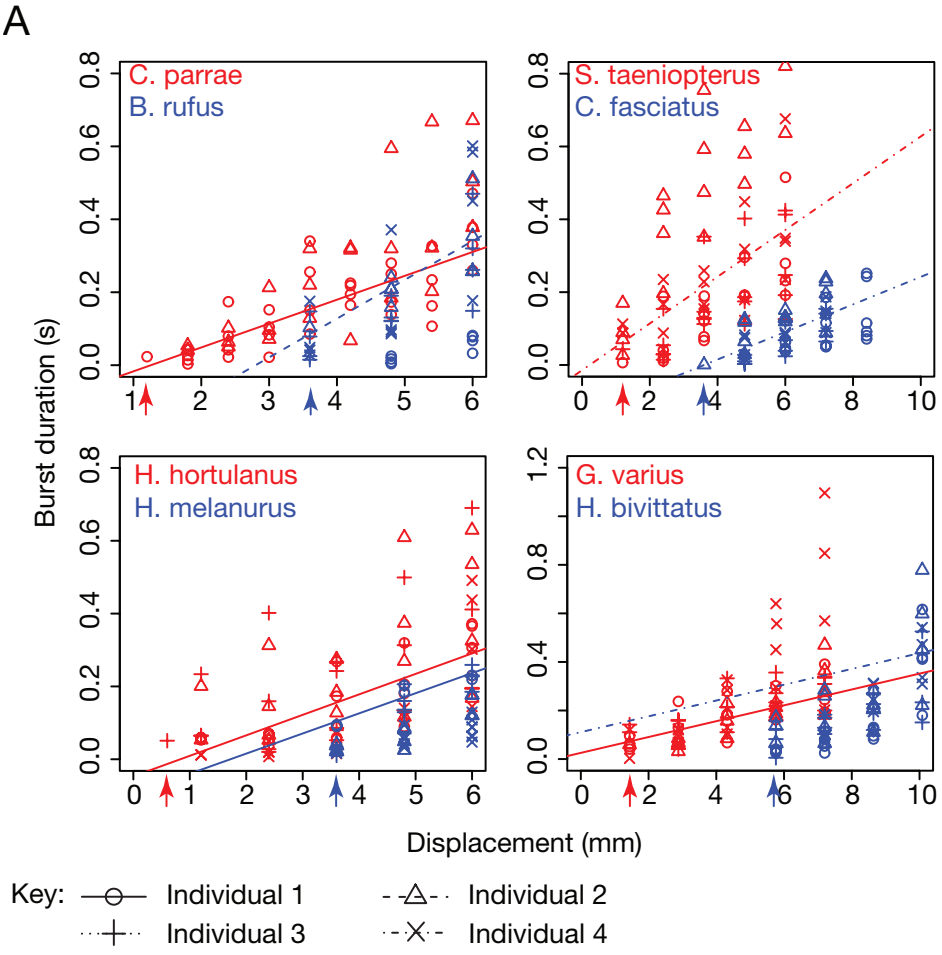

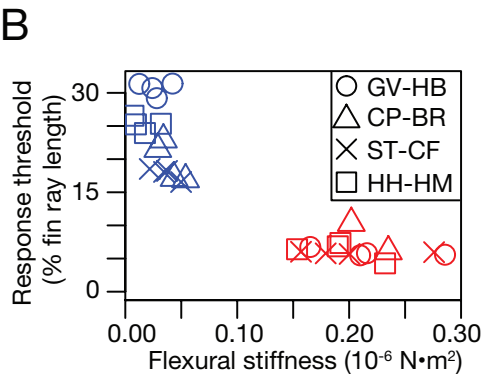

Figure 3. Summary of afferent response to fin ray bending. (A) Bivariate plots of burst duration by fin ray bending magnitude per species. The duration of bursts (three or more spikes within 50 ms of each other) associated with the onset of fin ray movement is positively and significantly correlated with fin ray bending magnitude. Regression lines are presented for one representative individual of each species, and regression statistics for all individuals are detailed in Table S3. Arrows represent minimum response amplitude per species. (B) Response threshold (the minimum bending amplitude needed to elicit a response) is plotted again fin ray flexural stiffness for every individual of each species. In all cases, the pectoral fin rays of high AR fins are significantly stiffer than those of low AR fins, and the proprioceptive system of high AR species is significantly more sensitive than that of low AR species. Blue = flexible low AR fins, red = stiff high AR fins.

response thresholds between the species of each pair

(p<0.0125; Fig. 5.3a). Furthermore, the slope of the regression between the duration of the afferent's initial burst associated with fin bending and fin bending amplitude was compared between the species of each pair to determine if the high and low AR species of each pair maintained similar stimulus intensity resolution (the ability to discern between two intensities of the same stimulus). The high and low AR species of each pair show no differences in intensity resolution (p-values range from 0.186 – 0.777).

We also assessed the relationship between response threshold and fin ray flexural stiffness. A multiple regression that nests species within subfamily and includes aspect ratio as a fixed effect found no significant correlation between response threshold and fin ray flexural stiffness (p-value = 0.2447; Table S5.7). Similarly, linear regressions conducted on these two variables for each species were never significant (p-values range from 0.101 – 0.965; Table S5.7). An additional regression between these two variables conducted on data from a single species that covered a larger ranger in body size (standard length: 6.3-15.2cm; N=6) was also not significant (p = 0.214; Table S5.7).

Discussion

The key results of this study are that (1) a phylogenetic analysis reveals extensive parallel evolution resulting in at least 22 independent origins of high aspect ratio, wing-like appendages in the Labridae, (2) the four pairs of species at low and high extremes on the AR spectrum showed significant differences in flexural stiffness, and (3) we found strong evidence of neuromechanical tuning, with elevated mechanosensory sensitivity in stiffer more wing-like fins.

This study investigates the relationship between limb mechanosensation and stiffness in four pairs of closely related species that employ divergent fin shapes, an independently evolved

high AR species and a plesiomorphic low AR species. In each pair, the high AR species employed significantly stiffer fin rays in comparison to the low AR species. Previous work has found a correlation between pectoral fin aspect ratio and swimming behavior (Wainwright et al., 2002). Therefore, these data suggest that differences in fin shape (aspect ratio) do not simply reflect change in movement and motor control of the fins but that the fins have evolved mechanically to function as effective propulsive structures, tuned to different performance capabilities. Importantly, the interspecific variation in fin ray stiffness observed and multiple independent evolutions of stiff fins, provided a phylogenetic framework in which to examine the correlated evolution of mechanics and mechanosensation.

In all eight species of wrasse studied here, spiking patterns of the mechanosensory afferents innervating each individual's pectoral fin rays were able to encode fin ray movement and position (Fig. 5.2c, 5.3a). These data are consistent with results from the bluegill sunfish (Williams et al., 2013). In combination with previous work in the pectoral fin (Williams et al., 2013; Hardy et al., 2016) and the adipose fin (Aiello et al., 2016), a central result of this study is the mechanosensory system's ability to encode information about both the static and dynamic qualities of a stimulus (i.e. position and movement) might be a general feature of actinopterygian fins. Further, we consistently found that species employing stiffer pectoral fins also exhibited greater mechanosensory sensitivity (a lower minimum bending amplitude needed to elicit a response) in comparison to species employing more flexible fins. These results suggest that sensory physiology can be tuned to the fin's mechanics through adaptation of the mechanosensory system's sensitivity to fin ray bending.

Our data supports the hypothesis of species-specific sensory phenotypes. We considered alternative explanations for the relationship between neural activity and mechanics. One

possibility is that interspecific variation in mechanosensory sensitivity arose as a plastic response to different behavioral repertoires. However, our data do not support either of these alternatives. If plasticity were the dominant process acting to produce the interspecific differences in response threshold, we would expect to see correlations between stiffness and sensory threshold across species and among individuals of a given species. If this were the case, within a given species and across all species, response threshold would decrease as stiffness increased. Instead, the mechanosensory sensitivity data show consistent sensitivity thresholds with little intraspecific variation (*p*-values range from 0.101 – 0.965; Table S7) for each species. To increase statistical power, a further multiple regression model that includes aspect ratio as a fixed effect to account for the two morphological groups was also conducted and also found no significant correlation between fin ray flexural stiffness and response threshold (*p*-value = 0.2447).

Body size and ontogeny may also impact the relationship between fin stiffness and afferent nerve activity. We performed the tests in this study on size-matched individuals with little variation in fin stiffness among the individuals of each species. To determine whether species-specific nerve activity patterns resulted from the narrow size range used, additional experiments were performed on individuals of a single species (*H. bivitattus*) that covered a large range in body size (standard length: 6.3-15.2cm; N=6). We found no significant correlation between fin stiffness or body size, and mechanosensory sensitivity ($p = 0.214$; Table S5.7), suggesting a species-specific match between stiffness and mechanosensory sensitivity across a wide range of sizes of adult wrasses.

The pectoral fin mechanosensory system is at the nexus of physics (mechanotransduction at the cellular level), biomechanics and behavior (the mechanics and motion of the fin), and neurobiology (the encoding of a signal and subsequent information processing). It is still under

debate whether mechanosensory cells sense stress or strain (Petzold et al., 2013; Wang, 2013), and whether the same mechanism of sensation is conserved across animals (Krieg et al., 2015). Our results do not suggest that species have retained a plesiomorphic response threshold where the same minimum force would elicit a response in all species. In this scenario, regardless of a species' fin stiffness, the application of the same given force would elicit a response in the pectoral fin afferents of any species. If this were true, a negative correlation would exist between response threshold and fin stiffness among the individuals within species and within behavior phenotypes, and fins of the same stiffness would exhibit the same response threshold. However, our data show a wide variety of response thresholds for fins of similar stiffness (Fig. 5.3b). These data provide support for the hypothesis that interspecific differences in mechanosensory sensitivity reflect species-specific phenotypes evolutionary tuned to the different magnitude bending regimes experienced by species with fins of high or low stiffness, respectively. Further, these results suggest that the pectoral fin mechanosensory system is responding to strain rather than differences in the applied stress.

The limbs of both biological organisms and robots with integrated sensors typically rely on sensory feedback to adjust output signals (Raibert, 1986; Phelan et al., 2010). In closed-loop control systems, the production of the desired output signal relies on extremely accurate sensory information and is sensitive to sensor error (Kuo, 2002). Novel engineering has led to the engineering of robots that employ dynamic limbs, which are capable of tuning their stiffness as they locomote in order to optimize limb mechanics and locomotor efficiency over variable terrain, payloads and speeds (Hurst, 2008; Galloway, 2011; Galloway et al., 2013). The application of robust sensors with wide stimulus ranges and high resolution could be implemented to meet the needs of dynamic limbs throughout the entirety of their stiffness

spectrum, but this will increase bandwidth requirements and sensory processing time. Limitations in neural bandwidth and delays in sensory processing in closed-loop control systems can have devastating effects on performance and stability in robotic models (Elzinga et al., 2012). The results presented here are a case study for how the mechanosensory system has been finely tuned through evolution to interspecific variation in appendage mechanics and may be useful in developing new sensors or control algorithms to maximize intensity resolution while maintaining low bandwidth and processing time.

In an evolutionary context, the phylogenetic analysis of fin shape reveals strong evidence of parallel evolution across the tree topology. In this study, we focused on four of the 22 known independent evolutions of high AR pectoral fins (Fig. 5.1, S5.2). In each of these four cases, high AR pectoral fins evolved in parallel from a similar low AR ancestor, and this same pattern is seen repeatedly across the tree topology (Fig. S5.1). In all four independently evolving species pairs, pectoral fin mechanics evolves in tandem with AR, and as fins evolve increased stiffness, the sensitivity of their mechanosensory system also increases. The close association between swimming behavior (Wainwright et al., 2002) and biomechanics (Walker and Westneat, 2000b; 2002a; b) with pectoral fin shape in these fishes suggests that the mechanosensory system has coevolved with the anatomical and behavioral diversification of the labrid fishes. We suggest that this is a clear example of parallel evolution in a complex neuromechanical system, with a strong link between multiple phenotypic characters: pectoral fin shape, swimming behavior, fin ray stiffness, and mechanosensory sensitivity. Further exploration of mechanosensation in this system, focused on species with a diversity of fin shapes, may yield information on the function of the mechanosensory system in intermediate forms, and the role that sensory neuromechanics plays in driving evolutionary trends in locomotor diversity.

Broadly across animals, a spectacular morphological and biomechanical diversity of appendages are used in a vast repertoire of behaviors. The locomotor appendages of animals, from insect wings to vertebrate limbs, perform dual roles as sensors and propulsors (Dickinson, 1990a; 1990b; Williams et al., 2013). We argue that the diversification of locomotor appendages involves the evolutionary tuning of mechanosensation to the concurrent evolutionary changes in the material and morphological properties of propulsors (wings, fins, limbs). This study demonstrates that the mechanosensory system has evolved to meet the dynamic range of fin movement in multiple independently evolving pairs of closely related fishes. The broad sampling of our study demonstrates that, as the fin evolves increased stiffness, the sensory system evolves increased sensitivity. These results suggest that the correlated evolution of the mechanosensory system and appendage biomechanics is a general principle of how neuromechanical systems evolve. As mechanosensation is a universal feature of organisms (Kung, 2005), this may be an evolutionary principle that shapes the functional capabilities of all animals.

CHAPTER SIX: BROADER THEMES AND FUTURE DIRECTIONS

The primary objective of this dissertation has been to integrate mechanical, morphological, and neurobiological data within a comparative framework to test hypotheses on the evolution of neuromechanical systems. In chapters two through four, I applied various approaches to answering specific questions in neuormechanics, and in chapter five, I examined how individual components of a neuromechanical system evolve in relation to each other. In this final chapter of the thesis, I will first justify the value of integrative research and the use of phylogeny when studying neuromechanical systems. Next, I will broadly evaluate the data of this thesis in relation to the evolution of neuromechanical systems, and discuss future directions of this work. Finally, I will discuss the potential for the data in this thesis to be applied to the development of bioinspired underwater robotic vehicles.

Evolutionary neuromechanics.

The functional capability of any neuromechanical system is the product of its numerous interconnected parts. Biomechanists often focus on the particular function of a specific morphological feature. Neurobiologists are often interested in the motor program used to generate a specific behavior, and/or how an animal senses a variety of stimuli while performing that behavior. Ultimately, the observed behavior of an animal is not simply the product of a given motor program, but results from a complex interaction between neurobiology, mechanics, morphology, and the physical interaction between the animal and its environment. Therefore, an integrative approach is necessary to answer questions on how the different axes of propulsor variation lead to effective locomotion and how the different components of a neuromechanical system change together. First, one should consider how the system as a whole is influenced by its

interaction with the environment (forces applied during locomotion) and the ecology of an animal, and how the animal senses its interaction with the environment and incorporates that feedback to adjust its motor program. Next, one should consider how a given motor program actuates an appendage, and how the mechanics of that appendage, which are influenced by its morphology, interact with the environment to produce a given behavior. Finally, it is important to test the consistency of these relationships across the phylogeny. If a certain phenomenon exists in a given species, can we expect to see the same pattern amongst these variables in other species? If not, how does the neuromechanical system change in response to selective pressures? Answering these questions in a phylogenetic context and examining trends across species can provide a more robust understanding of how different neuormechanical processes function together to produce effective locomotion. In other words, how many ways (e.g. constraint, independent evolution, convergent evolution, correlated evolution, etc)are there to produce a satisfactory answer?

Future directions.

It is clear that the loss of sensory feedback dramatically impacts the locomotor performance of animals across a wide variety of species. This thesis highlights the importance of sensory feedback during fin-based locomotion in fishes and that the biomechanical and sensory components of a neuromechanical system evolve together. However, there are still many unanswered questions that remain and that are of particular interest to me. (1) What strategies, if any, have fish evolved to sense muscle dynamics, and what is the structure and function of putative proprioceptors proximal to pectoral fin rays? (2) Does a neuromechanical system change

over ontogeny, and, if so, how do these changes effect sensation and motor control? (3) How does pectoral fin ray branching patterns evolve across wrasses and, more broadly, teleosts?

Proximal sensation.

There is likely a suite of proprioceptive sensors that innervate different aspects of the fin system that are located proximal to the fin rays. Evidence for such receptors is scarce, but their histology has been described in both specialized teleost fishes and several chondrichthyan species. Sensory endings have been found in the intramuscular connective tissue (Poloumordwinoff, 1898) and at the base (Wunderer, 1908; Bone, 1964) of the pectoral fins in chondrichthyans; the cells at the fin base fire in response to fin bending (Fessard and Sand, 1937; Lowenstein, 1956). In teleost fishes, free nerve endings are described innervating the tendon of the dorsal fin muscle in a seahorse (Pansini, 1888) and the tendons attached to the caudal fin in the tench fish and the goldfish (Ciaccio, 1890). Free nerve endings with and without vicrose endings have also been found to innervate the joint capsule in the modified pectoral fin rays of the searobin (Bone, 1964; Ono, 1979). Physiological evidence of muscle proprioception in teleost fishes exists only from a single recording of rhythmic activity from a nerve innervating a muscle in the searobin in response to sinusoidal bending of the muscle (Roberts, 1969). Other than a single study (Maeda et al., 1983) that has not been duplicated, spindles have not been identified in the muscles of teleost fishes despite investigation (Barker, 1974). Free sensory nerve endings have also been observed in the proximal connective tissue associated with the pectoral and pelvic fins of the African lungfish, *Protopterus annectens* (Barker, 1974). Together this begs two distinct questions: (1) What are the physiological properties of the sensory endings proximal to fin systems in teleost fishes, and what features of fin movement do they encode? (2)

When and why do muscle spindles evolve and how is their function different than the sensory endings found proximal to fin systems in teleosts?

The ontogeny of a fin.

Fin size, shape, kinematics, and mechanics, among other variables, will change over the life of a fish. Each of these variables is known to impact the hydrodynamic consequence of a flexible propulsor as it moves through a fluid medium. The hydrodynamic and inertial forces acting on the fin are complex; the fish's drag, the size and mass of the fin, and the amplitude and frequency of a fin beat will each influence the hydrodynamic and inertial forces experienced during a fin stroke (Daniel and Combes, 2002). There are significant differences in fin kinematics over the ontogeny of an animal, and larval and juvenile fish often use their fins at higher frequencies and at different Reynolds numbers in comparison to adults of the same species (Walker and Westneat, 1997; 2000a; Mussi et al., 2002; Hale et al., 2006). However, there has not been an investigation of the scaling of the combine hydrodynamic and inertial moment experience by a fish over its life.

The stiffness of a fin will also change over the life of a fish, and will impact the magnitude and pattern of shape change across the fin surface in response to application of an applied force (Vogel, 2003a). The deformation pattern of a propulsor will have a large impact on its propulsive capability. In the third chapter of this thesis I found that fin ray stiffness is strongly correlated with both body mass and fin ray length in two species (Figure 5.5). There is no difference in the slope of the regression between fin stiffness and body size between *G. varius* and *H. bivittatus*, which may be due to phylogenetic or developmental constraints. However, uncorrelated changes in the stiffness of a propulsor and the forces it experiences over an animal's

life could necessitate the need for a flexible motor-control system that changes over ontogeny in order to maintain efficient propulsion. Finer analysis of swimming behavior over a larger range of sizes and life stages will allow us to determine if the relative magnitude of fin bending is conserved over the life of an individual, or if there is evidence to suggest the need for continual adjustment of its innate CPG-driven motor plan.

The changes in fin size, shape, and stiffness that occur over ontogeny might also impact its role as a sensor. The larval pectoral fin membrane is innervated by a diffuse network of sensors that reorganize into distinct tracts that follow and run parallel to fin rays as they become ossified in the juvenile stage (Thorsen and Hale, 2007). How this reorganization occurs is unknown, but this general innervation pattern is maintained in the adult pectoral fin (Thorsen and Hale, 2007; Williams et al., 2013). Changes in fin size and shape as a fish continues to grow as a juvenile could have a significant impact on its sensory ability. For example, changes in the number and distribution of sensors across the fin surface will impact the signal to noise ratio and the spatiotemporal resolution of the sensory system. This leads to the question of whether or not the density and distribution of sensory endings changes as the fish grows over its life. Certain mechanosensory cells that innervate the body axis (Rohon-Beard cells) are lost through cell death in early development (Svoboda et al., 2001), and fin ray nerves are capable of regenerating with the ray skeleton after partial amputation (Geraudie and Singer, 1985). Together this suggests the capacity for an individual to maintain sensor density over ontogeny. Alternatively, a decrease in sensor density over time may be sufficient to maintain the sensory role of the fin or may even be helpful depending on the hydrodynamics of the fin. A detailed analysis of fin innervation over the course of juvenile and adult stages is needed to determine how fin innervation changes with fin size and shape.

My final question on potential changes in the pectoral fin system over ontogeny is whether or not pectoral fin rays have the potential to undergo bone modeling and remodeling. Fin rays are composite structures made up of two crescent–shaped hemitrichia (Geerlink and Videler, 1987) that surround a core of collagen gel (Goodrich, 1904). The hemitrichia are made of acellular bone (Goodrich, 1904). Vertebrate bone has the potential to model and remodel in response to increased use, loads, or micro-damage (Robling et al., 2006). Bone modeling and remodeling has traditionally be thought to require the presence of osteocytes, which are responsible for mechanotransduction in tetrapods (Klein-Nulend et al., 2013). Recently, a study found that acellular bone of billfishes is capable of remodeling despite the lack of osteocytes (Atkins et al., 2014). The potential for acellular bone remodeling in the fins of fish has not been explored and raises question on whether fin ray mechanics can be modified in response to the changes in kinematics and hydrodynamic loading that likely occur over the life of a fish.

Fin ray branching.

The pectoral fin rays branch and the fourth chapter of this thesis shows that interspecific differences exist among pectoral fin ray branching patterns. The analyses of fin ray branching found that the pectoral fin rays of a flapper are significantly more branched in comparison to the fin rays of a rower (Figure 4.4). I believe this result will act as the foundation of future studies testing the functional and evolutionary hypotheses presented in the discussion section of chapter four. First, is there a potential for fin ray branching to passively orient a fin ray at an advantageous angle of attack? This could be of great interest from both a functional biology and engineering perspective, as a passive mechanism to generate advantageous angles of attack would increase hydrodynamic efficiency and reduce energy requirements by eliminating the need for active muscle control. Second, can fin ray branching manipulate the apparent stiffness

of the fin webbing? In the discussion of chapter four I explain that a more branched fin ray will decreases the distance between adjacent supports, thereby increasing the resistance of the webbing to an applied bending force. The webbing stiffness hypothesis can be easily tested through the generation of several fin ray models with variation in the angle of the branch and the number of branching events that occur. Then mechanical tests can be conducted to test the "apparent" stiffness of webbing in each model. A further analysis would be to then take these models, place markers across the webbing, use an actuator to move them through a fluid-medium, and quantify the deformation pattern of the webbing in different models. This will allow for the simultaneous measure of stiffness, webbing strain, force generation, and the calculation of drag coefficients. Third, branching pattern is not a dichotomic trait and will have continuous variation across a group. Within wrasse, I have observed at least five different branching patterns in the fin rays of different flapping species. Rowing species also show great variability in the angle between primary branches. An understanding of the functional role of fin ray branching pattern will greatly benefit from an evolutionary analysis of this trait across the phylogeny.

Applied science.

The effective control of moving systems requires information to be acquired about its movement and its interaction with the external environment. Mobile neuromechanical systems simultaneously act as both sensors that encoding different stimuli and controllers that actuate the appendage. The processed information acquired about its movement and environment can then be used to maintain or adjust the motor program responsible for the generation of a certain movement. Ultimately, both animal and robotic limbs are highly integrated neuromechanical

systems that interact with various natural forces associated with the external environment to produce a given kinematic repertoire or behavior.

Advances in technology have now made it possible to build robots that are capable of behaving in a comparable way to animals. In order for bioinspired robots to produce animal-like behaviors and adjust that behavior in the face of an unexpected perturbation, it is necessary to understand the motor program responsible for a given behavior, the range of sensory stimuli associated with that behavior, how each stimulus is encoded in sensory afferents, and how sensory feedback is incorporated to modulate the motor program. Further, the physical interaction between the moving propulsor and its environment, which relies on the spatial distribution of propulsor mechanics, will be a key factor impacting the final product of a given movement. This thesis investigates the pectoral fin motor program, passive fin mechanics, the encoding strategy of simple mechanical stimuli applied to the fin rays, how this encoding strategy is tuned to the differences in fin mechanics and behaviors among species, and how the loss of sensory feedback affects the motor program. Here, I will outline how the data collected in this thesis can be applied to the design of bioinspired robots and some of the future work that needs to be completed for a more robust understanding of sensorimotor control.

Flexible propulsors are central to the development of bioinspired underwater autonoumous vehicles (Phelan et al., 2010; Tangorra et al., 2010; Lauder et al., 2006, 2011; Lucas et al., 2014). The three-dimensional deformation and kinematics of a flexible propulsor will largely impact its fluid-dynamic capabilities (Daniel and Combes, 2002; Young et al., 2009). The stiffness and distribution of that stiffness across a propulsor can be modified to change the magnitude and direction of the resultant force vector (Tangorra et al., 2010). In theory, the fins of fishes are dynamic and their curvature and stiffness can be actively controlled (Alben et al.,

2007), although data from this thesis do not suggest that happens during steady state swimming in at least the Quoyi parrotfish (Chapter 2). Terrestrial robots are already being outfitted with dynamic limbs that can tune their stiffness to optimize limb mechanics and locomotor efficiency over variable terrain, payloads, and speeds (Galloway et al., 2011, 2013).

The third chapter of this thesis is a case study on how pectoral fin stiffness has been finely tuned through evolution to interspecific variation in locomotor behavior, hydrodynamic capability, and ecology. I found that fish that employ relatively flexible fins live close to the reef bottom in complex environments and are capable of high degrees of maneuverability. In comparison to stiffer fins, it is likely that the high flexibility of these fins allows a wider range of thrust vectors to be achieved, which allows these fishes extreme maneuverability. Differently, stiff pectoral fins are employed by fishes that live in high-energy wave-swept environments and are capable of producing high thrust production, swimming at relatively high speeds, and exhibit greater mechanical efficiency in comparison to flexible-finned species. These data can be used in the development of underwater autonomous vehicles outfitted with propulsors that are finely tuned to specific tasks or outfitted with dynamic propuslors that are capable of rapidly adjusting their mechanics to different hydrodynamic environments or tasks.

The ultimate goal when designing a mobile robot is to be able to control dynamic propulsive forces produced by a propulsor over time, and the production of biologically inspired controllers will require the integration of sensory feedback (e.g. Phelan et al., 2010). If dynamic robotic propulsors are developed that can change stiffness in response to different functional needs or environmental pressures, so too will a dynamic sensory system need developed. Just as with biological mechanosensors, engineered sensors have a limited operating range and its output can saturate with the application of a high intensity stimulus. Sensors with wide stimulus

ranges and high resolution could be applied to dynamic limbs in order to encode the stimulus throughout the entire range of the limbs dynamic stiffness spectrum. However, this will increase bandwidth requirements and sensory processing time, and likely limit the intensity resolution of the sensor (the ability to discern between different intensities of the same stimulus). In closed loop systems, the performance and stability of a robotic model can be severely perturbed by limited bandwidth and prolonged processing of sensory feedback (Elzinga et al., 2012). Further, inaccurate sensory information and sensory error, which could be caused by low intensity resolution, can have devastating effects in the production of the desired output signal (Kuo, 2002). The fourth chapter of this thesis provide an example of how the mechanosensory system has been finely tuned through evolution to interspecific variation in appendage mechanics. These data might be helpful in developing new sensors or control algorithms to maximize intensity resolution while maintaining low bandwidth and processing time.

A dynamic propulsor can be outfitted with sensors designed to encode one of several different stimuli that includes strain, force, or pressure. As mentioned previously, the kinematics and deformation pattern of a flexible propulsor will have a large impact on its propulsive capability (Daniel and Combes, 2002). Therefore, to provide accurate sensory feedback to a robotic controller, it is necessary to accurately encode the deformation of the propuslor as well as predict the hydrodynamic forces (thrust, lift, etc) associated with the kinematics (velocity and acceleration) and deformation of the propuslor (associated with its movement). In a bioinspired fin-based system, it may be tempting to employ pressure sensors across the surface of the propulsor (Kahn et al., 2012). However, strain sensors are more consistent with biological sensors and likely more informative, especially if applied to a dynamic fin capable of changing its mechanics. While a debate exists over whether mechanosensory cells sense stress or strain

(Petzold et al., 2013, Wang et al., 2013), the data presented in chapter five of this thesis suggest that the mechanosensory cells innervating the pectoral fin of fishes sense strain rather than stress or force (Figure 5.3). In the fish fin system, a sense of stress or force would not be efficient in the ultimate calculation of fin deformation, which is the variable most relevant to hydrodynamics. The inefficiency would arise in a fin capable of changing its stiffness, which is thought to be the case for the fins of fishes (Alben et al., 2007), because the calculation of strain based on a given force would require knowledge of the stiffness of the material. This requires fish (and robots) using a dynamic fin to keep track of an additional variable and then use that variable to calculate fin deformation. The simple use of a strain sensor would eliminate this problem, as well as enable this input to be quickly processed to determine the velocity (1^{st} derivative of strain) and acceleration (2^{nd} derivative of strain) of any movement. Indeed, the prediction of propulsive forces generated by a robotic fin is more accurate through bending sensation via strain gauges in comparison to pressure sensation (Kahn et al., 2015).

The number and distribution of sensors across the propulsive surface will strongly impact the sensory capabilities of a propulsor. Increasing the number and distribution of sensors across a surface can maximize the signal to noise ratio and spatiotemporal resolution of a system. Maximizing these variables is necessary for the accurate adjustment of motor output that will produce a favorable behavioral outcome based on the sensory signal acquired. Yet, natural selection acts to reduce the total number of sensors needed to encode the relevant stimuli because of the high energetic cost associated with sensory systems (Laughlin et al., 1998; Niven and Laughlin, 2008). Therefore, the cost function associated with sensation leads to a fixed budget of sensors. Sparse sensing theory should be applied to animal and robotic propulsors to determine

the sensor locations that maximize the detection and classification of different features of propulsor movement with the fewest number of sensors (Brunton et al., 2016).

References

Abbott BC, Aubert XM. 1952. The force exerted by active striated muscle during and after change of length. The Journal of physiology 117(1):77-86.

Abelew TA, Miller MD, Cope TC, Nichols TR. 2000. Local loss of proprioception results in disruption of interjoint coordination during locomotion in the cat. Journal of neurophysiology 84(5):2709-2714.

Aiello BR, Blob RW, Butcher MT. 2013. Correlation of Muscle Function and Bone Strain in the Hindlimb of the River Cooter Turtle (Pseudemys concinna). J Morphol 274(9):1060-1069.

Aiello BR, Hardy AR, Cherian C, Olsen AM, Ahn SE, Hale ME, Westneat MW. 2017a. The relationship between pectoral fin stiffness and swimming behavior in Labridae: insights into design, performance, and ecology. In review at the Journal of Experimental Biology.

Aiello BR, King HM, Hale ME. 2014. Functional subdivision of fin protractor and retractor muscles underlies pelvic fin walking in the African lungfish Protopterus annectens. J Exp Biol 217(Pt 19):3474-3482.

Aiello BR, Stewart TA, Hale ME. 2016. Mechanosensation in an adipose fin. Proc R Soc B 283(20152794).

Aiello BR, Westneat MW, Hale ME. 2017b. Mechanosensation is evolutionarily tuned to locomotor mechanics. Proc Natl Acad Sci U S A 14(17):4459-4464.

Alben S, Madden PG, Lauder GV. 2007. The mechanics of active fin-shape control in ray-finned fishes. Journal of the Royal Society, Interface / the Royal Society 4(13):243-256.

Andersson MN, Larsson MC, Schlyter F. 2009. Specificity and redundancy in the olfactory system of the bark beetle Ips typographus: single-cell responses to ecologically relevant odors. Journal of insect physiology 55(6):556-567.

Arbuckle K, Bennett CM, Speed MP. 2014. A simple measure of the strength of convergent evolution. Methods Ecol Evol 5(7):685-693.

Atkins A, Dean MN, Habegger ML, Motta PJ, Ofer L, Repp F, Shipov A, Weiner S, Currey JD, Shahar R. 2014. Remodeling in bone without osteocytes: Billfish challenge bone structure-function paradigms. P Natl Acad Sci USA 111(45):16047-16052.

Bachmann T, Emmerlich J, Baumgartner W, Schneider JM, Wagner H. 2012. Flexural stiffness of feather shafts: geometry rules over material properties. J Exp Biol 215(3):405-415.

Barker D. 1974. Muscle Receptors. Handbook of Sensory Physiology. Springer- Verlag III:1-310.

Becerra J, Montes GS, Bexiga SRR, Junqueira LCU. 1983. Structure of the Tail Fin in Teleosts. Cell and tissue research 230(1):127-137.

Bellwood DR, Wainwright PC. 2001. Locomotion in labrid fishes: implications for habitat use and cross-shelf biogeography on the Great Barrier Reef. Coral Reefs 20(2):139-150.

Bennett MB, Ker RF, Dimery NJ, Alexander RM. 1986. Mechanical-Properties of Various Mammalian Tendons. J Zool 209:537-548.

Bernstein NA. 1967. Trends and problems in the study of investivation of physiology of activity. The Coordination and Regulation of Movements. Oxford: Pergamon.

Bickel A. 1897. Über den Einflug der sensibelen Nerven und der Labyrinthe auf die Bewegung der Tiere. Pflügers Arch ges Physiol 67:299-344.

Bilo D, Jahner A, Nachtigall W. 1980. Structure and innervation of wing muscle spindles in the domestic pigeon (Columba livia var. domestica); a light microscopical study. Zool J Anat 103:41-61.

Blob RW, LaBarbera M. 2001. Correlates of variation in deer antler stiffness: age, mineral content, intra-antler location, habitat, and phylogeny. Biological Journal of the Linnean Society 74:113-120.

Bone Q. 1964. Patterns of Muscular Innervation in the Lower Chordates. Int Rev Neurobiol 6:99-147.

Bonser RHC, Purslow PP. 1995. The Youngs-Modulus of Feather Keratin. J Exp Biol 198(4):1029-1033.

Bosco G, Poppele RE. 2001. Proprioception from a spinocerebellar perspective. Physiological reviews 81(2):539-568.

Brown TG, Sherrington CS. 1912. The rule of reflex response in the limb reflexes of the mammal and its exceptions. The Journal of physiology 44(3):125-130.

Brunton BW, Brunton SL, Proctor JL, Kutz JN. 2016. Sparse Sensor Placement Optimization for Classification. Siam J Appl Math 76(5):2099-2122.

Cardone BaF, J.H. 1981. Auditory characteristics and sexual dimorphism in the gypsy moth. Physiol Entomol 13:9-14.

Carruthers AC, Thomas AL, Taylor GK. 2007. Automatic aeroelastic devices in the wings of a steppe eagle Aquila nipalensis. J Exp Biol 210(Pt 23):4136-4149.

Cheney JA, Konow N, Middleton KM, Breuer KS, Roberts TJ, Giblin EL, Swartz SM. 2014. Membrane muscle function in the compliant wings of bats. Bioinspiration & biomimetics 9(2).

Ciaccio GV. 1890. Sur les plaques nerveuses finales darts les tendons des vertébrés. Archiv Ital de Biol 14:31-57.

Combes SA, Daniel TL. 2001. Shape, flapping and flexion: Wing and fin design for forward flight. J Exp Biol 204(12):2073-2085.

Combes SA, Daniel TL. 2003a. Flexural stiffness in insect wings. I. Scaling and the influence of wing venation. J Exp Biol 206(Pt 17):2979-2987.

Combes SA, Daniel TL. 2003b. Flexural stiffness in insect wings. II. Spatial distribution and dynamic wing bending. J Exp Biol 206(Pt 17):2989-2997.

Cooper BY, Glendinning DS, Vierck CJ. 1993. Finger Movement Deficits in the Stumptail Macaque Following Lesions of the Fasciculus-Cuneatus. Somatosens Mot Res 10(1):17-29.

Currey JD. 2002. Bones: structure and mechanics: Princeton University Press.

Daley MA, Biewener AA. 2003. Muscle force-length dynamics during level versus incline locomotion: a comparison of in vivo performance of two guinea fowl ankle extensors. J Exp Biol 206(Pt 17):2941-2958.

Daniel TL, Combes SA. 2002. Flexible wings and fins: bending by inertial or fluid-dynamic forces? Integrative and comparative biology 42(5):1044-1049.

Dekker T, Ibba I, Siju KP, Stensmyr MC, Hansson BS. 2006. Olfactory shifts parallel superspecialism for toxic fruit in Drosophila melanogaster sibling, D. sechellia. Current biology : CB 16(1):101-109.

Dickerson BH, Aldworth ZN, Daniel TL. 2014. Control of moth flight posture is mediated by wing mechanosensory feedback. J Exp Biol 217(13):2301-2308.

Dickinson MH. 1990a. Linear and nonlinear encoding properties of an identified mechanoreceptor on the fly wind measured with mechanical noise stimulation. J Exp Biol 151:219-244.

Dickinson MH. 1990b. Comparison of the encoding properties of campaniform sensilla on the fly wing. J Exp Biol 151:245-261.

Dingerkus G, Uhler LD. 1977. Enzyme Clearing of Alcian Blue Stained Whole Small Vertebrates for Demonstration of Cartilage. Stain Technol 52(4):229-232.

Drucker E, Jensen J. 1996. Pectoral fin locomotion in the striped surfperch. I. Kinematic effects of swimming speed and body size. J Exp Biol 199(Pt 10):2235-2242.

Drucker E, Jensen J. 1997. Kinematic and electromyographic analysis of steady pectoral fin swimming in the surfperches. J Exp Biol 200(Pt 12):1709-1723.

Eberle AL, Dickerson BH, Reinhall PG, Daniel TL. 2015. A new twist on gyroscopic sensing: body rotations lead to torsion in flapping, flexing insect wings. Journal of the Royal Society Interface 12(104).

Ellington CP. 1984. The Aerodynamics of Hovering Insect Flight .4. Aerodynamic Mechanisms. Philos T Roy Soc B 305(1122):79-&.

Elzinga MJ, Dickson WB, Dickinson MH. 2012. The influence of sensory delay on the yaw dynamics of a flapping insect. Journal of the Royal Society, Interface / the Royal Society 9(72):1685-1696.

Ennos AR. 1988a. The Importance of Torsion in the Design of Insect Wings. J Exp Biol 140:137-160.

Ennos AR. 1988b. The Inertial Cause of Wing Rotation in Diptera. J Exp Biol 140:161-169.

Etnier SA. 2001. Flexural and torsional stiffness in multi-jointed biological beams. Biol Bull 200(1):1-8.

Fessard A, Sand A. 1937. Stretch receptors in the muscles of fishes. J exp Biol 14(4):383-404.

Flammang BE, Alben S, Madden PG, Lauder GV. 2013. Functional morphology of the fin rays of teleost fishes. J Morphol 274(9):1044-1059.

Flammang BE, Lauder GV. 2008. Speed-dependent intrinsic caudal fin muscle recruitment during steady swimming in bluegill sunfish, Lepomis macrochirus. J Exp Biol 211(Pt 4):587-598.

Flammang BE, Lauder GV. 2013. Pectoral fins aid in navigation of a complex environment by bluegill sunfish under sensory deprivation conditions. J Exp Biol 216(Pt 16):3084-3089.

Frye MA. 2001. Encoding properties of the wing hinge stretch receptor in the hawkmoth Manduca sexta. J Exp Biol 204(Pt 21):3693-3702.

Fuchs E, Holmes P, David I, Ayali A. 2012. Proprioceptive feedback reinforces centrally generated stepping patterns in the cockroach. J Exp Biol 215(Pt 11):1884-1891.

Fulton CJ, Bellwood DR, Wainwright PC. 2001. The relationship between swimming ability and habitat use in wrasses (Labridae). Mar Biol 139(1):25-33.

Galloway KC, Clark JE, Koditschek DE. 2013. Variable Stiffness Legs for Robust, Efficient, and Stable Dynamic Running. J Mech Robot 5(1).

Galloway KC, Clark, J. E., Yim, M., and Koditschek, D. E. . 2011. Experimental investigations into the role of passive variable compliant legs for dynamic robotic locomotion. 2011 IEEE International Conference on Robotics and Automation:1243-1249.

Geerlink PJ, Videler JJ. 1987. The Relation between Structure and Bending Properties of Teleost Fin Rays. Neth J Zool 37(1):59-80.

Geraudie J, Singer M. 1985. Necessity of an Adequate Nerve Supply for Regeneration of the Amputated Pectoral Fin in the Teleost Fundulus. Journal of Experimental Zoology 234(3):367-374.

Gettrup E. 1965. Sensory Mechanisms in Locomotion - Campaniform Sensilla of Insect Wing and Their Function during Flight. Cold Spring Harb Sym 30:615-622.

Gettrup E. 1966. Sensory Regulation of Wing Twisting in Locusts. J Exp Biol 44(1):1-16.

Gettrup E, Wilson DM. 1964. Lift-Control Reaction of Flying Locusts. J Exp Biol 41(1):183-190.

Gibb AC, Jayne BC, Lauder GV. 1994. Kinematics of Pectoral Fin Locomotion in the Bluegill Sunfish Lepomis-Macrochirus. J Exp Biol 189:133-161.

Gillis GB, Biewener AA. 2002. Effects of surface grade on proximal hindlimb muscle strain and activation during rat locomotion. Journal of applied physiology 93(5):1731-1743.

Gillis GB, Blob RW. 2001. How muscles accommodate movement in different physical environments: aquatic vs. terrestrial locomotion in vertebrates. Comp Biochem Phys A 131(1):61-75.

Giuliani CA, Smith JL. 1987. Stepping Behaviors in Chronic Spinal Cats with One Hindlimb Deafferented. Journal of Neuroscience 7(8):2537-2546.

Goldberger ME. 1988. Partial and complete deafferentation of cat hindlimb: the contribution of behavioral substitution to recovery of motor function. Exp Brain Res 73(2):343-353.

Goodrich ES. 1904. On the dermal fin-rays of fishes - Living and extinct. Q J Microsc Sci 47(188):465-U418.

Gordon J, Ghilardi MF, Ghez C. 1995. Impairments of reaching movements in patients without proprioception. I. Spatial errors. J Neurophysiol 73(1):347-360.

Gordon JE. 1978. Structures: or Why Things Don’t Fall Down. . New York: Penguin Books.

Gray J, Lissmann HW. 1940. The effect of deafferentation upon the locomotory activity of amphibian limbs. J Exp Biol 17:227-237.

Grillner S. 1975. Locomotion in vertebrates: central mechanisms and reflex interaction. Physiological reviews 55(2):247-304.

Grillner S, Zangger P. 1975. How detailed is the central pattern generation for locomotion? Brain research 88(2):367-371.

Grillner S, Zangger P. 1984. The effect of dorsal root transection on the efferent motor pattern in the cat's hindlimb during locomotion. Acta Physiol Scand 120(3):393-405.

Haas HJ. 1962. Studies on Mechanisms of Joint and Bone Formation in Skeleton Rays of Fish Fins. Dev Biol 5(1):1-&.

Haga Y, Du SJ, Masui S, Fujinami Y, Aritaki M, Satoh S. 2010. Visualization of skeletons and intervertebral disks in live fish larvae by fluorescent calcein staining and disk specific GFP expression. J Appl Ichthyol 26(2):268-273.

Hale ME, Day RD, Thorsen DH, Westneat MW. 2006. Pectoral fin coordination and gait transitions in steadily swimming juvenile reef fishes. J Exp Biol 209(19):3708-3718.

Hall JM, McLoughlin DP, Kathman ND, Yarger AM, Mureli S, Fox JL. 2015. Kinematic diversity suggests expanded roles for fly halteres. Biology letters 11(11).

Hansson BS, Stensmyr MC. 2011. Evolution of insect olfaction. Neuron 72(5):698-711.

Hardy AR, Steinworth BM, Hale ME. 2016. Touch sensation by pectoral fins of the catfish *Pimelodus pictus*. Proc Roy Soc B 283(20152652).

Heathcote S, Wang Z, Gursul I. 2008. Effect of spanwise flexibility on flapping wing propulsion. J Fluid Struct 24(2):183-199.

Heide G. 1979. Proprioceptive Feedback Dominates the Central Oscillator in the Patterning of the Flight Motoneuron Output in Tipula (Diptera). J Comp Physiol 134(2):177-189.

Hering HW. 1983. Ueber die nach Durchschneidung der hinteren Wurzeln auftretende Bewegungslosigkeit des Rückenmarkfrosches. Pflügers Arch ges Physiol 54(614-640).

Higham TE, Birn-Jeffery AV, Collins CE, Hulsey CD, Russell AP. 2015. Adaptive simplification and the evolution of gecko locomotion: morphological and biomechanical consequences of losing adhesion. Proc Natl Acad Sci U S A 112(3):809-814.

Higham TE, Malas B, Jayne BC, Lauder GV. 2005. Constraints on starting and stopping: behavior compensates for reduced pectoral fin area during braking of the bluegill sunfish Lepomis macrochirus. J Exp Biol 208(24):4735-4746.

Higham TE, Russell AP, Birn-Jeffery A, Collins CE, Hulsey CD. 2014. Use it or lose it: locomotor evolution associated with the loss of adhesion in geckos. Integrative and comparative biology 54:E91-E91.

Hnik P, Vejsada R, Kasicki S. 1982. EMG changes in rat hind limb muscles following bilateral deafferentation. Pflugers Archiv : European journal of physiology 395(3):182-185.

Horton JM, Summers AP. 2009. The material properties of acellular bone in a teleost fish. J Exp Biol 212(9):1413-1420.

Hoyt DF, Taylor CR. 1987. Gait and the energetics of locmotion in horses. Nature 292:239-240.

Hurst J. 2008. The role and implementation of compliance in legged locomotion: Carnegie Mellon University.

Jensen M. 1956. Biology and Physics of Locust Flight .3. The Aerodynamics of Locust Flight. Philos T Roy Soc B 239(667):511-552.

Kahn JC, Flammang BE, Tangorra JL. 2012. Hover kinematics and distributed pressure sensing for force control of biorobotic fins. Intell Robot Syst IEEE 1460-1466.

Kahn JC, Peretz DJ, Tangorra JL. 2015. Predicting propulsive forces using distributed sensors in a compliant, high DOF, robotic fin. Bioinspiration & biomimetics 10(3).

Katz B. 1939. The relation between force and speed in muscular contraction. The Journal of physiology 96(1):45-64.

Katz PS, Harris-Warrick RM. 1990. Neuromodulation of the crab pyloric central pattern generator by serotonergic/cholinergic proprioceptive afferents. The Journal of neuroscience : the official journal of the Society for Neuroscience 10(5):1495-1512.

Kent GC, Carr RK. 2001. Comparative anatomy of the vertebrates. Boston: McGraw Hill. xvii, 524 p. p.

Klein-Nulend J, Bakker AD, Bacabac RG, Vatsa A, Weinbaum S. 2013. Mechanosensation and transduction in osteocytes. Bone 54(2):182-190.

Krieg M, Dunn AR, Goodman MB. 2015. Mechanical systems biology of C-elegans touch sensation. Bioessays 37(3):335-344.

Kung C. 2005. A possible unifying principle for mechanosensation. Nature 436(7051):647-654.

Kuo AD. 2002. The relative roles of feedforward and feedback in the control of rhythmic movements. Motor control 6(2):129-145.

Laska M, Seibt A, Weber A. 2000. 'Microsmatic' primates revisited: Olfactory sensitivity in the squirrel monkey. Chem Senses 25(1):47-53.

Lauder GV, Madden PG, Mittal R, Dong H, Bozkurttas M. 2006. Locomotion with flexible propulsors: I. Experimental analysis of pectoral fin swimming in sunfish. Bioinspiration & biomimetics 1(4):S25-34.

Lauder GV, Madden PGA, Tangorra JL, Anderson E, Baker TV. 2011. Bioinspiration from fish for smart material design and function. Smart Materials and Structures 20(9):094014.

Laughlin SB, van Steveninck RRD, Anderson JC. 1998. The metabolic cost of neural information. Nat Neurosci 1(1):36-41.

Liem KF. 1990. Aquatic Versus Terrestrial Feeding Modes - Possible Impacts on the Trophic Ecology of Vertebrates. Am Zool 30(1):209-221.

Liu P, Bose N. 1997. Propulsive performance from oscillating propulsors with spanwise flexibility. P Roy Soc a-Math Phy 453(1963):1763-1770.

Loeb GE, Gans C. 1986. Electromyography for experimentalists. Chicago: University of Chicago Press. xx, 373 p. p.

Losos JB. 1990. Ecomorphology, Performance Capability, and Scaling of West-Indian Anolis Lizards - an Evolutionary Analysis. Ecol Monogr 60(3):369-388.

Lowenstein O. 1956. Pressure receptors in the fins of the dogfish, Scyliorhinus canicula. J exp Biol 33(417-421).

Lundberg JG, Marsh E. 1976. Evolution and Functional-Anatomy of Pectoral Fin Rays in Cyprinoid Fishes, with Emphasis on Suckers (Family Catostomidae). Am Midl Nat 96(2):332-349.

Macleod GD. 1980. Mechanical-Properties of Contour Feathers. J Exp Biol 87(Aug):65-71.

Maeda N, Miyoshi S, Toh H. 1983. First observation of a muscle spindle in fish. Nature 302(5903):61-62.

Maier A. 1992a. The avian muscle spindle. Anatomy and embryology 186(1):1-25.

Maier A. 1992b. Sensory and motor innervation of bird intrafusal muscle fibers. Comparative biochemistry and physiology Comparative physiology 103(4):635-639.

Margaria R. 1938. Sulla fisiologica e specialmente sul consumo energetico
della corsa a varie velocita ed inclinazioni del terreno: Atti Accad. Naz.
Lincei Menorie. Biomechanics and Energetics of Muscular Exercise. Oxford: Clarendon Press. p 69-75.

Marsh E. 1977. Structural Modifications of Pectoral Fin Rays in Order Pleuronectiformes. Copeia(3):575-578.

Masino MA, Fetcho JR. 2005. Fictive swimming motor patterns in wild type and mutant larval zebrafish. J Neurophysiol 93(6):3177-3188.

Matthews PB. 1972. Mammalian muscle receptors and their central actions. Baltimore, MD: The Williams and Wilkins Co.

Miller S, Van Der Burg J, Van Der Meche FGA. 1975. Coordination of movements of the hindlimbs and forelimbs in different forms of locomotion in normal and decerebrate cats. . Brain Res 91:217-237.

Milner TE, Cloutier C. 1993. Compensation for Mechanically Unstable Loading in Voluntary Wrist Movement. Experimental Brain Research 94(3):522-532.

Mistick EA, Mountcastle AM, Combes SA. 2016. Wing flexibility improves bumblebee flight stability. J Exp Biol 219(21):3384-3390.

Möhl B. 1985. The role of proprioception in locust flight control. II. Information sugnalled by forewing stretch receptors. J Comp Physiol A 156:103-116.

Moir HM, Jackson JC, Windmill JF. 2013. Extremely high frequency sensitivity in a 'simple' ear. Biology letters 9(4):20130241.

Mongeau JM, Demir A, Dallmann CJ, Jayaram K, Cowan NJ, Full RJ. 2014. Mechanical processing via passive dynamic properties of the cockroach antenna can facilitate control during rapid running. J Exp Biol 217(18):3333-3345.

Montes GS, Becerra J, Toledo OMS, Gordilho MA, Junqueira LCU. 1982. Fine-Structure and Histochemistry of the Tail Fin Ray in Teleosts. Histochemistry 75(3):363-376.

Muniak MA, Ray S, Hsiao SS, Dammann JF, Bensmaia SJ. 2007. The neural coding of stimulus intensity: Linking the population response of mechanoreceptive Afferents with psychophysical Behavior. Journal of Neuroscience 27(43):11687-11699.

Mussi M, Summers AP, Domenici P. 2002. Gait transition speed, pectoral fin-beat frequency and amplitude in Cymatogaster aggregata, Embiotoca lateralis and Damalichthys vacca. J Fish Biol 61(5):1282-1293.

Nathan PW, Smith MC, Cook AW. 1986. Sensory Effects in Man of Lesions of the Posterior Columns and of Some Other Afferent Pathways. Brain 109:1003-1041.

Nelson FE, Jayne BC. 2001. The effects of speed on the in vivo activity and length of a limb muscle during the locomotion of the iguanian lizard Dipsosaurus dorsalis. J Exp Biol 204(Pt 20):3507-3522.

Newman DJS, Wootton RJ. 1986. An Approach to the Mechanics of Pleating in Dragonfly Wings. J Exp Biol 125:361-372.

Niven JE, Laughlin SB. 2008. Energy limitation as a selective pressure on the evolution of sensory systems. J Exp Biol 211(Pt 11):1792-1804.

Olsen AM, Westneat MW. 2015. StereoMorph: an R package for the collection of 3D landmarks and curves using a stereo camera set-up. Methods Ecol Evol 6(3):351-356.

Ono RD. 1979. Sensory nerve endings of highly mobile structures in two marine teleost fishes. Zoomorphologie 92:107-114.

Paillard J. 1960. The patterning of skilled movements, Sec. 1: Neurophysiology. In: Field J, Magoun HW, Hall VE, editors. Handbook of Physiology. Washington: Amer. Physiol. Ass. p 1679-1708.

Pansini S. 1888. Delle terminazioni dei nervi sui tendini nei Vertebrati. Boll Soc Nat Napoli 1(2):135-160.

Paradis E, Claude J, Strimmer K. 2004. APE: Analyses of Phylogenetics and Evolution in R language. Bioinformatics 20(2):289-290.

Passe DH, Walker JC. 1985. Odor Psychophysics in Vertebrates. Neurosci Biobehav R 9(3):431-467.

Pearson KG, Wolf H. 1987. Comparison of motor patterns in the intact and deafferented flight system of the locust. I. Electromyographic analysis. J Comp Physiol A 160:259-268.

Perret C, Cabelguen JM. 1976. Central and Reflex Participation in Timing of Locomotor Activations of a Bifunctional Muscle, Semi-Tendinosus, in Cat. Brain research 106(2):390-395.

Perret C, Cabelguen JM. 1980. Main Characteristics of the Hindlimb Locomotor Cycle in the Decorticate Cat with Special Reference to Bifunctional Muscles. Brain research 187(2):333-352.

Petzold BC, Park SJ, Mazzochette EA, Goodman MB, Pruitt BL. 2013. MEMS-based force-clamp analysis of the role of body stiffness in C. elegans touch sensation. Integr Biol-Uk 5(6):853-864.

Phelan C, Tangorra J, Lauder G, Hale M. 2010. A biorobotic model of the sunfish pectoral fin for investigations of fin sensorimotor control. Bioinspiration & biomimetics 5(3):035003.

Pierce SE, Clack JA, Hutchinson JR. 2012. Three-dimensional limb joint mobility in the early tetrapod Ichthyostega. Nature 486(7404):523-U123.

Plassmann W, Kadel M. 1991. Low-Frequency Sensitivity in a Gerbilline Rodent, Pachyuromys-Duprasi. Brain Behav Evolut 38(2-3):115-126.

Polit A, Bizzi E. 1978. Processes controlling arm movements in monkeys. Science 201(4362):1235-1237.

Polit A, Bizzi E. 1979. Characteristics of motor programs underlying arm movements in monkeys. J Neurophysiol 42(1 Pt 1):183-194.

Poloumordwinoff D. 1898. Recherches sur les terminaisons nerveuses sensitives darts les muscles volontaires. Société Scientifique et Station Zoologique d' Arcachon 3:73-79.

Potthoff T. 1984. Clearing and staining techniques. In: Moser HG, editor. Ontogeny and Systematics of Fishses, Special Publication - American Society of Ichthyologist and Herpetologist. Lawrence, KS. p 35-37.

Prochazka A, Gritsenko V, Yakovenko S. 2002. Sensory control of locomotion: reflexes versus higher-level control. In: Gan-devia SG, Proske U, Stuart DG, editors. Sensorimotor control. London, U.K.: Kluwer Academic/Plenum Publishers. p 1-13.

Purslow PP, Vincent JFV. 1978. Mechanical-Properties of Primary Feathers from Pigeon. J Exp Biol 72(Feb):251-260.

Quist BW, Faruqi RA, Hartmann MJZ. 2011. Variation in Young's modulus along the length of a rat vibrissa. Journal of biomechanics 44(16):2775-2781.

Raibert MH. 1986. Legged robots that balance: MIT press.

Rayner JMV. 1993. On aerodynamics and the energetics of vertebrate flapping flight. Contemp Math 141:351-400.

Revell LJ. 2012. phytools: An R package for phylogenetic comparative biology (and other things). Methods Ecol Evol 3:217-223.

Reye DN, Pearson KG. 1988. Entrainment of the locust central flight oscillator by wing stretch receptor stimulation. J Comp Physiol A 162:77-89.

Roberts BL. 1969. Response of a Proprioceptor to Undulatory Movements of Dogfish. J Exp Biol 51(3):775-&.

Robling AG, Castillo AB, Turner CH. 2006. Biomechanical and molecular regulation of bone remodeling. Annu Rev Biomed Eng 8:455-498.

Romanovsky D, Moseley AE, Mrak RE, Taylor MD, Dobretsov M. 2007. Phylogenetic preservation of alpha3 Na+,K+-ATPase distribution in vertebrate peripheral nervous systems. The Journal of comparative neurology 500(6):1106-1116.

Ross CF, Blob RW, Carrier DR, Daley MA, Deban SM, Demes B, Gripper JL, Iriarte-Diaz J, Kilbourne BM, Landberg T, Polk JD, Schilling N, Vanhooydonck B. 2013. The evolution of locomotor rhythmicity in tetrapods. Evolution; international journal of organic evolution 67(4):1209-1217.

Sainburg RL, Ghilardi MF, Poizner H, Ghez C. 1995. Control of limb dynamics in normal subjects and patients without proprioception. J Neurophysiol 73(2):820-835.

Sainburg RL, Poizner H, Ghez C. 1993. Loss of proprioception produces deficits in interjoint coordination. J Neurophysiol 70(5):2136-2147.

Sane SP, Dieudonne A, Willis MA, Daniel TL. 2007. Antennal mechanosensors mediate flight control in moths. Science 315(5813):863-866.

Sanes JN, Mauritz KH, Dalakas MC, Evarts EV. 1985. Motor control in humans with large-fiber sensory neuropathy. Human neurobiology 4(2):101-114.

Schindelin J, Arganda-Carreras, I., Frise, E., Kaynig, V., Longair, M., Pietzsch, T., Preibisch, S., Rueden, C., Saalfeld, S., Schmid, B. and Tinevez, J.Y. 2012. Fiji: an open-source platform for biological-image analysis. Nature methods 9(7):676-682.

Sherrington CS. 1913. Further observations on the production of reflex stepping by combination of reflex excitation with reflex inhibition. The Journal of physiology 47(3):196-214.

Simoncelli EPaO, B. A. . 2001. Neural image statistics and neural representation. Annu Rev Neurosci 24:1193-1216.

Smith LL, Fessler JL, Alfaro ME, Streelman JT, Westneat MW. 2008. Phylogenetic relationships and the evolution of regulatory gene sequences in the parrotfishes. Molecular phylogenetics and evolution 49(1):136-152.

Standen EM, Lauder GV. 2005. Dorsal and anal fin function in bluegill sunfish Lepomis macrochirus: three-dimensional kinematics during propulsion and maneuvering. J Exp Biol 208(Pt 14):2753-2763.

Steppan SJ. 2000. Flexural stiffness patterns of butterfly wings (Papilionoidea). Journal of Research on the Lepidoptera 35:61-77.

Stevenson PA, Kutsch W. 1986. Basic circuitry of an adult-specific motor program completed with embryogenesis. Naturwissenschaften 73:741-743.

Stevenson PA, Kutsch W. 1987. A reconsideration of the central pattern generator concept for locust flight. J Comp Physiol A 161:115-129.

Stevenson PA, Kutsch W. 1988. Demonstration of functional connectivity of the flight motor system in all stages of the locust. J Comp Physiol A 162:247-259.

Svoboda KR, Linares AE, Ribera AB. 2001. Activity regulates programmed cell death of zebrafish Rohon-Beard neurons. Development 128(18):3511-3520.

Swartz SM, Groves MS, Kim HD, Walsh WR. 1996. Mechanical properties of bat wing membrane skin. J Zool 239:357-378.

Swartz SM, Middleton KM. 2008. Biomechanics of the bat limb skeleton: scaling, material properties and mechanics. Cells, tissues, organs 187(1):59-84.

Székely G, Czeh G, Voros G. 1969. The activity pattern of limb muscles in freely moving normal and deafferented newts. Exp Brain Res 9(1):53-72.

Taft NK. 2011. Functional implications of variation in pectoral fin ray morphology between fishes with different patterns of pectoral fin use. J Morphol 272(9):1144-1152.

Taft NK, Taft BN. 2012. Functional implications of morphological specializations among the pectoral fin rays of the benthic longhorn sculpin. J Exp Biol 215(15):2703-2710.

Tangorra JL, Lauder GV, Hunter IW, Mittal R, Madden PG, Bozkurttas M. 2010. The effect of fin ray flexural rigidity on the propulsive forces generated by a biorobotic fish pectoral fin. J Exp Biol 213(23):4043-4054.

Thorsen DH, Westneat MW. 2005. Diversity of pectoral fin structure and function in fishes with labriform propulsion. J Morphol 263(2):133-150.

Thoumie P, Do MC. 1996. Changes in motor activity and biomechanics during balance recovery following cutaneous and muscular deafferentation. Exp Brain Res 110(2):289-297.

Tourtellotte WG, Milbrandt J. 1998. Sensory ataxia and muscle spindle agenesis in mice lacking the transcription factor Egr3. Nature genetics 20(1):87-91.

Vogel S. 1967. Flight in Drosophila .3. Aerodynamic Characteristics of Fly Wings and Wing Models. J Exp Biol 46(3):431-&.

Vogel S. 2003a. Comparative biomechanics : life's physical world. Princeton, NJ: Princeton University Press. xii, 580 p. p.

Vogel S. 2003b. Comparative biomechanics: life's physical world.: Princeton University Press.

Vogel S, Labarbera M. 1978. Simple Flow Tanks for Research and Teaching. Bioscience 28(10):638-643.

Wainwright PC, Bellwood DR, Westneat MW. 2002. Ecomorphology of locomotion in labrid fishes. Environmental Biology of Fishes 65(1):47-62.

Wainwright PC, Reilly SM. 1994. Ecological morphology : integrative organismal biology. Chicago: University of Chicago Press. viii, 367 p. p.

Walker JA, Westneat MW. 1997. Labriform propulsion in fishes: kinematics of flapping aquatic flight in the bird wrasse Gomphosus varius (Labridae). J Exp Biol 200(Pt 11):1549-1569.

Walker JA, Westneat MW. 2000a. Mechanical performance of aquatic rowing and flying. Proceedings Biological sciences / The Royal Society 267(1455):1875-1881.

Walker JA, Westneat MW. 2000b. Mechanical performance of aquatic rowing and flying. P Roy Soc B-Biol Sci 267(1455):1875-1881.

Walker JA, Westneat MW. 2002a. Kinematics, dynamics, and energetics of rowing and flapping propulsion in fishes. Integrative and comparative biology 42(5):1032-1043.

Walker JA, Westneat MW. 2002b. Performance limits of labriform propulsion and correlates with fin shape and motion. J Exp Biol 205(2):177-187.

Wang YM, K. L.; Baba, Y.; Lumpkin, E. A.; and Gerling, G. J. 2013. Natural variation in skin thickness argues for mechanical stimulus control by force instead of displacement. In World Haptics Conference (WHC) IEEE:645-650.

Warrant E. 2004. Vision in the dimmest habitats on earth. Journal of comparative physiology A, Neuroethology, sensory, neural, and behavioral physiology 190(10):765-789.

Webb PW. 1973. Kinematics of Pectoral Fin Propulsion in Cymatogaster-Aggregata. J Exp Biol 59(3):697-710.

Webster DB, Webster M. 1971. Adaptive Value of Hearing and Vision in Kangaroo Rat Predator Avoidance. Brain Behav Evolut 4(4):310-&.

Webster DB, Webster M. 1972. Kangaroo Rat Auditory Thresholds before and after Middle-Ear Reduction. Brain Behav Evolut 5(1):41-&.

Weis-Fogh T. 1956. Biology and physics of locust flight, IV. Notes on sensory mechanisms in locust flight. Phil Trans B 339:553-584.

Wenger MPE, Bozec L, Horton MA, Mesquida P. 2007. Mechanical properties of collagen fibrils. Biophys J 93(4):1255-1263.

Westneat M, Walker J. 1997. Motor patterns of labriform locomotion: kinematic and electromyographic analysis of pectoral fin swimming in the labrid fish Gomphosus varius. J Exp Biol 200(Pt 13):1881-1893.

Westneat MW, Alfaro ME. 2005. Phylogenetic relationships and evolutionary history of the reef fish family Labridae. Molecular phylogenetics and evolution 36(2):370-390.

Westneat MW, Thorsen DH, Walker JA, Hale ME. 2004. Structure, function, and neural control of pectoral fins in fishes. Ieee J Oceanic Eng 29(3):674-683.

Williams CM, Kramer EM. 2010. The Advantages of a Tapered Whisker. Plos One 5(1).

Williams R, Hale ME. 2015. Fin ray sensation participates in the generation of normal fin movement in the hovering behavior of the bluegill sunfish (Lepomis macrochirus). J Exp Biol 218(Pt 21):3435-3447.

Williams R, Neubarth N, Hale ME. 2013. The function of fin rays as proprioceptive sensors in fish. Nature communications 4:1729.

Wilson DM. 1961. The central nervous control of locust flight. J Exp Biol 38:471-490.

Wilson DM, Gettrup E. 1963. A Stretch Reflex Controlling Wingbeat Frequency in Grasshoppers. J Exp Biol 40(1):171-&.

Wolf H, Pearson KG. 1987. Intracellular recordings from interneurons and motoneurons in intact flying locusts. Journal of neuroscience methods 21(2-4):345-354.

Woo SH, Lukacs V, de Nooij JC, Zaytseva D, Criddle CR, Francisco A, Jessell TM, Wilkinson KA, Patapoutian A. 2015. Piezo2 is the principal mechanotransduction channel for proprioception. Nat Neurosci 18(12):1756-1762.

Wootton RJ. 1981. Support and Deformability in Insect Wings. J Zool 193(Apr):447-468.

Wootton RJ. 1992. Functional-Morphology of Insect Wings. Annu Rev Entomol 37:113-140.

Wunderer H. 1908. Über Terminalkörperchen der Anamnien. Archiv für mikroskop Anat Entwicklungsmech 71:504-569.

Yakhnitsa IA, Bulgakova NV, Pilyavskii AI. 1987. Kinematics of different types of locomotor movements in the deafferented rat. Neurophysiol 19:394-398.

Yamamoto I, Terada Y, Nagamatu T, Imaizumi Y. 1995. Propulsion System with Flexible Rigid Oscillating Fin. Ieee J Oceanic Eng 20(1):23-30.

Young J, Walker SM, Bomphrey RJ, Taylor GK, Thomas AL. 2009. Details of insect wing design and deformation enhance aerodynamic function and flight efficiency. Science 325(5947):1549-1552.

Young WC, Budynas RG, Sadegh A. 2012. Roark's formulas for stress and strain. New York: McGraw-Hill.

Zhu Q, Shoele K. 2008. Propulsion performance of a skeleton-strengthened fin. J Exp Biol 211(Pt 13):2087-2100.